DYNAMIC AND CONDITIONALLY ACTIVATED NUCLEIC ACID NANOPARTICLES

by

Morgan Renee Chandler

A dissertation submitted to the faculty of
The University of North Carolina at Charlotte
in partial fulfillment of the requirements
for the degree of Doctor of Philosophy in
Nanoscale Science

Charlotte

2021

Approved by:

_____
Dr. Kirill Afonin

_____
Dr. Juan Vivero-Escoto

_____
Dr. Joanna Krueger

_____
Dr. Kausik Chakrabarti

_____
Dr. Craig Allan

ABSTRACT

MORGAN RENEE CHANDLER. Dynamic and Conditionally Activated Nucleic Acid Nanoparticles. (Under the direction of DR. KIRILL AFONIN)

Programmed interactions of nucleic acids—including DNA and RNA—orchestrate genetic expression and downstream cellular processes at every level. The structures of nucleic acids rely on their sequences, which include traditional Watson-Crick base pairing as well as non-canonical interactions and which make bottom-up structural design predictable and feasible. By utilizing these biopolymers as materials for the design and assembly of nucleic acid nanoparticles (NANPs), defined scaffolds can be constructed to carry out specific interactions with other nucleic acids, immune receptors, and pathways. The design of NANPs offers the advantage of modularity over traditional therapeutic approaches, as the targeting features can be tailored without alteration of the overall pharmacokinetic profile. Here, the immunostimulatory design parameters of therapeutic NANPs are explored as well as the conditional activation of those therapeutic moieties, which work via the RNA interference pathway for post-transcriptional gene knockdown. Overall, the further development of dynamic NANPs aims to treat disease with greater individualized specificity and to induce strategic immune responses towards the development of personalized medicine.

Acknowledgments

I would like to express my deepest gratitude to the "village" it took to help me grow and learn, full of those who have continued to inspire and support me along the way. First and foremost, my advisor, Dr. Kirill Afonin, has been an incredible mentor. His investment in teaching me and the opportunities he has provided me with have had an enormous impact on the direction of my life and career. I may have found my passion working within "the emerging field," but I was also very fortunate that I found an advisor working to push the boundaries within it which have made this work so fulfilling.

I am grateful for the time and expertise offered by my committee members—Dr. Joanna Krueger, Dr. Juan Vivero-Escoto, Dr. Kausik Chakrabarti, and Dr. Craig Allan—as they have guided me along this process. I am thankful for Dr. Caryn Striplin for her encouragement and pursuit of adventure in the lab and in life, Dr. Brittany Johnson for sharing her expertise and paving the road for the next generation of incredible PIs, Dr. Martin Panigaj for his timeless wisdom and good humor, and Dr. Angelica Martins who has shown me what it means to be an extraordinary leader and role model.

To my parents, Barry and Lynn Chandler, any goal that I accomplish is driven by your unconditional love and support from my earliest days. There was never a project—not a Grand Canyon, an algebraic park, nor a milk carton town—which you hesitated to stay up all night working with me on. Thank you for taking the time to elevate my tiniest accomplishments and never doubting my latest pitch. To Ryan, your incredible fortitude has been an endless source of inspiration not only to overcome obstacles, but to work towards overcoming the maladies that serve as obstacles to others. To Jordan, Jenni, and Olive, thank you for always uplifting creativity and inspiring me to conjure up the kind of passion that you pour into your projects. To

Tom Ouellette, thank you for embracing me and every one of my papers with your unwavering excitement and love. To Dava Anderson, who has been a part of my academic journey for almost two decades, your navigation and endless support has meant so much to me.

To Dr. Justin Halman, my greatest advocate and co-author in life, I am forever grateful that this research brought us together through a series of incredibly fortunate happenstances. I am excited to keep problem solving with you in every capacity and hope our desks will always be side-by-side. I also want to express my gratitude to the Halman family—Gary, Jill, Alexander, and Susanna—who welcomed me with such warmth and have never stopped cheering me on.

I am extremely thankful to have worked alongside so many cherished labmates during my time here, especially fellow graduate students Alex, Damian, Jessica, Kyle, Leyla, Oleg, Sameer, Sandra, Weina, and Yelixza, as well our many undergraduate students and summer scholars. I would also like to thank all the collaborators and co-authors I've had the chance to work alongside, especially Dr. Marina Dobrovolskaia and the team at NCL as well as Dr. Roger Chammas and the team at USP for the opportunities they gave me visit, work, and learn from their vast knowledgebases. I am extremely grateful for Dr. Chandra Williams and the team at the Vivarium for their experimental support. Thank you to Dr. Bernadette Donovan-Merkert, Rebecca Hawes, Nancy Queen, Lisa Carlin, Paul Bainbridge, Brenda Fandrey, Deborah Howard, and the rest of the Department who have helped me in almost every capacity along the way.

Finally, I am grateful to funding from the Thomas L. Reynolds Graduate Student Research Award and the UNC Charlotte Graduate School Summer Fellowship.

Table of Contents

List of Figures

List of Abbreviations

°C	Degrees Celsius
µg	Microgram
µL	Microliter
µm	Micrometer
1D	One-dimensional
2D	Two-dimensional
3D	Three-dimensional
3p-hpRNA	5’ triphosphate hairpin ribonucleic acid
3WJ	Three-way junction
A	Adenine
a.u.	Arbitrary units
AB	Assembly Buffer
Abs	Absorbance
AFM	Atomic force microscopy
ANOVA	Analysis of variance
ATCC	American Type Culture Collection
BD	Becton, Dickinson and Company
BDNA	Synthetic analog of B-form deoxyribonucleic acid
Biosg	5’ Biotin
bp	Basepair
BP	Bandpass
C	Cytosine

CARPA	Complement activation-related pseudoallergies
cGAMP	Cyclic guanosine monophosphate-adenosine monophosphate
cGAS	Cyclic guanosine monophosphate-adenosine monophosphate synthase
cm	Centimeter
CO_2	Carbon dioxide
CpG	Cytosine-phosphodiester bond-guanine
Cryo-EM	Cryogenic electron microscopy
d	Distance
DAMP	Damage-associated molecular pattern
ddiH_2O	Double-deionized water
DFHBI	(Z)-4-(3,5-Difluoro-4-hydroxybenzylidene)-1,2-dimethyl-1*H*-imidazol-5(4*H*)-one
DFHBI-1T	(Z)-4-(3,5-Difluoro-4-hydroxybenzylidene)-2-methyl-1-(2,2,2-trifluoroethyl)-1*H*-imidazol-5(4*H*)-one
DIC	Differential interference contrast
DLS	Dynamic light scattering
DMEM	Dulbecco's Modified Eagle Medium
DNA	Deoxyribonucleic acid
DNase	Deoxyribonuclease
DS RNA	Dicer substrate ribonucleic acid
dsDNA	Double-stranded deoxyribonucleic acid
dsRNA	Double-stranded ribonucleic acid
DTT	Dithiothreitol
EDTA	Ethylenediaminetetraacetic acid

eGFP	Enhanced green fluorescent protein
ELISA	Enzyme-linked immunosorbent assay
Em	Emission
EMEM	Eagle's Minimum Essential Medium
EMSA	Electrophoretic mobility shift assay
ER	Endoplasmic reticulum
EtBr	Ethidium bromide
EtOH	Ethanol
FBS	Fetal bovine serum
FRET	Förster resonance energy transfer
G	Guanine
g	Gram, Gravity
GC	Guanine-cytosine
GFP	Green fluorescent protein
gMFI	Geometric mean fluorescence intensity
h	Hours
H_ant	Hybrid antisense duplex
H_sen	Hybrid sense duplex
HBS	Human blood serum
HBSS	Hanks' Balanced Salt Solution
HEK	Human Embryonic Kidney
HEPES	4-(2-hydroxyethyl)-1-piperazineethanesulfonic acid
hIFN-β	Human interferon beta

hIL-1β	Human interleukin one beta
hIL-6	Human interleukin six
hIL-8	Human interleukin eight
HIV-KL	Human immunodeficiency virus-derived kissing loop
HRP	Horseradish peroxidase
hTLR3	Human toll-like receptor 3
hTLR7	Human toll-like receptor 7
hTLR8	Human toll-like receptor 8
hTLR9	Human toll-like receptor 9
IDT	Integrated DNA Technologies
IFI16	Interferon-γ-inducible protein sixteen
IFIT	Interferon-induced proteins with tetratricopeptide repeats
IFN	Interferon
IFN-α	Interferon alpha
IFN-β	Interferon beta
IFN-λ	Interferon lambda
IFN-ω	Interferon omega
IL-1β	Interleukin one beta
IL-6	Interleukin six
IL-8	Interleukin eight
IR	Infrared
IRF	Interferon regulatory factor
IRF3	Interferon regulatory factor three

IRF7	Interferon regulatory factor seven
ITA	Investigational Testing Authorization
ITK	Innovator's Tool Kit
IκB	Nuclear factor of kappa light polypeptide gene enhancer in B-cells inhibitor
kcal	Kilocalorie
KCl	Potassium chloride
K_d	Dissociation constant
KL	Kissing loop
KOH	Potassium hydroxide
kV	Kilovolt
L2K	Lipofectamine 2000
M	Molar
MAVS	Mitochondrial antiviral-signaling protein
MD	Molecular Dynamics
MDA5	Melanoma differentiation-associated protein five
mDC	Myeloid dendritic cell
MEM	Minimum Essential Medium
MG	Malachite Green
Mg^{2+}	Magnesium cation
$MgCl_2$	Magnesium chloride
min	Minutes
mL	Milliliter
mM	Millimolar

mo	Monocyte
moDC	Monocyte-derived dendritic cell
mol	Mole
MP	Multiplex
mRNA	Messenger RNA
ms	Millisecond
MTS	3-(4,5-dimethylthiazol-2-yl)-5-(3-carboxymethoxyphenyl)-2-(4-sulfophenyl)-2H-tetrazolium, inner salt
MW	Molecular weight
MΩ	Megaohm
NA	Nucleic acid
NaCl	Sodium chloride
NANP	Nucleic acid nanoparticle
NC	Negative control
NCL	Nanotechnology Characterization Laboratory
ncRNA	Noncoding ribonucleic acid
ND	Nearest distances
NF-κB	Nuclear factor kappa-light-chain-enhancer of activated B cells
ng	Nanogram
nM	Nanomolar
nm	Nanometer
NMR	Nuclear magnetic resonance
nr	Nanoring

nt	Nucleotide
NUPACK	Nucleic Acid Package
ODN	Oligodeoxynucleotide
p	Phosphate
PAGE	Polyacrylamide gel electrophoresis
PAMP	Pathogen-associated molecular pattern
PBMC	Peripheral blood mononuclear cell
PBS	Phosphate-buffered saline
PCR	Polymerase Chain Reaction
pDC	Plasmacytoid dendritic cell
PenStrep	Penicillin-Streptomycin
pg	Picogram
Phos	Phosphate
PK	Pseudoknot
Pol III	Ribonucleic acid polymerase III
Poly I:C	Polyinosinic:polycytidylic acid
pRNA	Packing ribonucleic acid
PRR	Pattern recognition receptor
QD	Quantum dot
QD525	Quantum dot, 525 nanometer emission
QD545	Quantum dot, 545 nanometer emission
QD605	Quantum dot, 605 nanometer emission
Qdot	Quantum dot

QSAR	Quantitative structure-activity relationship
r_1	Radius of identified point
r_2	Radius of identified neighbor
R848	Resiquimod
RFU	Relative fluorescence units
RIG-I	Retinoic acid-inducible gene I
RISC	Ribonucleic acid-induced silencing complex
RLR	Retinoic acid-inducible gene I-like receptor
RNA	Ribonucleic acid
RNAi	RNA interference
RNase	Ribonuclease
rNTP	Ribonucleotide triphosphate
RPMI	Roswell Park Memorial Institute
RQ1	Ribonucleic acid-qualified
RT	Room temperature
s	Second
SARS-CoV-2	Severe acute respiratory syndrome coronavirus 2
SEAP	Secreted alkaline phosphatase
SELEX	Systematic evolution of ligands by exponential enrichment
SEM	Standard error of the mean
siRNA	Short interfering ribonucleic acid
SMART	Specific, Manageable, Adjustable, Reproducible, and Targeted
ssDNA	Single-stranded deoxyribonucleic acid

ssRNA	Single-stranded ribonucleic acid
STING	Stimulator of interferon genes
T	Thymine, Temperature
$t_{½}$	Half-life
TB	Tris/Borate
TBE	Tris/Borate/Ethylenediaminetetraacetic acid
TEM	Transmission electron microscopy
TLR	Toll-like receptor
TLR3	Toll-like receptor 3
TLR7	Toll-like receptor 7
TLR8	Toll-like receptor 8
TLR9	Toll-like receptor 9
T_m	Melting temperature
TNA	Therapeutic nucleic acid
tRNA	Transfer ribonucleic acid
U	Uracil, Units
UTR	Untranslated region
UV	Ultraviolet
V	Volts
v/v	Volume per volume
τ	Stability in blood serum

CHAPTER 1: INTRODUCTION: INNATE IMMUNE RESPONSES TRIGGERED BY NUCLEIC ACIDS INSPIRE THE DESIGN OF IMMUNOMODULATORY NUCLEIC ACID NANOPARTICLES

1.1 Introduction

Nucleic acid biopolymers (RNA and DNA) have evolved to preserve and regulate the flow of genetic information across all forms of life. Drawing from the variety of available structures of naturally occurring or experimentally selected nucleic acid motifs, mostly manifested in RNAs, a vast library of nucleic acid nanoparticles (NANPs) has been demonstrated (**Figure 1**) and further investigated for the delivery of therapeutic moieties[1-2], material organization[3-5], or conditional operations in mammalian cells[6-9].

However, as a result of evolutionary ubiquity, nucleic acids (NAs) have well-established patterns of recognition and thus, the manner in which mammalian cells can interpret NANPs is built upon the pre-existing machinery for bacterial and viral immune recognition. While the recognition of exogenous NAs serves to defend against pathogen invasion, one key challenge for cells remains to avoid an innate immune response to their own endogenous NAs. Four main determinants have been identified to balance the recognition of self from non-self NAs: patterns (foreign NAs are recognized based on the structure, sequence, or composition), location (occurrence of NAs in compartments unusual for their presence), quantity (changes in relative amounts of NAs compared to physiological conditions), and threshold (regulation of expression of components for NA sensing and downstream signaling)[10]. Accordingly, cells express pattern recognition receptors (PRRs) that precisely identify signature motifs termed pathogen-associated or danger-associated molecular patterns (PAMPs and DAMPs) in main cellular locations[11-13]. Numerous key PRRs specializing in NA recognition will be discussed in this review with the emphasis on NANP recognition pathways (**Figure 2**).

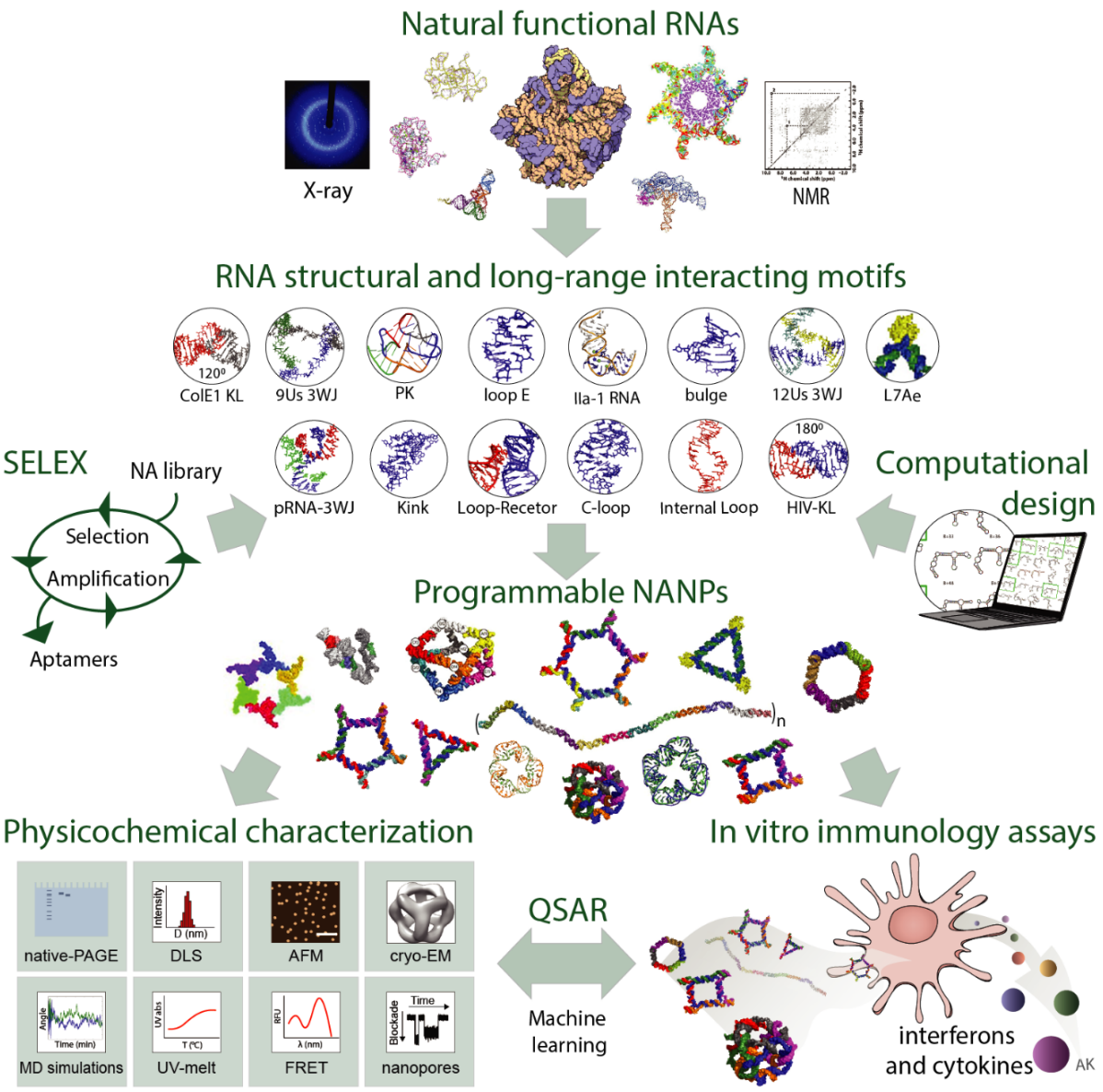

Figure 1. The flow of NANP design and characterization. Structural and long-range interacting motifs that can be either mined from natural NAs, selected via systematic evolution of ligands by exponential enrichment (SELEX), or designed computationally are combined for the rational design of programmable NANPs. All new NANPs are then extensively characterized and their immunostimulation is assessed. Machine learning approaches such as quantitative structure-activity relationship (QSAR) modeling which relates the physicochemical parameters to relative immune response can be utilized to predict and optimize future NANP designs suitable for specific biomedical tasks. (Additional abbreviations: three-way junction (3WJ); atomic force microscopy (AFM); dynamic light scattering (DLS); electron microscopy (EM); Förster Resonance Energy Transfer (FRET); human immunodeficiency virus (HIV); kissing loop (KL); molecular dynamics (MD); nuclear magnetic resonance (NMR); polyacrylamide gel electrophoresis (PAGE); pseudoknot (PK); packing RNA (pRNA); ultraviolet (UV))

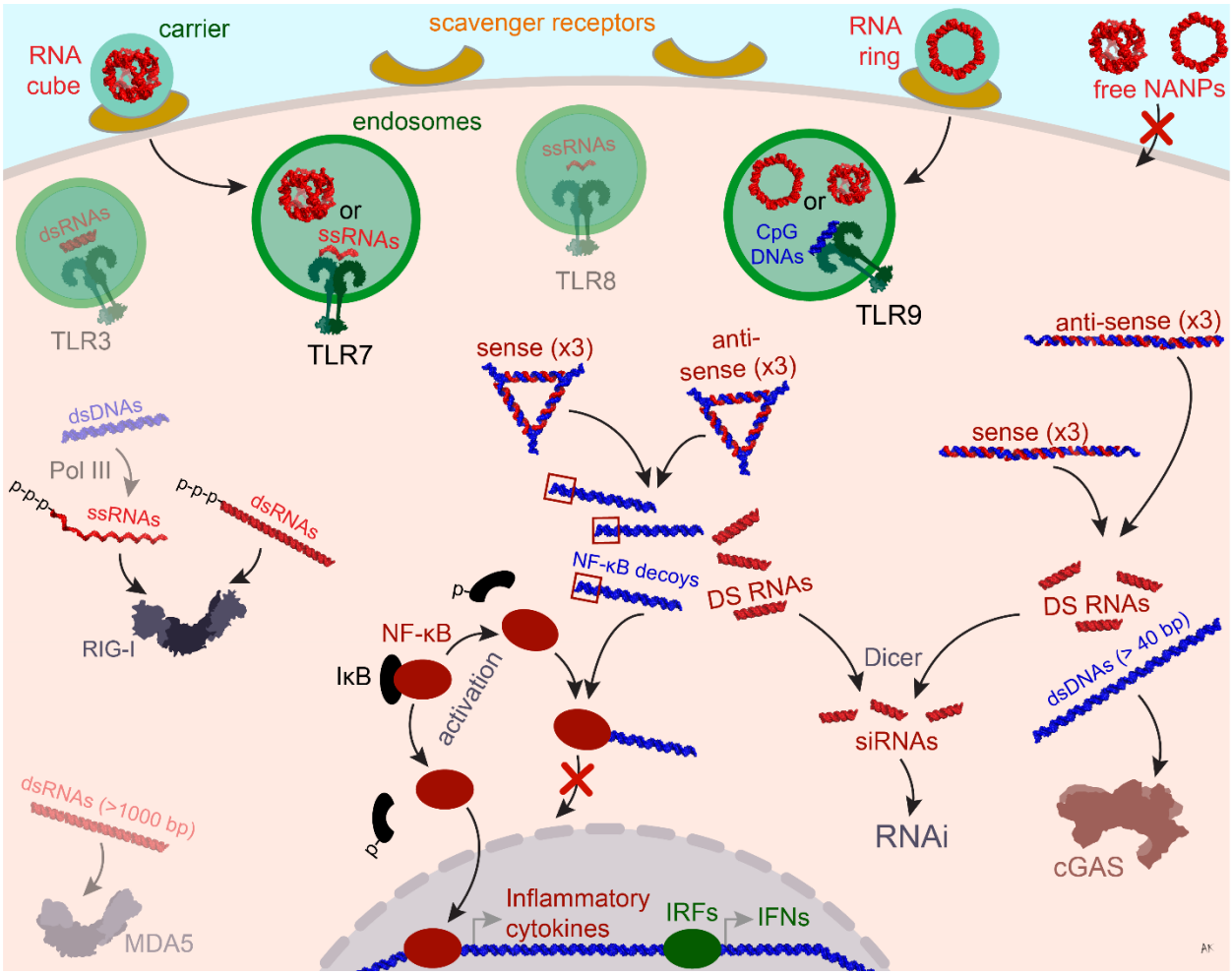

Figure 2. Possible ways of NANP processing in the cellular environment. NANPs complexed with a polycationic carrier enter the cell via scavenger receptor-mediated endocytosis and get recognized by TLRs (*e.g.*, TLR7 for RNA cubes and TLR9 for both RNA cubes and rings). In the cytoplasm, non-functional RNA/DNA hybrid NANPs can dynamically interact with each other to activate pre-programmed functionalities such as the release of Dicer Substrate (DS) RNAs, later processed into siRNAs, and NF-κB decoy containing dsDNAs which prevent NF-κB translocation into the nucleus and the subsequent production of inflammatory cytokines. The use of longer byproduct dsDNAs helps to activate the cGAS-STING pathway leading to the expression of inflammatory genes.

As the first line of cellular defense, four endosomal membrane-located Toll-like receptors (TLRs 3, 7, and 8 sensing RNAs and TLR9 sensing DNA) compose the group of PRRs that recognize extracellularly invading bacterial and viral NAs[11, 14]. Another group of PRRs that

resides in the cytoplasm and nucleus include RIG-I-like (RLRs) and MDA5 receptors sensing non-self RNAs along with cyclic GMP-AMP synthase (cGAS) and interferon-γ-inducible protein 16 (IFI16) sensing cytoplasmic DNA[15]. The abundance of individual PRRs differs among various tissues and cell types[16]. While TLRs are mostly specific for cells of the immune system, intracellular PRRs are broadly expressed. Detection of NA-based PAMPs triggers intricate signaling cascades that pass through the pathway's specific adaptor proteins defined by the type of NA trigger and finally merge to the transcription factors NF-κB, IRF3, and IRF7[15, 17]. PRR activation culminates in expression of host defense genes and translation of water-soluble proteins (*e.g.*, interferons, proinflammatory cytokines, and chemokines) essential for defense against pathogens. However, the same immune responses that diligently defend against pathogens can create an immunological hurdle for broad applications of therapeutic nucleic acids (TNAs) and NANPs. While some recent TNA formulations have successfully overcome immunological toxicities using chemical modifications and carriers, unwanted immunostimulation remains the major challenge for further clinical translation[18]. Establishing trends in NANP recognition based on design and composition introduces new possibilities to tailor NANPs for emulating the activations of specific immune pathways. Additionally, viral and bacterial pathogens have evolved methods to circumvent, avoid, or enhance the innate surveillance system. Therefore, critically examining the mechanisms of pathogen recognition and manipulation of NA immune responses will provide valuable insight into the development of NANP technology for clinical applications.

1.2 Recognition Receptors

As the field moves towards the development of rationally engineered NANPs with controlled immunostimulation[9, 19-22], it becomes crucial to consider PRRs' expression which is

often cell type-specific. For example, TLRs 7 and 8 can both recognize ssRNA; however, plasmacytoid dendritic cells (pDC) and B cells can only express TLR7 while monocytes, macrophages, and myeloid DCs preferentially express TLR8 with minimal expression of TLR7[23-25]. Also, TLR7 can detect short stretches of dsRNAs[26-28] and as a result, pDCs have been shown to be the primary source of interferon production in response to cubic RNA NANPs via the TLR7 pathway[22, 29]. Recent studies have also suggested the possible involvement of TLR9 in the recognition of RNA cubes and rings in human peripheral blood mononuclear cells (PBMCs)[29]. However, the mechanism of recognition has yet to be determined.

It is important to note that the expression of PRRs often changes during a diseased state and, for example, the upregulation of TLR9 has been observed in patients with autoimmune thyroid disease[30]. As such, when choosing the designing principles of therapeutic NANPs, it is vital to consider any disease-specific changes in expression patterns of relevant PRRs.

Expression of PRRs is also tightly regulated on the subcellular level to strategically encounter pathogenic NAs while avoiding any recognition of self-NAs. The endosomal TLRs 3, 7, and 8 are synthesized in the ER and traffic from the Golgi to either endosomes or lysosomes, while TLR9 traffics from the ER directly to the endosomal compartment[17, 31]. Additionally, proteolytic processing of TLR ectodomains is required for receptor signaling and, therefore, is limited to the endosomal compartment[32]. This tightly regulated trafficking of TLRs provides an important means for avoiding the recognition of self-NAs. However, some pathogens evolved several mechanisms aimed at escaping TLR-mediated detection. For example, some bacteria utilize the endosomal compartment to create an intracellular replication niche[33-34], whereas other microbes use effector proteins to decrease phagosomal calcium concentration, increase phagosome pH, and avoid or reduce fusion with lysosomes[35-38]. Manipulating phagosome maturation prevents

bacterial degradation and reduces the presence of NA ligands for endosomal TLRs. Alternating phagosome maturation may also alter the presence or function of these TLRs in the endocytic compartment. Therefore, pathogen recognition within the endosome is dependent on the presence of functional TLRs.

While mechanisms of endosomal and TLR escape by pathogens may have deleterious consequences for the host, they could be employed for designing SMART (Specific, Manageable, Adjustable, Reproducible, and Targeted) NANPs for biomedical applications. Since NANPs are made of nucleic acids which, when delivered into the endosomal compartment, could elicit TLR-driven interferon responses, this property is beneficial for applications in which activation of the immune system is desirable (*e.g.*, vaccines and immunotherapies). In contrast, the mechanisms analogous to those utilized by microbes escaping immune recognition could potentially be implemented into the NANP design to diminish the immunorecognition of therapeutic cargo in conditions for which immunostimulation is undesirable (*e.g.*, drug delivery).

Similarly, the delivery and intracellular trafficking of NANPs are key determinants in immune receptor recognition or avoidance. Due to their negative charge, free NANPs are unable to enter the cell without the use of a carrier and are immunoquiescent[22]. Activation of the NANPs' immune recognition can, therefore, be controlled by selecting a delivery carrier with specificity to certain routes of uptake, and, consequently, to various intracellular compartments. For example, delivery via receptor-mediated endocytosis allows for the targeting of endosomal TLRs, while delivery to the cytosol would introduce NANPs directly to cytosolic NA sensors such as RIG-I and MDA5. Since TLR and RIG-I/MDA5 pathways have different threshold concentrations for activation by NA ligands, such flexibility in delivery would allow for dose-control over beneficial type I interferon (IFN) responses. For example, when a robust type I IFN response is wanted,

delivery into the endosomal TLR-rich compartment is the optimal solution. In contrast, when it is desired to activate a type I IFN by a higher concentration of NANPs, then delivery into cytosol is the most optimal route.

An alternative strategy is the use of dynamic hybrid DNA-RNA NANPs which can surpass recognition until they intracellularly re-associate with one another to release functional RNA interference inducers (Dicer Substrate (DS) RNAs) and double-stranded (ds) DNA byproducts (**Figure 2**)[39-40]. Longer dsDNA, however, can activate the cGAS-cGAMP-STING pathway and trigger the expression of inflammatory genes[40]. To avoid this, the designed dsDNA byproducts can be shortened and programmed to carry additional functions such as binding NF-κB and lowering the subsequent production of proinflammatory cytokines[19]. Tightly controlling NANP intracellular trafficking via the use of specific carriers or development of tools that emulate bacterial phagosome manipulation are essential next steps in the therapeutic application of NANPs.

1.3 Signature Motifs

Mirroring pathogenic strategies, NANPs can be designed to either avoid PRRs entirely by mimicking host NAs or to elicit specific signaling brought about by selective binding or inhibition[41-42]. While PRRs may have evolved to detect and disallow foreign NAs from entering the cell, the use of NANPs has the potential to take advantage of well-established and predictable NA processing. Using this strategy, an additional layer of programmability—tailored processing—can be embedded into NANP structures.

Vaccine adjuvants which serve to enhance the immune response against an antigen are an especially promising route for NANP technology. In addition to incorporating the most immunostimulatory design principles into a NANP, there are also motifs which can direct immune

stimulation. Unmethylated CpG oligodeoxynucleotides which are common in bacterial genomes are processed by TLR9[43]. Many nanoformulations have utilized CpG motifs to consistently induce strong immune responses[44]. For NANPs, sequence-specific activation can be incorporated directly as part of a multi-stranded assembly[21].

In order to evade detection and be seen as "self," pathogens can mimic host mRNA by protecting their own RNA with a 5' end cap. Since viral RNAs lack RNA cap modification, its absence is sensed by interferon-stimulated genes that regulate protein synthesis[45]. Utilizing these approaches, RNA strands in NANP assemblies can be modified with a 5' end cap if detection is not desirable. Besides alternative routes to obtain cap structures or use cap-independent translation, alphaviruses or filoviruses can use secondary structural motifs in the 5′ UTR to alter IFIT (interferon-induced proteins with tetratricopeptide repeats) binding and function[45]. Almost each virus is generating noncoding RNAs (ncRNAs) with diverse roles in the virus life cycle. These ncRNAs modulating immune responses in favor of viral infection have medical potential as targets for the development of novel antiviral therapeutics. Furthermore, RNA motifs or RNA modifications involved in subverting cellular immunity can enrich the field of NA nanotechnology. Embedding such motifs in NANPs would allow for designing assemblies with attenuated immunogenicity and enhanced stability for transfected or *in vivo* co-transcriptionally assembled nanoparticles.

Taking the programmability of NANPs into consideration at the very initial stages of design, the composition and dimensionality of NANPs have been shown to greatly dictate their processing and subsequent initiation of immune responses[22]. Globular NANPs have been shown to be more immunostimulatory than planar NANPs, which in turn are more immunostimulatory than fibrous NANP structures (**Figure 3A**). Within the same dimensions, the composition (RNA,

DNA, or an RNA/DNA hybrid) also influences the extent of immune response[22, 46]. NANPs made of DNA have been shown to be less immunostimulatory than the RNA counterparts[47] and thus can act as an immunoquiescent carrier for the delivery of therapeutic cargos. However, DNA NANPs can also be advantageous for strategic activation, as DNA constructs have been utilized to bind to TLR9 in the endosome, causing downstream production of type I IFNs for immune modulation[48-51]. With increasing numbers of RNAs in their composition, NANPs become more immunostimulatory[47]. RNA NANP interactions with endosomal TLRs 7 and 9[22] as well as with RLRs[29] induce the production of pro-inflammatory cytokines and type I IFNs downstream. Upon functionalization with DS RNAs, each NANP becomes relatively more immunostimulatory. However, the orientation of functional moieties has been shown to regulate the magnitude of stimulation[44, 52]. Additionally, despite the basic sequence of the NANP, the structural trends prevail, with reverse complement "anti" NANPs producing the same relative stimulation. In order to stimulate any immune response, NANPs must be taken up by cells utilizing a carrier and the greatest IFN production comes from pDCs (**Figure 3B**). Other trends in NANP design parameters have been investigated using QSAR modeling, during which a library of polygonal NANPs was designed based upon the minimal changes in their sequences, but varying between their composition, relative blood stability, melting temperature, molecular weight, GC content, K_d, and size[46]. Analyzing these descriptors in addition to their relative levels of immune stimulation allowed for correlations between physicochemical and immunostimulatory properties of NANPs, suggesting that molecular weight, melting temperature, and relative blood stability might be the most closely linked descriptors to immune response (**Figure 3C**).

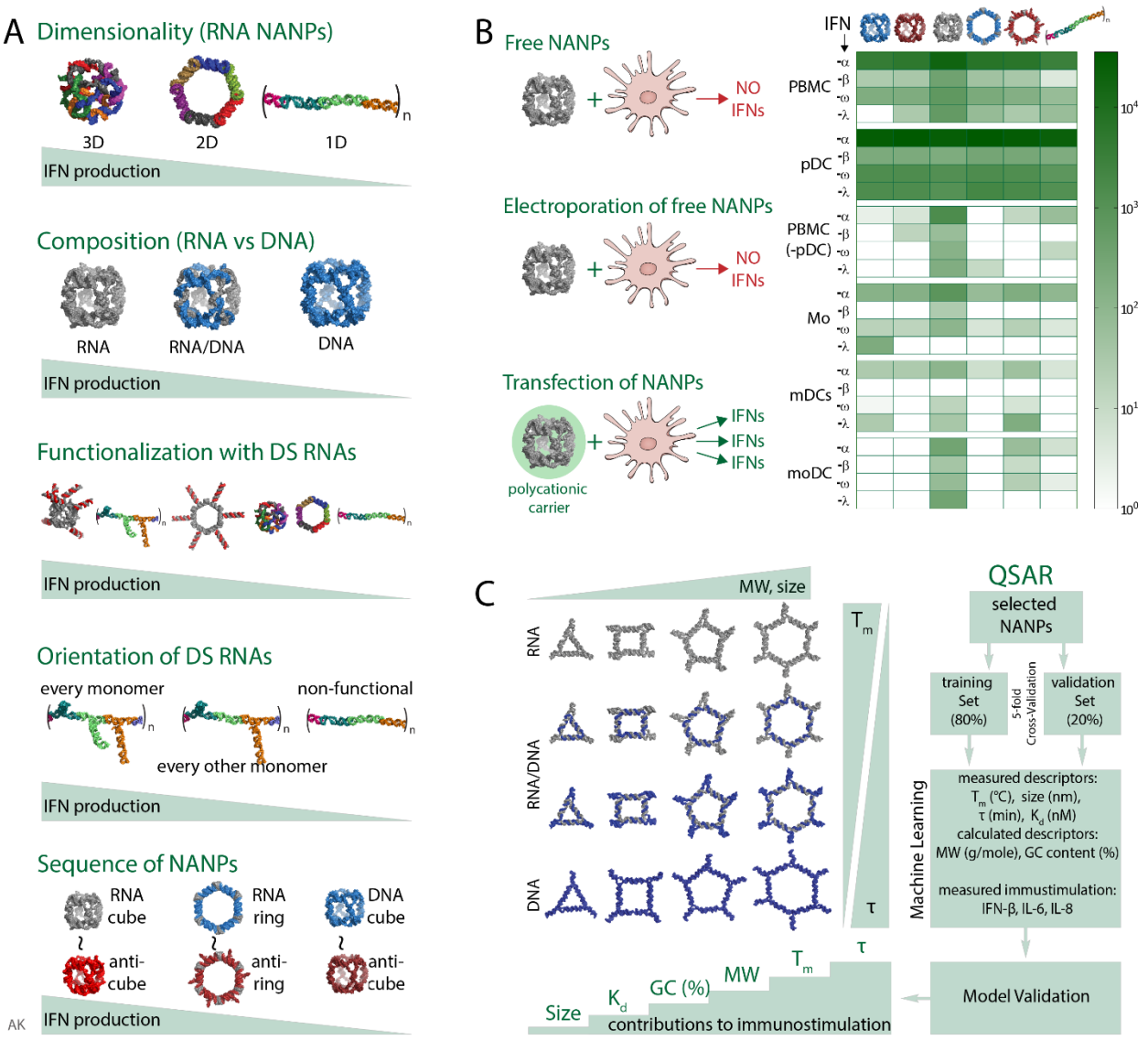

Figure 3. Trends in immune stimulation by NANPs. (A) The dimensionality, composition, functionalization, orientation, and sequence of NANPs have been evaluated relative to contributions to immunostimulation. Globular NANPs are more immunostimulatory than planar NANPs, which are in turn more immunostimulatory than fiborous. For composition, an increasing number of RNA strands in an assembly over DNA strands yields a greater subsequent immune response. Increased functionalization of NANPs with DS RNAs increases relative IFN production, while the orientation of DS RNAs within a single fibrous structure can decrease the effect. Finally, the sequences between variations of the structure have no effect on immune stimulation, while the structure itself is what dictates the response. (B) Neither free NANPs without a carrier nor electroporated free NANPs induce any IFN response. Instead, transfection using a polycationic carrier is necessary to trigger the IFN production. Across multiple immune cell types including PBMCs, plasmacytoid dendritic cells (pDCs), monocytes (Mo), myeloid dendritic cells (mDCs), and monocyte-derived dendritic cells (moDCs), pDCs show the greatest production of types I and III IFNs in response to various NANPs. (C) A library of RNA, RNA/DNA, and DNA NANP polygons composed of the same set of sequences but varying in

relative blood stability (τ), melting temperature (T_m), molecular weight (MW, g/mole), GC content, K_d (nM), and size (nm) revealed that those descriptors had the respective impact on NANP-induced immune stimulation.

1.4 Safety considerations and future directions

The immune stimulation by TNAs and NANPs has been a significant challenge to the transition of these biotechnologies into the clinical setting[53]. Since overwhelming immunostimulation may have deleterious consequences to the host, understanding the mechanisms by which NANPs activate the immune cells while monitoring the biomarkers of inflammation in the context of NANPs' physicochemical properties constitute a framework for responsible and safe use of these materials. Infusion reactions resulting from cytokine storms or complement activation-related pseudoallergies (CARPA) have adverse systemic effects which can surpass the efficacy of therapeutics and deprecate their biocompatibility. Therefore, recent studies have investigated patterns of immune recognition between different designing strategies of NANPs in order to more accurately predict their immune responses[22, 29, 46].

Preestablished and well-evolved immunorecognition pathways by bacterial and viral pathogens present a direct means for NANP recognition, but also offer a great advantage to the field of TNAs by offering a known road map around which therapeutic strategies can be planned. With this in mind, predictable immune activation can be incorporated into the design of NANPs which could be a boon for immunotherapy and the use of vaccine adjuvants in one direction, as well as for immunoquiescent drug delivery in another.

1.5 Future Directions and Theme

With individualized approaches to sequencing becoming more and more accessible, the future for personalized therapeutic approaches has great potential, especially when it comes to sequence-related ailments which can be directly targeted by sequence-composed therapeutics. Nucleic acid nanotechnology presents a unique opportunity for tailoring formulations directly to

clinically relevant applications where specific disease signatures can be addressed with the modularity and programmability of NANPs. As naturally occurring functional biomaterials, nucleic acids can interact directly with one another and with other classes of biomolecules such that nucleic acid-based constructs inspired by naturally occurring motifs can also be imbued with biological functions. The rational design of the sequences, composition, dimensionality, and incorporation of TNAs, chemical modifications, and drug delivery agents make this platform highly tailorable for interactions with specific cellular components. In particular, these dynamic systems can be designed to interact with PRRs of the innate immune system for control over the immunostimulation generated upon their introduction into the cellular environment.

Given this background, the following works aim to expand upon this general theme of dynamic NANP platforms. The NANPs and nucleic acid assemblies discussed herein are designed to present or conditionally release DS RNAs for gene knockdown via RNAi while their general immunostimulatory properties are explored in cell lines. This combination of functions aims to optimize the choice of NANPs which may be utilized for carrying out dynamic therapeutic activities in vitro and in vivo.

1.6 References

1. Jasinski, D.; Haque, F.; Binzel, D. W.; Guo, P., Advancement of the Emerging Field of RNA Nanotechnology. ACS Nano 2017, 11 (2), 1142-1164.
2. Afonin, K. A.; Kasprzak, W. K.; Bindewald, E.; Kireeva, M.; Viard, M.; Kashlev, M.; Shapiro, B. A., In silico design and enzymatic synthesis of functional RNA nanoparticles. Acc. Chem. Res. 2014, 47 (6), 1731-1741.
3. Osada, E.; Suzuki, Y.; Hidaka, K.; Ohno, H.; Sugiyama, H.; Endo, M.; Saito, H., Engineering RNA-protein complexes with different shapes for imaging and therapeutic applications. ACS Nano 2014, 8 (8), 8130-40.
4. Schwarz-Schilling, M.; Dupin, A.; Chizzolini, F.; Krishnan, S.; Mansy, S. S.; Simmel, F. C., Optimized Assembly of a Multifunctional RNA-Protein Nanostructure in a Cell-Free Gene Expression System. Nano letters 2018, 18 (4), 2650-2657.
5. Jepsen, M. D. E.; Sparvath, S. M.; Nielsen, T. B.; Langvad, A. H.; Grossi, G.; Gothelf, K. V.; Andersen, E. S., Development of a genetically encodable FRET system using fluorescent RNA aptamers. Nat Commun 2018, 9 (1), 18.

6. Shibata, T.; Fujita, Y.; Ohno, H.; Suzuki, Y.; Hayashi, K.; Komatsu, K. R.; Kawasaki, S.; Hidaka, K.; Yonehara, S.; Sugiyama, H.; Endo, M.; Saito, H., Protein-driven RNA nanostructured devices that function in vitro and control mammalian cell fate. Nat Commun 2017, 8 (1), 540.
7. Chandler, M.; Afonin, K. A., Smart-Responsive Nucleic Acid Nanoparticles (NANPs) with the Potential to Modulate Immune Behavior. Nanomaterials (Basel) 2019, 9 (4).
8. Bindewald, E.; Afonin, K. A.; Viard, M.; Zakrevsky, P.; Kim, T.; Shapiro, B. A., Multistrand Structure Prediction of Nucleic Acid Assemblies and Design of RNA Switches. Nano letters 2016, 16 (3), 1726-35.
9. Afonin, K. A.; Viard, M.; Kagiampakis, I.; Case, C. L.; Dobrovolskaia, M. A.; Hofmann, J.; Vrzak, A.; Kireeva, M.; Kasprzak, W. K.; KewalRamani, V. N.; Shapiro, B. A., Triggering of RNA Interference with RNA-RNA, RNA-DNA, and DNA-RNA Nanoparticles. ACS Nano 2015, 9 (1), 251-9.
10. Roers, A.; Hiller, B.; Hornung, V., Recognition of Endogenous Nucleic Acids by the Innate Immune System. Immunity 2016, 44 (4), 739-54.
11. Takeuchi, O.; Akira, S., Pattern recognition receptors and inflammation. Cell 2010, 140 (6), 805-20.
12. Pandey, S.; Kawai, T.; Akira, S., Microbial sensing by Toll-like receptors and intracellular nucleic acid sensors. Cold Spring Harb Perspect Biol 2014, 7 (1), a016246-a016246.
13. Patel, S., Danger-Associated Molecular Patterns (DAMPs): the Derivatives and Triggers of Inflammation. Current allergy and asthma reports 2018, 18 (11), 63.
14. Tan, X.; Sun, L.; Chen, J.; Chen, Z. J., Detection of Microbial Infections Through Innate Immune Sensing of Nucleic Acids. Annual review of microbiology 2018, 72, 447-478.
15. Luecke, S.; Paludan, S. R., Molecular requirements for sensing of intracellular microbial nucleic acids by the innate immune system. Cytokine 2017, 98, 4-14.
16. Broz, P.; Monack, D. M., Newly described pattern recognition receptors team up against intracellular pathogens. Nature reviews. Immunology 2013, 13 (8), 551-65.
17. Blasius, A. L.; Beutler, B., Intracellular toll-like receptors. Immunity 2010, 32 (3), 305-15.
18. Dobrovolskaia, M. A.; McNeil, S. E., Strategy for selecting nanotechnology carriers to overcome immunological and hematological toxicities challenging clinical translation of nucleic acid-based therapeutics. Expert Opinion on Drug Delivery 2015, 12 (7), 1163-1175.
19. Ke, W.; Hong, E.; Saito, R. F.; Rangel, M. C.; Wang, J.; Viard, M.; Richardson, M.; Khisamutdinov, E. F.; Panigaj, M.; Dokholyan, N. V.; Chammas, R.; Dobrovolskaia, M. A.; Afonin, K. A., RNA-DNA fibers and polygons with controlled immunorecognition activate RNAi, FRET and transcriptional regulation of NF-kappaB in human cells. Nucleic acids research 2018.
20. Bui, M. N.; Brittany Johnson, M.; Viard, M.; Satterwhite, E.; Martins, A. N.; Li, Z.; Marriott, I.; Afonin, K. A.; Khisamutdinov, E. F., Versatile RNA tetra-U helix linking motif as a toolkit for nucleic acid nanotechnology. Nanomedicine 2017, 13 (3), 1137-1146.
21. Khisamutdinov, E. F.; Li, H.; Jasinski, D. L.; Chen, J.; Fu, J.; Guo, P., Enhancing immunomodulation on innate immunity by shape transition among RNA triangle, square and pentagon nanovehicles. Nucleic acids research 2014, 42 (15), 9996-10004.

22. Hong, E.; Halman, J. R.; Shah, A. B.; Khisamutdinov, E. F.; Dobrovolskaia, M. A.; Afonin, K. A., Structure and Composition Define Immunorecognition of Nucleic Acid Nanoparticles. Nano Letters 2018, 18 (7), 4309-4321.
23. Eng, H. L.; Hsu, Y. Y.; Lin, T. M., Differences in TLR7/8 activation between monocytes and macrophages. Biochemical and biophysical research communications 2018, 497 (1), 319-325.
24. Ito, T.; Amakawa, R.; Kaisho, T.; Hemmi, H.; Tajima, K.; Uehira, K.; Ozaki, Y.; Tomizawa, H.; Akira, S.; Fukuhara, S., Interferon-alpha and interleukin-12 are induced differentially by Toll-like receptor 7 ligands in human blood dendritic cell subsets. The Journal of experimental medicine 2002, 195 (11), 1507-12.
25. Hornung, V.; Rothenfusser, S.; Britsch, S.; Krug, A.; Jahrsdorfer, B.; Giese, T.; Endres, S.; Hartmann, G., Quantitative expression of toll-like receptor 1-10 mRNA in cellular subsets of human peripheral blood mononuclear cells and sensitivity to CpG oligodeoxynucleotides. Journal of immunology (Baltimore, Md. : 1950) 2002, 168 (9), 4531-7.
26. Hornung, V.; Guenthner-Biller, M.; Bourquin, C.; Ablasser, A.; Schlee, M.; Uematsu, S.; Noronha, A.; Manoharan, M.; Akira, S.; de Fougerolles, A.; Endres, S.; Hartmann, G., Sequence-specific potent induction of IFN-alpha by short interfering RNA in plasmacytoid dendritic cells through TLR7. Nature medicine 2005, 11 (3), 263-70.
27. Judge, A. D.; Sood, V.; Shaw, J. R.; Fang, D.; McClintock, K.; MacLachlan, I., Sequence-dependent stimulation of the mammalian innate immune response by synthetic siRNA. Nature biotechnology 2005, 23 (4), 457-62.
28. Sioud, M., Induction of inflammatory cytokines and interferon responses by double-stranded and single-stranded siRNAs is sequence-dependent and requires endosomal localization. J Mol Biol 2005, 348 (5), 1079-90.
29. Hong, E.; Halman, J. R.; Shah, A.; Cedrone, E.; Truong, N.; Afonin, K. A.; Dobrovolskaia, M. A., Toll-Like Receptor-Mediated Recognition of Nucleic Acid Nanoparticles (NANPs) in Human Primary Blood Cells. Molecules 2019, 24 (6), 1094.
30. Peng, S.; Li, C.; Wang, X.; Liu, X.; Han, C.; Jin, T.; Liu, S.; Zhang, X.; Zhang, H.; He, X.; Xie, X.; Yu, X.; Wang, C.; Shan, L.; Fan, C.; Shan, Z.; Teng, W., Increased Toll-Like Receptors Activity and TLR Ligands in Patients with Autoimmune Thyroid Diseases. Front Immunol 2016, 7, 578-578.
31. Lee, B. L.; Barton, G. M., Trafficking of endosomal Toll-like receptors. Trends in cell biology 2014, 24 (6), 360-9.
32. Ewald, S. E.; Engel, A.; Lee, J.; Wang, M.; Bogyo, M.; Barton, G. M., Nucleic acid recognition by Toll-like receptors is coupled to stepwise processing by cathepsins and asparagine endopeptidase. The Journal of experimental medicine 2011, 208 (4), 643-51.
33. Lebreton, A.; Stavru, F.; Cossart, P., Organelle targeting during bacterial infection: insights from Listeria. Trends in cell biology 2015, 25 (6), 330-8.
34. Omotade, T. O.; Roy, C. R., Manipulation of Host Cell Organelles by Intracellular Pathogens. Microbiology spectrum 2019, 7 (2).
35. Shaughnessy, L. M.; Hoppe, A. D.; Christensen, K. A.; Swanson, J. A., Membrane perforations inhibit lysosome fusion by altering pH and calcium in Listeria monocytogenes vacuoles. Cell Microbiol 2006, 8 (5), 781-792.
36. Vergne, I.; Chua, J.; Lee, H. H.; Lucas, M.; Belisle, J.; Deretic, V., Mechanism of phagolysosome biogenesis block by viable Mycobacterium tuberculosis. Proceedings of

the National Academy of Sciences of the United States of America 2005, 102 (11), 4033-8.
37. Vergne, I.; Chua, J.; Deretic, V., Tuberculosis toxin blocking phagosome maturation inhibits a novel Ca2+/calmodulin-PI3K hVPS34 cascade. The Journal of experimental medicine 2003, 198 (4), 653-659.
38. Spano, S.; Gao, X.; Hannemann, S.; Lara-Tejero, M.; Galan, J. E., A Bacterial Pathogen Targets a Host Rab-Family GTPase Defense Pathway with a GAP. Cell Host Microbe 2016, 19 (2), 216-26.
39. Afonin, K. A.; Viard, M.; Martins, A. N.; Lockett, S. J.; Maciag, A. E.; Freed, E. O.; Heldman, E.; Jaeger, L.; Blumenthal, R.; Shapiro, B. A., Activation of different split functionalities on re-association of RNA-DNA hybrids. Nat Nanotechnol 2013, 8 (4), 296-304.
40. Afonin, K. A.; Desai, R.; Viard, M.; Kireeva, M. L.; Bindewald, E.; Case, C. L.; Maciag, A. E.; Kasprzak, W. K.; Kim, T.; Sappe, A.; Stepler, M.; KewalRamani, V. N.; Kashlev, M.; Blumenthal, R.; Shapiro, B. A., Co-transcriptional production of RNA–DNA hybrids for simultaneous release of multiple split functionalities. Nucleic Acids Research 2013, 42 (3), 2085-2097.
41. Ariza-Mateos, A.; Gómez, J., Viral tRNA Mimicry from a Biocommunicative Perspective. Front. Microbiol. 2017, 8.
42. Greenbaum, B. D.; Levine, A. J.; Bhanot, G.; Rabadan, R., Patterns of Evolution and Host Gene Mimicry in Influenza and Other RNA Viruses. PLOS Pathogens 2008, 4 (6), e1000079.
43. Lester, S. N.; Li, K., Toll-like receptors in antiviral innate immunity. J Mol Biol 2014, 426 (6), 1246-64.
44. Guo, S.; Li, H.; Ma, M.; Fu, J.; Dong, Y.; Guo, P., Size, Shape, and Sequence-Dependent Immunogenicity of RNA Nanoparticles. Mol Ther Nucleic Acids 2017, 9, 399-408.
45. Hyde, J. L.; Gardner, C. L.; Kimura, T.; White, J. P.; Liu, G.; Trobaugh, D. W.; Huang, C.; Tonelli, M.; Paessler, S.; Takeda, K.; Klimstra, W. B.; Amarasinghe, G. K.; Diamond, M. S., A viral RNA structural element alters host recognition of nonself RNA. Science (New York, N.Y.) 2014, 343 (6172), 783-787.
46. Johnson, M. B.; Halman, J. R.; Satterwhite, E.; Zakharov, A. V.; Bui, M. N.; Benkato, K.; Goldsworthy, V.; Kim, T.; Hong, E.; Dobrovolskaia, M. A.; Khisamutdinov, E. F.; Marriott, I.; Afonin, K. A., Programmable Nucleic Acid Based Polygons with Controlled Neuroimmunomodulatory Properties for Predictive QSAR Modeling. Small 2017, 13 (42), 1701255.
47. Halman, J. R.; Satterwhite, E.; Roark, B.; Chandler, M.; Viard, M.; Ivanina, A.; Bindewald, E.; Kasprzak, W. K.; Panigaj, M.; Bui, M. N.; Lu, J. S.; Miller, J.; Khisamutdinov, E. F.; Shapiro, B. A.; Dobrovolskaia, M. A.; Afonin, K. A., Functionally-interdependent shape-switching nanoparticles with controllable properties. Nucleic Acids Research 2017, 45 (4), 2210-2220.
48. Schmidt, N. W.; Jin, F.; Lande, R.; Curk, T.; Xian, W.; Lee, C.; Frasca, L.; Frenkel, D.; Dobnikar, J.; Gilliet, M.; Wong, G. C. L., Liquid-crystalline ordering of antimicrobial peptide–DNA complexes controls TLR9 activation. Nature Materials 2015, 14, 696.
49. Tursi, S. A.; Lee, E. Y.; Medeiros, N. J.; Lee, M. H.; Nicastro, L. K.; Buttaro, B.; Gallucci, S.; Wilson, R. P.; Wong, G. C. L.; Tükel, Ç., Bacterial amyloid curli acts as a

carrier for DNA to elicit an autoimmune response via TLR2 and TLR9. PLOS Pathogens 2017, 13 (4), e1006315-e1006315.

50. Lande, R.; Lee, E. Y.; Palazzo, R.; Marinari, B.; Pietraforte, I.; Santos, G. S.; Mattenberger, Y.; Spadaro, F.; Stefanantoni, K.; Iannace, N.; Dufour, A. M.; Falchi, M.; Bianco, M.; Botti, E.; Bianchi, L.; Alvarez, M.; Riccieri, V.; Truchetet, M.-E.; C.L. Wong, G.; Chizzolini, C.; Frasca, L., CXCL4 assembles DNA into liquid crystalline complexes to amplify TLR9-mediated interferon-α production in systemic sclerosis. Nature Communications 2019, 10 (1), 1731.
51. Lee, E. Y.; Zhang, C.; Di Domizio, J.; Jin, F.; Connell, W.; Hung, M.; Malkoff, N.; Veksler, V.; Gilliet, M.; Ren, P.; Wong, G. C. L., Helical antimicrobial peptides assemble into protofibril scaffolds that present ordered dsDNA to TLR9. Nature Communications 2019, 10 (1), 1012.
52. Rackley, L.; Stewart, J. M.; Salotti, J.; Krokhotin, A.; Shah, A.; Halman, J. R.; Juneja, R.; Smollett, J.; Lee, L.; Roark, K.; Viard, M.; Tarannum, M.; Vivero-Escoto, J.; Johnson, P. F.; Dobrovolskaia, M. A.; Dokholyan, N. V.; Franco, E.; Afonin, K. A., RNA Fibers as Optimized Nanoscaffolds for siRNA Coordination and Reduced Immunological Recognition. Advanced Functional Materials 2018, 28 (48), 1805959.
53. Dobrovolskaia, M. A.; McNeil, S. E., Immunological and hematological toxicities challenging clinical translation of nucleic acid-based therapeutics. Expert opinion on biological therapy 2015, 15 (7), 1023-48.

2 CHAPTER 2: BROCCOLI FLUORETS: SPLIT APTAMERS AS A USER-FRIENDLY FLUORESCENT TOOLKIT FOR DYNAMIC RNA NANOTECHNOLOGY

2.1 Introduction

DNA and RNA, which are best known for their roles in processing genetic information, are natural biopolymers that are also increasingly utilized in the design and construction of nucleic acid nanoparticles (NANPs)[1–4]. Predictable pairing between canonical Watson–Crick bases (A–U (or T) and G–C) in RNA and DNA as well as the possibility for additional non-canonical base pairs, generally characteristic of RNA[5], allow for the assembly of programmable and well-defined structures that can coordinate an array of functions[6]. Such functions can be demonstrated by the diverse roles of natural nucleic acids (mostly RNA) as exemplified by riboswitches, ribozymes, mRNAs, aptamers, and siRNAs that are capable of fine-tuning and orchestrating biological environments[6]. RNA nanotechnology aims to design functional NANPs based on RNA's ability to self-assemble, interact with other molecules, and exhibit fine-tunable physicochemical properties[2,7–9]. Rationally designed nucleic acids which are programmed to interact with other sequences, molecules, or in response to various stimuli have led to the development of molecular logic gates and biosensors[10–15]. The most recent achievements take advantage of these properties in constructing NANPs which are dynamic in structure and can independently[16,17] or interdependently[18,19] act in human cells, conditionally activating pre-programmed functionalities and triggering responses. Similar design principles can be applied to engineer diagnostic devices and smart therapeutics[20]. The rapid development of NANP-based dynamic platforms demands synchronized advancements in various robust visualization and tracking techniques that are user-friendly and biocompatible.

The responsive behaviors of NANPs can be directly visualized in living cells using complementary strands labeled with pairs of dyes that can undergo Förster resonance energy transfer (FRET). Tracing changes in FRET signals that result upon re-hybridization of labeled strands entering the compositions of cognate NANPs confirms the dynamicity of their behavior in real time[18,21,22]. The integrity of NANPs in cells can be verified through the co-localization of multiple different fluorophores simultaneously entering the composition of NANPs[23,24]. RNA probes also allow for a modular approach to visualization; fluorescent in situ hybridization, or FISH, and molecular beacons have been introduced to cells to give a fluorescent response upon binding to a target sequence[25–27]. However, for all aforementioned techniques, the fluorescent dyes must be covalently linked to either the 5'- or 3'-end of nucleic acids, which makes the techniques limited to only exogenously introduced NANPs.

For visualizing intracellular RNAs, the MS2-green fluorescent protein (GFP) system has been utilized to tag and image endogenous RNAs in cells[28]. However, this approach requires tagging RNAs with multiple copies of GFP systems in order to separate the desired signal from the background noise. This may affect the mobility of labeled RNAs and drastically alter their function. In turn, the split GFP system, in which two halves of the GFP are brought within binding proximity for restored fluorescence, has allowed for a conditionally activated fluorescence signal[18] and this approach can potentially be used to validate the formation of NANPs in cells[29,30]. The combination of several fluorescent proteins forming FRET pairs is another possible way for NANP visualizations[31]. However, all these systems require the presence of bulky tags and may be limited to the intracellular compartmentalization of NANPs.

The development of RNA aptamers which activate fluorophores upon binding has been a major improvement over these imaging techniques, offering a high signal-to-noise ratio,

modularity for simple sequence incorporation and tagging, and real-time protein-free imaging in cells[25]. Using systematic evolution of ligands by exponential enrichment, or SELEX, to select a unique RNA sequence which binds and activates a normally non-fluorescent dye, the malachite green (MG) aptamer was first developed[32]. Similar to split protein systems, splitting MG aptamers allowed for fluorescence detection of nucleic acids[33,34]. In nucleic acid nanotechnology, any fluorescent aptamers can act as functional units which can be easily embedded into the NANPs' structures by simple extension of individual strands. By doing this, NANPs' assembly verification[35], tracking NANPs' co-transcriptional assembly[7,35], and monitoring the dynamic behavior of interdependent RNA-DNA hybrids[22,36] have been successfully achieved. However, the high cytotoxicity of MG (a triphenylmethane dye) and its non-specific binding to cellular components warranted the further search for new biocompatible RNA aptamers which could be used at higher concentrations in cells[25]. Using SELEX, a Spinach aptamer was selected to bind a GFP fluorophore analog, the dye (Z)-4-(3,5-difluoro-4-hydroxybenzylidene)-1,2-dimethyl-1*H*-imidazol-5(4*H*)-one (DFHBI), and to exhibit green fluorescence when bound[37,38]. The Spinach aptamer was further optimized into Spinach2 for greater thermostability and brightness, yet still required a tRNA scaffold to promote folding and stability which made it susceptible to endonucleases and limited cellular activity[39,40]. A new aptamer with a three-way junction scaffold called F30-Broccoli was subsequently developed with a higher T_m and higher binding affinity for ligand DFHBI-1T, an optimized dye[25,40–42].

Fluorescent RNA aptamers such as Spinach, Broccoli, and Mango have been used to monitor a variety of metabolites and proteins in mammalian and bacterial cells[38,43–46]. To assess the actions of dynamic NANPs, these new aptamers were also split such that fluorescence is restored only upon the subsequent halves of the aptamer being brought into close proximity to

re-associate and bind to a dye. Split Spinach[47] and split Broccoli[18] have been developed as tools for assessing the conditional activation of fluorescence. Based on the studied G-quadruplex structure of the Spinach aptamer which is involved in binding DFHBI, the sequence of Spinach was shortened into Baby Spinach while exhibiting comparable fluorescence[48]. As the Broccoli aptamer is also expected to depend on a G-quadruplex for fluorescence activation, we set out to optimize the split F30-Broccoli aptamer experimentally in order to produce several conditionally activated splits, that here we call fluorets, without the complexities of solving for multiple cocrystal structures of Broccoli bound to DFHBI-1T[40,48]. We suggest several experimental schemes allowing for both conditional activation and deactivation of fluorescent responses using the split aptamers technology.

2.2 Results and Discussion

Rationally designed (as described in Methods) split F30-Broccoli (or original F30-Broccoli) aptamers were assembled in the presence of DFHBI-1T to assess their responses to an array of stimuli (**Figure 4A**) which would allow for their optimized utilization as tools in RNA nanotechnology. Potential folding and assembly of fluorets were assessed using NUPACK[49] (**Figure A1**) and from this library, eight different variations of the split F30-Broccoli aptamer were experimentally tested for assembly and fluorescence activation by non-denaturing polyacrylamide gel electrophoresis (native-PAGE) and fluorescence measurements. The results revealed that out of eight of the chosen fluorets, only five exhibited detectable fluorescence (**Figure 4B**). Because the fluorets have an additional starting sequence necessary for synthesis by in vitro transcription, their assemblies appear slightly higher on the gel when compared to the complete F30 aptamer. Fluorets D and E which appear to fluoresce the brightest in the presence of DFHBI-1T do not assemble; the Broc half of each fluoret fluoresces on its own, as the

G-quadruplex DFHBI-1T-binding structure is not affected by the location of the split (**Figure A2**). This suggests using the individual Broc strands of D and E as truncated versions of F30 Broccoli. Once the active fluorets were identified, we then tested various stimuli to conditionally activate or deactivate them (**Figure 4C**). We proposed several important stimuli such as the presence of enzymes (RNase, DNase, or T7 RNA polymerase), responses to changes in temperature, presence of divalent ions, and programmability via the addition of complementary strands. Developing molecular devices able to respond to these stimuli may potentially assist in studies of metabolic processes and the dynamic behavior of NANPs.

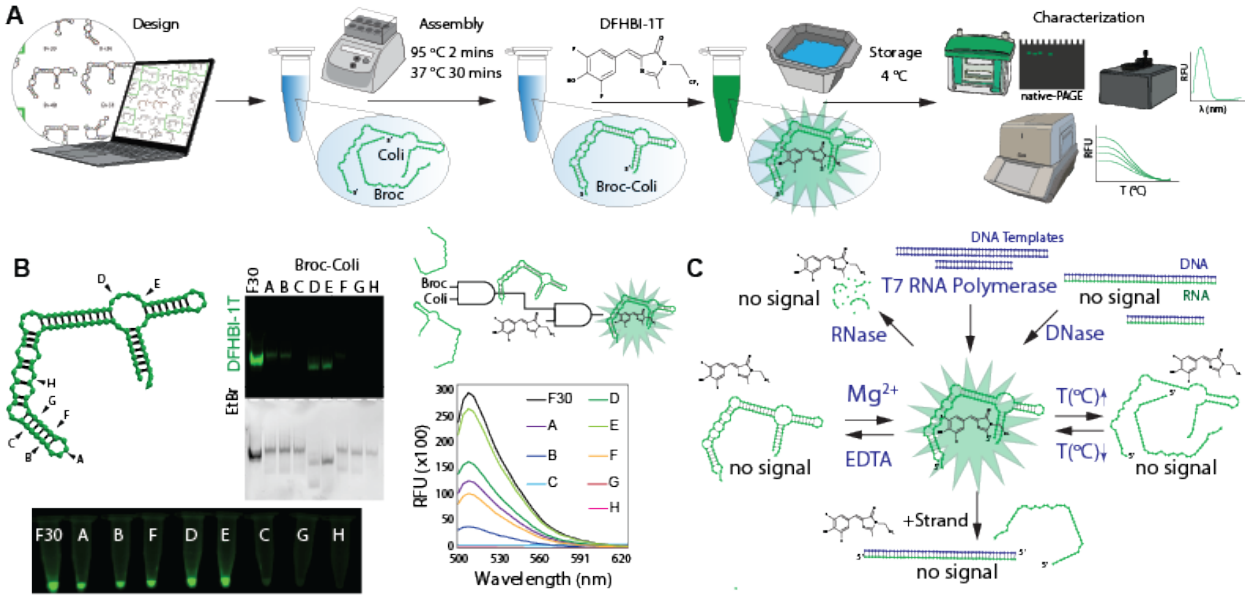

Figure 4. Computer-aided design, assembly, and characterization of fluorets. (A) Schematic representation of experimental pipeline with used experimental techniques indicated. (B) Positions of cuts (denoted A–H) chosen to be tested in this work and assessment of functionalities with native-PAGE and fluorimetry. Conditional activation of fluorescence is schematically demonstrated by AND gates. (C) Schematic representation of conditional activation and deactivation of fluorets tested in this work.

We first experimentally confirmed that fluorets can be assembled co-transcriptionally while activating DFHBI-1T fluorescence. We followed the protocols of previously established generalized in vitro methodology for the one-pot T7 RNA polymerase-driven co-transcriptional

assembly of different RNA NANPs[35], including those functionalized with up to ten siRNAs for co-RNAi[50]. In vitro run-off transcription performed with the mixture of DNA duplexes carrying T7 RNA polymerase promoters resulted in relatively high NANP assembly yields. In this work, using DNA templates of complementary fluorets in the presence of T7 RNA polymerase and transcription mix, complete fluoret RNAs were transcribed and assembled over 3.5 h, visualized by native-PAGE, and tracked in real-time using fluorescence (**Figure 5A**). The results suggest this system for further investigation with NANP production in cells. The ability to transcribe and assemble NANPs co-transcriptionally in mammalian cells is a promising avenue for their applications in vivo and assemblies with incorporated fluorets would allow for their simple visualization[35]. The use of mammalian cell lines for large-scale NANP production is expected to reduce endotoxin contamination and pave the way towards NANP-based personalized therapeutics. T7 RNA polymerase, which can be expressed in mammalian cells[51,52], would provide tight control over transcription regulation (cytoplasmic polymerase with unique 20 bps promoter), permits the use of shorter DNA templates, and offers faster transcription rates compared to RNA polymerase II.

It is beneficial to trace the activity and involvement of various enzymes in real time. As a proof of concept, we tested if the presence of different nucleases can conditionally drive either assembly or disassembly of fluorescent fluorets. Hybrid DNA/RNA duplexes for each fluoret monomer with an excess of DNA were incubated with DNase, resulting in the assembly of complete RNA fluorets which were then further deactivated by RNase (**Figure 5B**). The increased chemical stability of RNA/DNA hybrids[22] offers a way to keep fluorets dormant (thus, extending their shelf-life) until activation is desired.

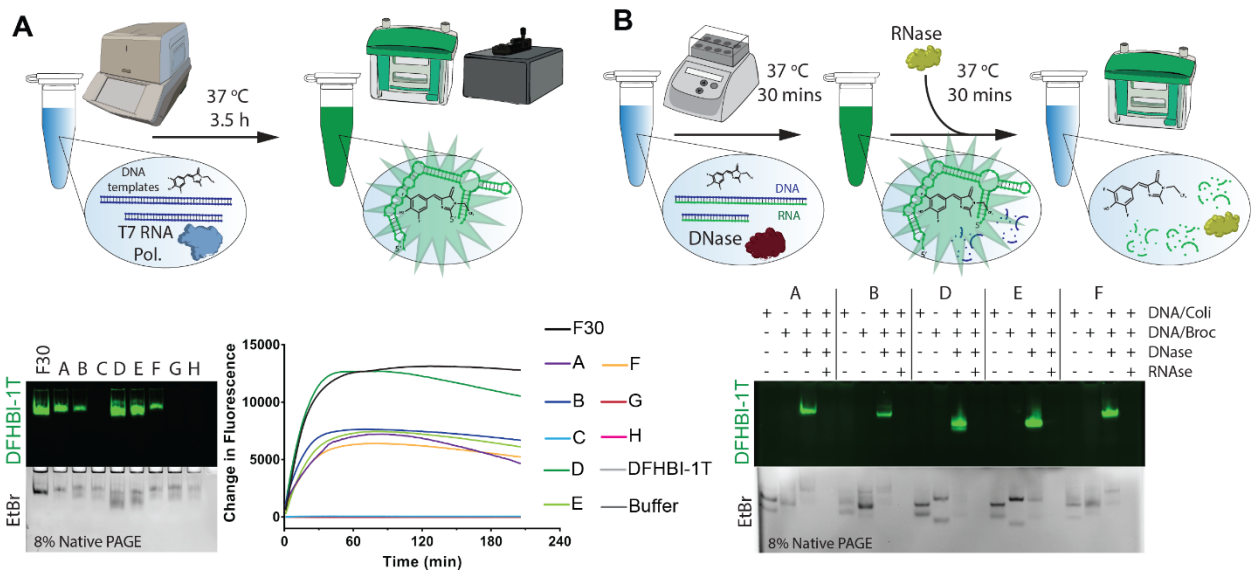

Figure 5. Enzyme-assisted activation and deactivation of fluorescent responses. (A) Co-transcriptional assembly of fluorets in the presence of DFHBI-1T. (B) DNase-assisted production of active fluorets from RNA/DNA duplexes, and their further deactivation with RNases.

The temperature-responsive behavior of fluorets may enable them to act as "molecular thermometers" in that their fluorescence can be turned "off" and "on" again upon reaching a specific melting temperature (**Figure 6A and Figure A3**). This responsiveness allows for a personalized selection of the splits to be incorporated into NANPs based on their T_ms and the temperature of the environment in which they will be functioning. The fluorets also demonstrate some minor variations in stability in human blood serum (**Figure 6B**), allowing them to act as "molecular clocks" for tracking in circulation during in vivo studies. The thermal and chemical stability of fluorets can be extended by potentially elongating their flanking helices or changes in Mg^{2+} concentrations. Oscillations between the activation and deactivation of the fluorescence can not only be controlled with temperature, but also upon the addition of a chelating agent such as ethylenediaminetetraacetic acid (EDTA) that removes the Mg^{2+} ions necessary for forming the tertiary structure of the aptamers required for binding and activating DFHBI-1T fluorescence.

Importantly, the functional structure can be restored upon the subsequent addition of Mg^{2+} and the oscillation can continue based on repeated additions (**Figure 6C**).

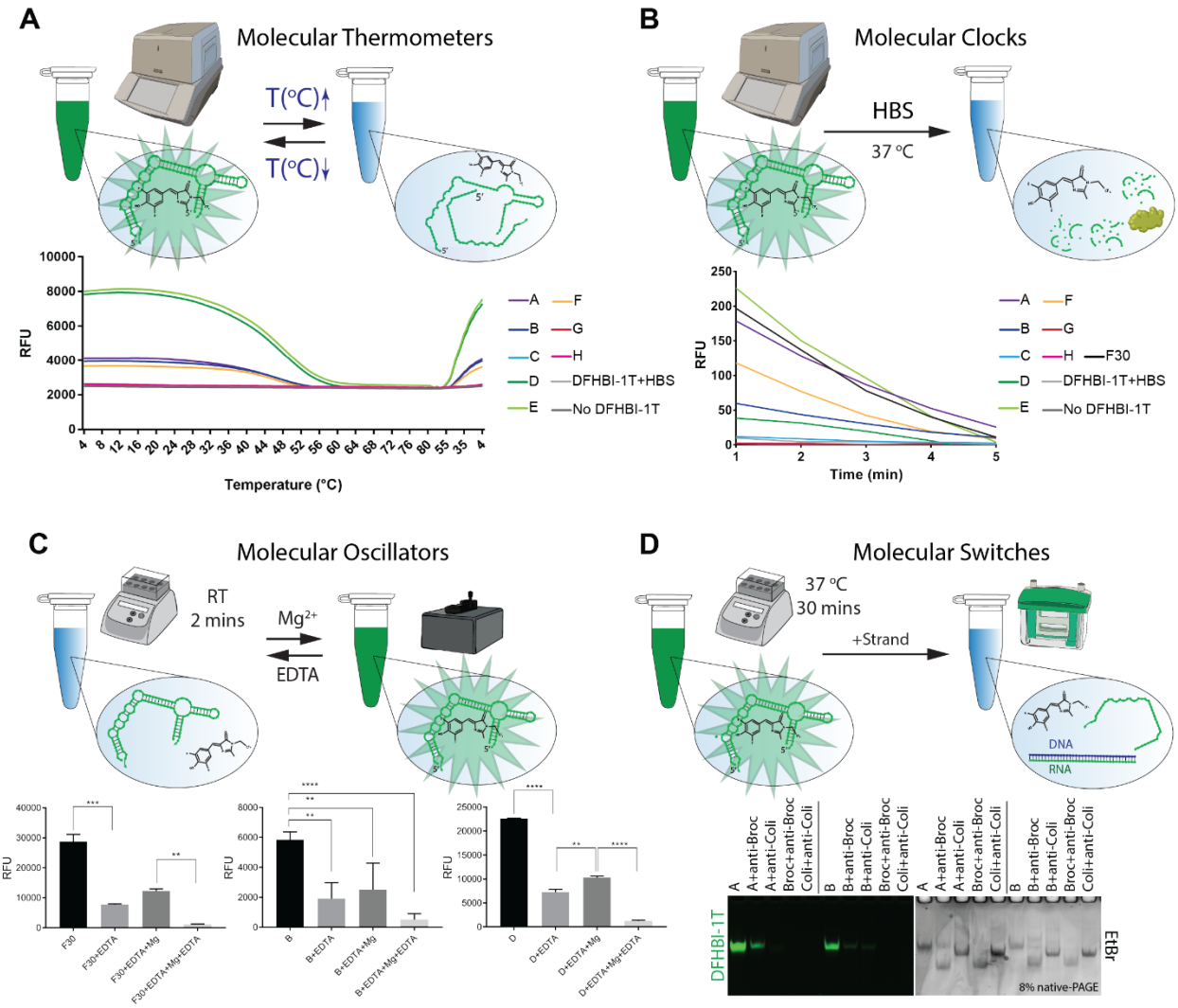

Figure 6. Molecular devices built with fluorets. (A) "Molecular Thermometer" that tracks the temperature changes via fluorescence activation and deactivation. (B) "Molecular Clock" that can trace the presence of sample in human blood serum via the fluorescence deactivation. (C) "Molecular Oscillators" working in response to the presence of magnesium ions. Statistical analysis was performed by one-way ANOVA (** $p < 0.01$, *** $p < 0.001$, **** $p = 0.0001$). (D) "Molecular Switches" responding to the introduction of oligonucleotides.

Logic gating and the development of programmable NANPs often utilize strand displacement for triggering dynamic interactions[53]. Likewise, the fluorets can act as "molecular switches" which are activated or de-activated by the addition of other oligonucleotides[54].

Complementary DNAs to the split Broc or Coli strands which contain programmable toeholds can be used to disassemble fluorets and can in turn be displaced by full complement strands for the re-assembly of the fluoret with restored fluorescence (**Figure 6D**). Single stranded fluorets D and E can be deactivated by adding the complementary strands. This isothermal strand displacement is thermodynamically driven and becomes possible due to the presence of unpaired nucleotides in the secondary structure of F30-Broccoli as well as T7 RNA polymerase starting sequences added to the 5′-ends of all fluorets. The deactivation of F30-Broccoli, however, requires at least five-fold excess of complementary strand (**Figure A5**). Fluorets as output strands in molecular circuits can be used to provide a fluorescent response only when both are produced. While current applications for logic gating remain in vitro, future work will characterize the brightness of fluorets in various cell lines separately and when incorporated into dynamic NANP assemblies[55] for their transition to in vivo work.

2.3 Materials and Methods

2.3.1 Design of Broccoli Fluorets

Starting with the original split F30-Broccoli aptamer[18] with a cut after U45 separating Broc (45 nts) from Coli (72 nts), the fluorets were designed by simply moving the location of the split downstream 3 bases or upstream 3 bases. The +/− number indicates how many bases away from the original split site the new cut was made (*e.g.*, B + 6 is 51 nts long, Coli − 6 is 66 nts long). The final group of eight fluorets was chosen via the analysis of NUPACK[49] predicted secondary structures (**Figure A1**), looking for either the greatest similarity to the original F30-Broccoli aptamer or for structures which addressed the importance of various functional regions in the aptamer sequence. With the original split[18] labeled as A, splits B, C, F, G and H were selected to be within close proximity in order to elucidate the relationship between the structure

of the hairpin containing the original split and DFHBI-1T binding. Splits D and E were chosen to test the truncated versions of the F30-Broccoli scaffold.

2.3.2 RNA Preparation

DNA strands were purchased from Integrated DNA Technologies (Coralville, IA, USA) (Sequences available in Supporting Information) and PCR-amplified using MyTaq™ Mix from Bioline (London, UK). PCR products containing T7 RNA polymerase promoters were purified using the DNA Clean and Concentrator™ kit from Zymo Research (Irvine, CA, USA). RNAs were produced by in vitro run-off transcription with T7 RNA polymerase (80 mM HEPES-KOH (pH 7.5), 2.5 mM spermidine, 50 mM DTT, 25 mM $MgCl_2$, 5 mM each rNTP). After 3.5 h at 37 °C, the reaction was incubated with RQ1 RNase-free DNase (New England BioLabs, Ipswich, MA, USA) prior to purification using denaturing 8 M urea polyacrylamide gel electrophoresis (PAGE, 15%). RNA bands were visualized under UV (short wavelength), cut, and eluted in crush and soak buffer (300 mM NaCl, 89 mM tris-borate (pH 8.2), 2 mM EDTA) overnight. Precipitation of the RNA was done in 2.5 volumes of 100% ethanol for 3 h at −20 °C. Samples were rinsed with 90% ethanol, vacuum dried, and dissolved in double-deionized water (17.8 MΩ·cm).

2.3.3 Broccoli Aptamer and Fluoret Assembly

F30-Broccoli RNA or Broc and Coli RNA strands composed of unmodified nucleotides were mixed in an equimolar ratio in double-deionized water. The samples were heated to 95 °C for 2 min, snap-cooled to 4 °C for 2 min, and assembly buffer (89 mM tris-borate (pH 8.2), 2 mM $MgCl_2$, 50 mM KCl) was added, followed by 30 min of incubation at 37 °C.

2.3.4 Co-Transcriptional Assembly

PCR-amplified DNA templates for complementary splits were added 1:1 as 20% final volume with T7 RNA polymerase (80 mM HEPES-KOH (pH 7.5), 2.5 mM spermidine, 50 mM DTT, 25 mM $MgCl_2$, 5 mM each rNTP) and 10 μM DFHBI-1T in buffer. Samples in triplicate were placed at 37 °C on a Bio-Rad CFX96 Touch Real-Time PCR Detection System (Bio-Rad, Hercules, CA, USA) for 3.5 h. Fluorescence was measured every minute, using 10 μM DFHBI-1T in buffer and transcription reactions at the above concentrations but without pDNA as negative controls.

2.3.5 Electrophoretic Mobility Shift Assays

For analysis, 8% non-denaturing native-PAGE (37.5:1) was used in the presence of 89 mM tris-borate (pH 8.2) and 2 mM $MgCl_2$. Native-PAGE gels were run for 20 min (Mini-PROTEAN® Tetra system by Bio-Rad, Hercules, CA, USA) at 4 °C and 300 V. Prior to staining, gels were washed 3 × 5 min in water and stained for 15 min in 10 μM DFHBI-1T in buffer (50 mM HEPES (pH 7.4), 100 mM KCl, 1 mM $MgCl_2$) as previously reported[40]. Gels were imaged using a ChemiDoc MP system (Bio-Rad) for Alexa488. Afterwards, gels were washed again with water and stained for 10 min with ethidium bromide for total visualization.

2.3.6 EDTA Degradation and Mg^{2+} Formation

Fluorets were assembled as normal at a concentration of 4 μM with 10 μM DFHBI-1T in buffer and measured using a NanoDrop 3300 (Thermo Scientific, Waltham, MA, USA). An amount of 1 μL of 10 mM EDTA was added to the sample, which was incubated at room temperature for 2 min before measuring again with a NanoDrop 3300. This was repeated using 1 μL of 10 mM Mg^{2+} and incubating for 2 min at room temperature and again using 10 mM EDTA.

2.3.7 Nuclease-Driven Assembly/Degradation

Split Broc RNA strands were assembled with Coli DNA strands (and vice-versa) by mixing in an equimolar ratio in double-deionized water. The samples were heated to 95 °C for 2 min, snap-cooled to 4 °C for 2 min, and assembly buffer (89 mM tris-borate (pH 8.2), 2 mM $MgCl_2$, 50 mM KCl) was added, followed by 20 min of incubation at room temperature. Each hybrid split was then added with its opposite hybrid split (*e.g.,* dBroc + rColi was added with rBroc + dColi) in an equimolar ratio at a final concentration of 1 μM with 2/15 volume of RQ1 RNase-free DNase (New England BioLabs). This was incubated at 37 °C for 30 min, then 2/5 of the volume were added to RNase ONE™ (Promega, Madison, WI, USA) at a volume equal to the RQ1 RNase-free DNase added previously. This was incubated at 37 °C for 30 min. Samples were visualized on an 8% non-denaturing native-PAGE (37.5:1) in the presence of 89 mM tris-borate (pH 8.2) and 2 mM $MgCl_2$ run for 20 min at 4 °C and 300 V.

2.3.8 Strand Displacement

Fluorets were assembled as previously described and then added in an equimolar ratio with either DNA for Broc or DNA for Coli prior to incubation at 37 °C for 30 min. RNA fluoret monomers were also assembled with their complementary DNAs as controls by mixing in an equimolar ratio in double-deionized water, heating to 95 °C for 2 min, snap-cooling to 4 °C for 2 min, and adding assembly buffer (89 mM tris-borate (pH 8.2), 2 mM $MgCl_2$, 50 mM KCl) followed by 20 min of incubation at room temperature.

2.3.9 Thermal Deactivation/Activation

Aptamers were assembled as previously described. For in vitro staining with DFHBI-1T, assemblies were mixed in a 1:1 volumetric ratio with 20 μM DFHBI-1T in buffer (100 mM HEPES (pH 7.4), 200 mM KCl, 2 mM $MgCl_2$) and incubated for 30 min at 37 °C. Assemblies at

a final concentration of 1.25 μM underwent a 4 °C to 80 °C thermal gradient with a step size of 0.5 °C per 5 s using a Bio-Rad CFX96 Touch Real-Time PCR Detection System. For the reactivation of fluorets, assemblies were programmed to undergo cooling from 80 °C to 4 °C with a step size of 2 °C per 45 s. Fluorescence of thermal deactivation was measured in triplicate for all fluorets using 10 μM DFHBI-1T in buffer and F30-Broccoli without DFHBI-1T (1.25 μM) as negative controls. Analysis of $T_m \pm$ SEM was done in GraphPad Prism Software (Version 7, GraphPad Software, San Diego, CA, USA) with a Boltzmann sigmoidal curve fit.

2.3.10 Blood Stability

Aptamers were assembled as previously described, mixed in a 1:1 volumetric ratio with 20 μM DFHBI-1T in buffer, and incubated for 30 min at 37 °C. An amount of 9 μL of assembled aptamer at a final concentration of 1.25 μM was added with 1 μL of 20% HBS and placed at 37 °C on a Bio-Rad CFX96 Touch Real-Time PCR Detection System. Fluorescence was measured every min, using 2% HBS with 10 μM DFHBI-1T in buffer and 1.25 μM of F30-Broccoli with 2% HBS without DFHBI-1T as negative controls. Analysis of $t_{1/2}$ was done in GraphPad Prism Software with a linear fit.

2.3.11 Statistics

Statistical analysis was done by one-way analysis of variance (ANOVA) using GraphPad Prism Software. All column means were compared by Tukey's multiple comparison test. A p-value of less than 0.05 was considered to be statistically significant.

2.4 Conclusions

In conclusion, the experimental design reported in this work is anticipated to lead the development of several robust strategies allowing for real-time fluorescence-assisted tracking of various processes at the nanoscale level. The reported system is made of biocompatible materials

that can be used for a broad range of biological and nanotechnological applications both in vitro and potentially in vivo. The developed experimental schemes are expected to help address some fundamental questions such as co-transcriptional folding of RNAs, formation of multi-stranded RNA NANPs, and their responses to various stimuli. Such complex behaviors will definitely promote fields such as synthetic biology or applications such as the stimulation of differentiating cells during basic research and tissue engineering. Although only eight different variations in the split aptamer were tested, optimized fluorescence of the split was demonstrated and shown to be responsive to various stimuli.

2.5 References

1. Shukla, G.C., Haque, F., Tor, Y., Wilhelmsson, L.M., Toulme, J.J., Isambert, H., Guo, P., Rossi, J.J., Tenenbaum, S.A. and Shapiro, B.A. (2011) A Boost for the Emerging Field of RNA Nanotechnology. *ACS nano*, **5**, 3405-3418.
2. Afonin, K.A., Kasprzak, W.K., Bindewald, E., Kireeva, M., Viard, M., Kashlev, M. and Shapiro, B.A. (2014) In silico design and enzymatic synthesis of functional RNA nanoparticles. *Acc. Chem. Res.*, **47**, 1731-1741.
3. Pinheiro, A.V., Han, D., Shih, W.M. and Yan, H. (2011) Challenges and opportunities for structural DNA nanotechnology. *Nat Nanotechnol*, **6**, 763-772.
4. Hong, E., Halman, J.R., Shah, A.B., Khisamutdinov, E.F., Dobrovolskaia, M.A. and Afonin, K.A. (2018) Structure and Composition Define Immunorecognition of Nucleic Acid Nanoparticles. *Nano letters*, **18**, 4309-4321.
5. Leontis, N.B., Stombaugh, J. and Westhof, E. (2002) The non-Watson-Crick base pairs and their associated isostericity matrices. *Nucleic Acids Res*, **30**, 3497-3531.
6. Jasinski, D., Haque, F., Binzel, D.W. and Guo, P. (2017) Advancement of the Emerging Field of RNA Nanotechnology. *ACS nano*, **11**, 1142-1164.
7. Afonin, K.A., Viard, M., Koyfman, A.Y., Martins, A.N., Kasprzak, W.K., Panigaj, M., Desai, R., Santhanam, A., Grabow, W.W., Jaeger, L. *et al.* (2014) Multifunctional RNA nanoparticles. *Nano letters*, **14**, 5662-5671.
8. Shibata, T., Fujita, Y., Ohno, H., Suzuki, Y., Hayashi, K., Komatsu, K.R., Kawasaki, S., Hidaka, K., Yonehara, S., Sugiyama, H. *et al.* (2017) Protein-driven RNA nanostructured devices that function in vitro and control mammalian cell fate. *Nat Commun*, **8**, 540.
9. Li, H., Lee, T., Dziubla, T., Pi, F., Guo, S., Xu, J., Li, C., Haque, F., Liang, X.J. and Guo, P. (2015) RNA as a stable polymer to build controllable and defined nanostructures for material and biomedical applications. *Nano today*, **10**, 631-655.
10. Xie, Z., Liu, S.J., Bleris, L. and Benenson, Y. (2010) Logic integration of mRNA signals by an RNAi-based molecular computer. *Nucleic Acids Research*, **38**, 2692-2701.

11. Xie, Z., Wroblewska, L., Prochazka, L., Weiss, R. and Benenson, Y. (2011) Multi-Input RNAi-Based Logic Circuit for Identification of Specific Cancer Cells. *Science*, **333**, 1307.
12. Rinaudo, K., Bleris, L., Maddamsetti, R., Subramanian, S., Weiss, R. and Benenson, Y. (2007) A universal RNAi-based logic evaluator that operates in mammalian cells. *Nature Biotechnology*, **25**, 795.
13. Penchovsky, R. and Breaker, R.R. (2005) Computational design and experimental validation of oligonucleotide-sensing allosteric ribozymes. *Nat Biotechnol*, **23**, 1424-1433.
14. Soukup, G.A. and Breaker, R.R. (1999) Nucleic acid molecular switches. *Trends in Biotechnology*, **17**, 469-476.
15. Roark, B.K., Tan, L.A., Ivanina, A., Chandler, M., Castaneda, J., Kim, H.S., Jawahar, S., Viard, M., Talic, S., Wustholz, K.L. *et al.* (2016) Fluorescence blinking as an output signal for biosensing. *ACS sensors*, **1**, 1295-1300.
16. Zakrevsky, P., Parlea, L., Viard, M., Bindewald, E., Afonin, K.A. and Shapiro, B.A. (2017) Preparation of a Conditional RNA Switch. *Methods Mol Biol*, **1632**, 303-324.
17. Bindewald, E., Afonin, K.A., Viard, M., Zakrevsky, P., Kim, T. and Shapiro, B.A. (2016) Multistrand Structure Prediction of Nucleic Acid Assemblies and Design of RNA Switches. *Nano letters*, **16**, 1726-1735.
18. Halman, J.R., Satterwhite, E., Roark, B., Chandler, M., Viard, M., Ivanina, A., Bindewald, E., Kasprzak, W.K., Panigaj, M., Bui, M.N. *et al.* (2017) Functionally-interdependent shape-switching nanoparticles with controllable properties. *Nucleic Acids Res*, **45**, 2210-2220.
19. Chandler, M., Ke, W., Halman, J., Panigaj, M. and Afonin, K.A. (2018) Reconfigurable nucleic acid materials for cancer therapy. *In: Gonçalves G., Tobias G. (eds) Nanooncology. Nanomedicine and Nanotoxicology. Springer, Cham, Chapter 11:* , 365-385.
20. Douglas, S.M., Bachelet, I. and Church, G.M. (2012) A logic-gated nanorobot for targeted transport of molecular payloads. *Science (New York, N.Y.)*, **335**, 831-834.
21. Afonin, K.A., Viard, M., Kagiampakis, I., Case, C.L., Dobrovolskaia, M.A., Hofmann, J., Vrzak, A., Kireeva, M., Kasprzak, W.K., KewalRamani, V.N. *et al.* (2015) Triggering of RNA Interference with RNA-RNA, RNA-DNA, and DNA-RNA Nanoparticles. *ACS nano*, **9**, 251-259.
22. Afonin, K.A., Viard, M., Martins, A.N., Lockett, S.J., Maciag, A.E., Freed, E.O., Heldman, E., Jaeger, L., Blumenthal, R. and Shapiro, B.A. (2013) Activation of different split functionalities upon re-association of RNA-DNA hybrids. *Nature nanotechnology*, **8**, 296-304.
23. Sajja, S., Chandler, M., Fedorov, D., Kasprzak, W.K., Lushnikov, A., Viard, M., Shah, A., Dang, D., Dahl, J., Worku, B. *et al.* (2018) Dynamic Behavior of RNA Nanoparticles Analyzed by AFM on a Mica/Air Interface. *Langmuir*.
24. Rackley, L., Stewart, J.M., Salotti, J., Krokhotin, A., Shah, A., Halman, J., Juneja, R., Smollett, J., Roark, B., Viard, M. *et al.* (2018) RNA Fibers as Optimized Nanoscaffolds for siRNA Coordination and Reduced Immunological Recognition. *Adv Funct Mater*.
25. Ouellet, J. (2016) RNA Fluorescence with Light-Up Aptamers. *Frontiers in Chemistry*, **4**.
26. Marras, S.A., Kramer, F.R. and Tyagi, S. (1999) Multiplex detection of single-nucleotide variations using molecular beacons. *Genet Anal*, **14**, 151-156.

27. Feng, S., Shang, Y., Wu, F., Ding, F., Li, B., Xu, J., Xu, L. and Zhou, X. (2014) DNA nanomachines as evolved molecular beacons for in vitro and in vivo detection. *Talanta*, **120**, 141-147.
28. Bertrand, E., Chartrand, P., Schaefer, M., Shenoy, S.M., Singer, R.H. and Long, R.M. (1998) Localization of ASH1 mRNA particles in living yeast. *Mol Cell*, **2**, 437-445.
29. Valencia-Burton, M., McCullough, R.M., Cantor, C.R. and Broude, N.E. (2007) RNA visualization in live bacterial cells using fluorescent protein complementation. *Nat Methods*, **4**, 421-427.
30. Demidov, V.V., Dokholyan, N.V., Witte-Hoffmann, C., Chalasani, P., Yiu, H.-W., Ding, F., Yu, Y., Cantor, C.R. and Broude, N.E. (2006) Fast complementation of split fluorescent protein triggered by DNA hybridization. *Proceedings of the National Academy of Sciences*, **103**, 2052-2056.
31. Schwarz-Schilling, M., Dupin, A., Chizzolini, F., Krishnan, S., Mansy, S.S. and Simmel, F.C. (2018) Optimized Assembly of a Multifunctional RNA-Protein Nanostructure in a Cell-Free Gene Expression System. *Nano letters*, **18**, 2650-2657.
32. Grate, D. and Wilson, C. (1999) Laser-mediated, site-specific inactivation of RNA transcripts. *Proceedings of the National Academy of Sciences of the United States of America*, **96**, 6131-6136.
33. Stojanovic, M.N. and Kolpashchikov, D.M. (2004) Modular aptameric sensors. *Journal of the American Chemical Society*, **126**, 9266-9270.
34. Kolpashchikov, D.M. (2005) Binary malachite green aptamer for fluorescent detection of nucleic acids. *Journal of the American Chemical Society*, **127**, 12442-12443.
35. Afonin, K.A., Bindewald, E., Yaghoubian, A.J., Voss, N., Jacovetty, E., Shapiro, B.A. and Jaeger, L. (2010) In vitro assembly of cubic RNA-based scaffolds designed in silico. *Nature Nanotechnology*, **5**, 676-682.
36. Afonin, K.A., Desai, R., Viard, M., Kireeva, M.L., Bindewald, E., Case, C.L., Maciag, A.E., Kasprzak, W.K., Kim, T., Sappe, A. *et al.* (2014) Co-transcriptional production of RNA-DNA hybrids for simultaneous release of multiple split functionalities. *Nucleic Acids Research*, **42**, 2085-2097.
37. Paige, J.S., Wu, K.Y. and Jaffrey, S.R. (2011) RNA mimics of green fluorescent protein. *Science (New York, N.Y.)*, **333**, 642-646.
38. Paige, J.S., Nguyen-Duc, T., Song, W. and Jaffrey, S.R. (2012) Fluorescence imaging of cellular metabolites with RNA. *Science*, **335**, 1194.
39. Strack, R.L., Disney, M.D. and Jaffrey, S.R. (2013) A superfolding Spinach2 reveals the dynamic nature of trinucleotide repeat–containing RNA. *Nature Methods*, **10**, 1219.
40. Filonov, G.S., Kam, C.W., Song, W. and Jaffrey, S.R. (2015) In-gel imaging of RNA processing using broccoli reveals optimal aptamer expression strategies. *Chem. Biol.*, **22**, 649-660.
41. Filonov Grigory, S. and Jaffrey Samie, R. (2016) RNA Imaging with Dimeric Broccoli in Live Bacterial and Mammalian Cells. *Current Protocols in Chemical Biology*, **8**, 1-28.
42. Filonov, G.S., Moon, J.D., Svensen, N. and Jaffrey, S.R. (2014) Broccoli: rapid selection of an RNA mimic of green fluorescent protein by fluorescence-based selection and directed evolution. *Journal of the American Chemical Society*, **136**, 16299-16308.
43. Svensen, N. and Jaffrey, S.R. (2016) Fluorescent RNA aptamers as a tool to study RNA-modifying enzymes. *Cell chemical biology*, **23**, 415-425.

44. Autour, A., C. Y. Jeng, S., D. Cawte, A., Abdolahzadeh, A., Galli, A., Panchapakesan, S.S.S., Rueda, D., Ryckelynck, M. and Unrau, P.J. (2018) Fluorogenic RNA Mango aptamers for imaging small non-coding RNAs in mammalian cells. *Nature Communications*, **9**, 656.
45. Jepsen, M.D.E., Sparvath, S.M., Nielsen, T.B., Langvad, A.H., Grossi, G., Gothelf, K.V. and Andersen, E.S. (2018) Development of a genetically encodable FRET system using fluorescent RNA aptamers. *Nat Commun*, **9**, 18.
46. Song, W., Filonov, G.S., Kim, H., Hirsch, M., Li, X., Moon, J.D. and Jaffrey, S.R. (2017) Imaging RNA polymerase III transcription using a photostable RNA–fluorophore complex. *Nature chemical biology*, **13**, 1187.
47. Rogers, T.A., Andrews, G.E., Jaeger, L. and Grabow, W.W. (2015) Fluorescent monitoring of RNA assembly and processing using the split-spinach aptamer. *ACS synthetic biology*, **4**, 162-166.
48. Warner, K.D., Chen, M.C., Song, W., Strack, R.L., Thorn, A., Jaffrey, S.R. and Ferre-D'Amare, A.R. (2014) Structural basis for activity of highly efficient RNA mimics of green fluorescent protein. *Nature structural & molecular biology*, **21**, 658-663.
49. Zadeh, J.N., Steenberg, C.D., Bois, J.S., Wolfe, B.R., Pierce, M.B., Khan, A.R., Dirks, R.M. and Pierce, N.A. (2011) NUPACK: Analysis and design of nucleic acid systems. *J Comput Chem*, **32**, 170-173.
50. Afonin, K.A., Kireeva, M., Grabow, W.W., Kashlev, M., Jaeger, L. and Shapiro, B.A. (2012) Co-transcriptional assembly of chemically modified RNA nanoparticles functionalized with siRNAs. *Nano letters*, **12**, 5192-5195.
51. Britton, P., Green, P., Kottier, S., Mawditt, K.L., Penzes, Z., Cavanagh, D. and Skinner, M.A. (1996) Expression of bacteriophage T7 RNA polymerase in avian and mammalian cells by a recombinant fowlpox virus. *The Journal of general virology*, **77 (Pt 5)**, 963-967.
52. Elroy-Stein, O. and Moss, B. (1990) Cytoplasmic expression system based on constitutive synthesis of bacteriophage T7 RNA polymerase in mammalian cells. *Proceedings of the National Academy of Sciences of the United States of America*, **87**, 6743-6747.
53. Goldsworthy, V., LaForce, G., Abels, S. and Khisamutdinov, E. (2018) Fluorogenic RNA Aptamers: A Nano-platform for Fabrication of Simple and Combinatorial Logic Gates. *Nanomaterials*, **8**, 984.
54. Lloyd, J., Tran, C.H., Wadhwani, K., Cuba Samaniego, C., Subramanian, H.K.K. and Franco, E. (2018) Dynamic Control of Aptamer-Ligand Activity Using Strand Displacement Reactions. *ACS synthetic biology*, **7**, 30-37.
55. Ke, W.; Hong, E.; Saito, R.F.; Rangel, M.C.; Wang, J.; Viard, M.; Richardson, M.; Khisamutdinov, E.F.; Panigaj, M.; Dokholyan, N.V.; et al. RNA-DNA fibers and polygons with controlled immunorecognition activate RNAi, FRET, and transcriptional regulation of NF-Kb in human cells. *Nucleic Acids Res.* **2018.**

2.6 Appendices: Supporting Information for Split Aptamers as a User-Friendly Fluorescent Toolkit for Dynamic RNA Nanotechnology

2.6.1 Sequences Designed in this Project

Sequences which were tested experimentally, listed 5’ to 3’:

F30 Broccoli:

GGGAAAGUUGCCAUGUGUAUGUGGGAGACGGUCGGGUCCAGAUAUUCGUAUCUG

UCGAGUAGAGUGUGGGCUCCCACAUACUCUGAUGAUCCUUCGGGAUCAUUCAUG

GCAA

Free energy: -42.50 kcal/mol

Broc:

GGGAAAUUGCCAUGUGUAUGUGGGAGACGGUCGGGUCCAGAUAUU

Coli:

GGGAAACGUAUCUGUCGAGUAGAGUGUGGGCUCCCACAUACUCUGAUGAUCCUU

CGGGAUCAUUCAUGGCAA

Broc + Coli free energy: -44.78 kcal/mol

Broc+3:

GGGAAAUUGCCAUGUGUAUGUGGGAGACGGUCGGGUCCAGAUAUUCGU

Coli-3:

GGGAAAAUCUGUCGAGUAGAGUGUGGGCUCCCACAUACUCUGAUGAUCCUUCGG

GAUCAUUCAUGGCAA

(Broc+3)+(Coli-3) free energy: -46.08 kcal/mol

Broc+6:

GGGAAAUUGCCAUGUGUAUGUGGGAGACGGUCGGGUCCAGAUAUUCGUAUC

Coli-6:

GGGAAAUGUCGAGUAGAGUGUGGGCUCCCACAUACUCUGAUGAUCCUUCGGGAU

CAUUCAUGGCAA

(Broc+6)+(Coli-6) free energy: -42.98 kcal/mol

Broc+36:

GGGAAAUUGCCAUGUGUAUGUGGGAGACGGUCGGGUCCAGAUAUUCGUAUCUGU

CGAGUAGAGUGUGGGCUCCCACAUACU

Coli-36:

GGGAAACUGAUGAUCCUUCGGGAUCAUUCAUGGCA

(Broc+36)+(Coli-36) free energy: -47.88 kcal/mol

Broc+39:

GGGAAAUUGCCAUGUGUAUGUGGGAGACGGUCGGGUCCAGAUAUUCGUAUCUGU

CGAGUAGAGUGUGGGCUCCCACAUACUCUG

Coli-39:

GGGAAAAUGAUCCUUCGGGAUCAUUCAUGGCA

(Broc+39)+(Coli-39) free energy: -47.98 kcal/mol

Broc-3:

GGGAAAUUGCCAUGUGUAUGUGGGAGACGGUCGGGUCCAGAU

Coli+3:

GGGAAAAUUCGUAUCUGUCGAGUAGAGUGUGGGCUCCCACAUACUCUGAUGAUC

CUUCGGGAUCAUUCAUGGCAA

(Broc-3)+(Coli+3) free energy: -42.48 kcal/mol

Broc-6:

GGGAAAUUGCCAUGUGUAUGUGGGAGACGGUCGGGUCCA

Coli+6:

GGGAAAGAUAUUCGUAUCUGUCGAGUAGAGUGUGGGCUCCCACAUACUCUGAUG

AUCCUUCGGGAUCAUUCAUGGCAA

(Broc-6)+(Coli+6) free energy: -46.68 kcal/mol

Broc-12:

GGGAAAUUGCCAUGUGUAUGUGGGAGACGGUCG

Coli+12:

GGGAAAGGUCCAGAUAUUCGUAUCUGUCGAGUAGAGUGUGGGCUCCCACAUACU

CUGAUGAUCCUUCGGGAUCAUUCAUGGCAA

(Broc-12)+(Coli+12) free energy: -46.68 kcal/mol

2.6.2 Supporting Figures

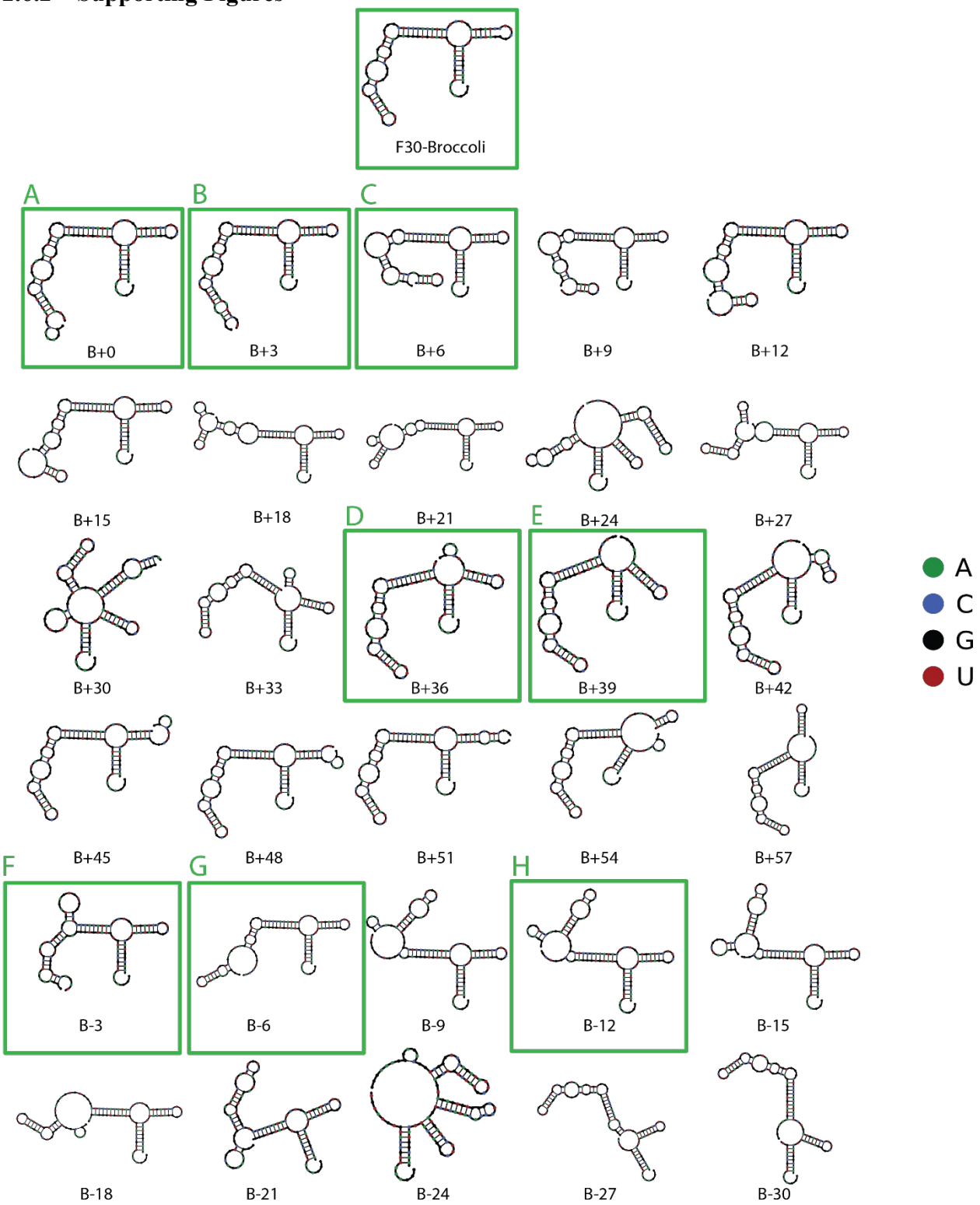

Figure A1: Secondary structures of designed Broccoli Fluorets, predicted by NUPACK at 37 °C. Some of them are completely misfolded (*e.g.*, B-24, B-27, etc.) when compared to the secondary structure of original F30 Broccoli. Based on the secondary structure analysis, eight fluorets

(boxed in green) were chosen for further experimental characterization. The splits of chosen constructs address the potential influence of different areas of F30-Broccoli aptamer on its fluorescent properties. The choice of ± 3 nts was arbitrary.

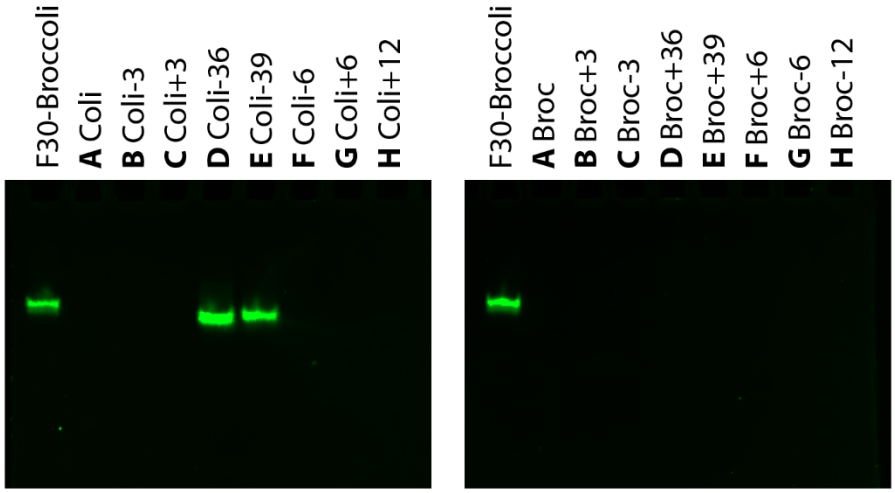

Figure A2: Fluorescence of individual monomer strands. Strands were visualized on an 8% native-PAGE stained with DFHBI-1T.

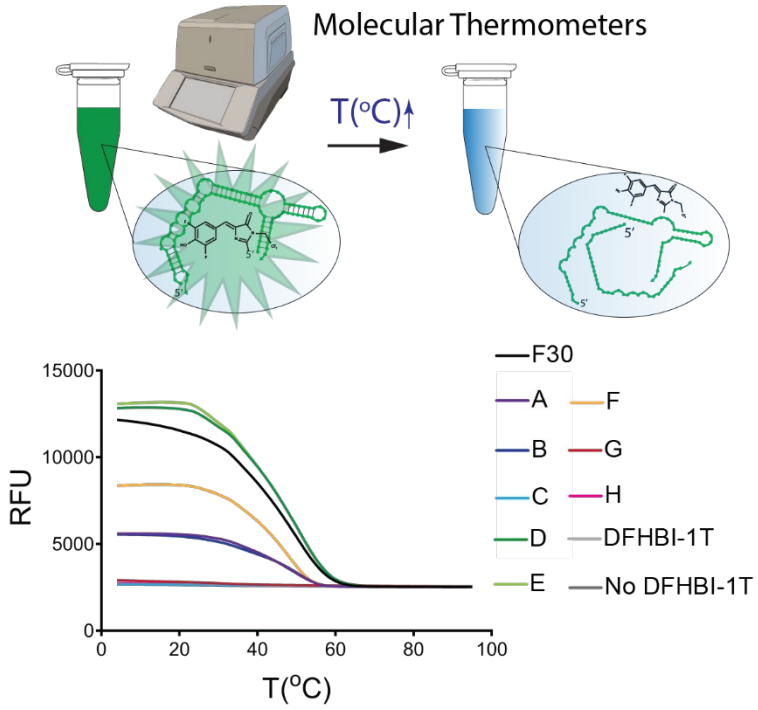

Figure A3: "Molecular Thermometers" that track the temperature changes via fluorescence deactivation.

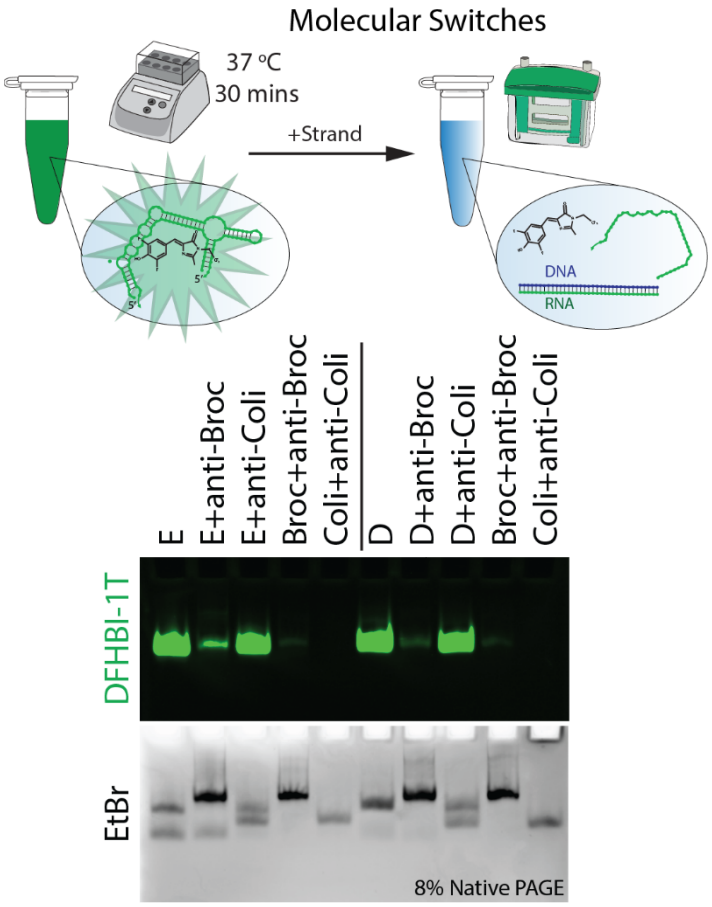

Figure A4: “Molecular Switches” responding to the introduction of oligonucleotides.

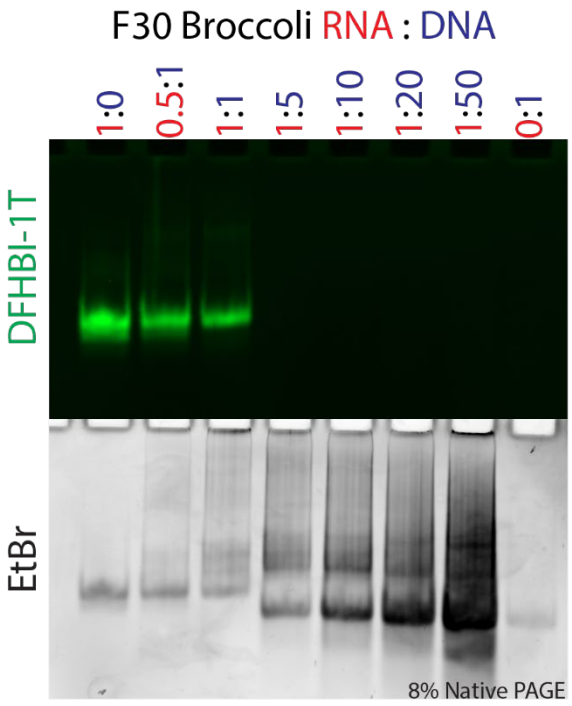

Figure A5: F30 Broccoli RNA assembled with increasing ratios of its complementary DNA. All RNAs are added at 1 μM.

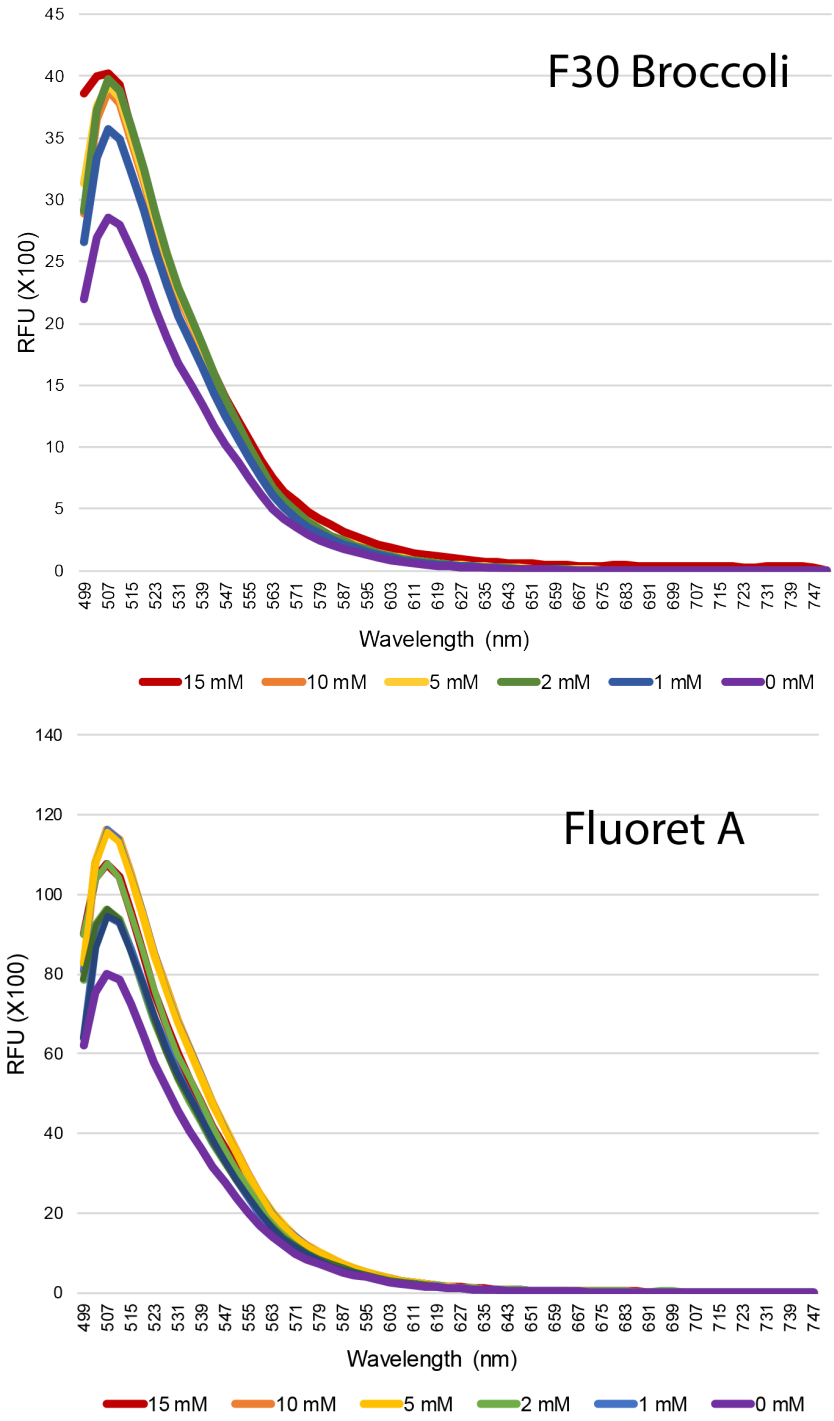

Figure A6: Assembly of F30-Broccoli aptamer and Fluoret A demonstrated at varying concentrations of Mg^{2+}.

3 CHAPTER 3: CONTROLLED ORGANIZATION OF INORGANIC MATERIALS USING BIOLOGICAL MOLECULES FOR ACTIVATING THERAPEUTIC FUNCTIONALITIES

3.1 Introduction

The organization of inorganic materials in diverse 3D nanostructures with hierarchical complexity mimics biological approaches by combining nanoscale components of distinct physicochemical properties with promising applications in imaging[1], sensing[2], drug delivery[3], and tissue engineering[4] with a variety of assembly strategies. Generally, there are two approaches for the fabrication of materials with defined features and functionality at the nanometer scale: top-down and bottom-up. In several top-down approaches, inorganic structures of cellular origin can serve as templates for the organization of nanomaterials. Attachment to these template surfaces can be nonspecific, or microorganisms can be genetically engineered to express functional groups for selective interactions with nanoparticles or their adsorption with increased affinity.[5-7] The top-down methods for nanoparticle organization on the cellular scale are intrinsically less controllable and highly depend on the structure/shape of the template. Therefore, the bottom-up approach for *de novo* organization of inorganic particles by natural polymers such as polypeptides and nucleic acids offers advantages for regulating assembly behavior and morphology.[8]

Nucleic acids are materials with programmable, dynamic, and environmentally responsive functional components for hybrid nanoparticle systems. Due to their simple primary structure and known rules that guide the formation of their secondary and tertiary conformations, nucleic acids are robust materials for scaffolding in comparison to proteins or other biopolymers. The use of Watson-Crick base pairing as a means of prescribing bottom-up assembly strategies has been shown to control and rationally program the 3D self-assembly of functional particles into

well-ordered organizations from the nano- to microscale.[9-12] Several experiments have demonstrated the versatility of nucleic acid scaffolds for displaying functional DNA/RNA motifs with intrinsic functionalities and promising applications in biotechnology or biomedicine.[13-19] The ability to dynamically respond to the environment makes nucleic acids an attractive biomaterial for tailormade structures with desired responsiveness[20-21]. In recent decades, a wide array of artificially designed dynamic nucleic acid assemblies have been shown to react on the broad spectrum of physicochemical or biological stimuli (*e.g.* pH, light, ion concentration, small metabolites, enzymes, or nucleic acid strands).[22-31]

DNA oligonucleotides have been conjugated to a wide range of inorganic particles with distinct physicochemical properties.[32-33] In particular, semiconductor nanocrystals or quantum dots (QDs) are attractive for the development of nanotheranostic concepts for simultaneous diagnostics and therapy.[34] In comparison to organic fluorophores, QDs are strongly luminescent, have increased stability, and have higher brightness and resistance to photobleaching, as well as narrower and symmetric fluorescence spectra with tunable colors controlled by their size. Using DNA for linking, QDs can be utilized to create assemblies with controlled bonding, valency, and photoluminescence.[35-36] Over the last two decades, numerous studies have developed approaches for modifying the surface of QDs with biomolecules for the attachment of functionalized moieties such as DNA/RNA oligonucleotides, antibodies, and peptides.[2] Almost exclusively as optical labels, functionalized QDs have found many applications in biosensing and bioimaging.[37-39] Instead of fluorescent dyes, QDs can be conjugated to aptamers for the visualization of aptamer binding and subsequent intracellular trafficking.[40] Aptamer-QD complexes have been examined to detect a wide range of targets, from simple metal ions, drugs, or toxins to proteins.[41]

Although most biosensing and bioimaging applications of QDs rely on the measurement of changes in fluorescence (color or intensity), QDs offer additional properties for detection. The fluorescence intermittency or blinking is an inherent random fluctuation between ON (bright) and OFF (dark) states of individual QDs.[42] The phenomenon is observable only in a single QD, while in aggregated QDs, the signal is semi-steady. Therefore, differences in signal between the single QDs versus an accumulated group of QDs can be distinguished and used for the detection of target molecules. The principle of this strategy is strand displacement triggered by a target sequence, leading to the re-association of two split biotinylated oligonucleotides that subsequently promote the arrangement and assembly of streptavidin-decorated QDs.[43]

In this work, we set out to design a biocompatible nucleic acid-based scaffold for the assembly of QDs and delivery of functional therapeutics. The developed system uses both RNA and biotinylated DNA as a means to drive the 3D organization of streptavidin-decorated QDs. We first interrogated several approaches for the formation of bioresponsive QD 3D assemblies using sets of QDs functionalized with complementary single-stranded (ss)DNAs, combined with double-biotinylated DNA duplexes, or decorated with DNA/RNA hybrids that re-associate to release Dicer Substrate (DS) RNAs via an isothermal strand displacement reaction[19, 44-48]. The results from each method of assembly were extensively characterized via electrophoretic mobility shift assays (EMSA) and transmission electron microscopy (TEM). Next, we studied relative cellular uptake efficiencies, immunostimulatory properties, and intracellular co-localization of the 3D assemblies and their individual components. We have shown that intracellular formation of QD assemblies in human breast cancer cells releases DS RNAs and, upon dicing, triggers targeted gene silencing.

3.2 Results

The assembly strategy, as dictated by the way nucleic acids are introduced, offers versatility in the resulting 3D assemblies with varying kinetics and functionalities. Three methods of QD assembly were evaluated. First, through the introduction of 39 bp double-stranded (ds)DNA oligonucleotides with a single biotin present on both ends of each duplex, binding with streptavidin-coated QDs which are 15-16 nm in diameter drives the rapid (~30 seconds) formation of assembled structures (**Figure 7**). As seen in the agarose gel, the QDs alone begin to migrate upon the addition of an ssDNA. However, full assembly at a 1 QD:10 DNA molar ratio into larger-scale organization over time results in morphologies that are too large to enter the gel and can thus be observed in the loading wells only (**Figure A1**).[43] In comparison, if individual fully complementary DNA strands are added separately to QDs and then combined, it takes closer to 30 minutes for the aggregate to fully assemble (**Figure 7B**).

As the third approach, QDs were separately conjugated to complementary dsDNA/RNA hybrid duplexes via the biotinylated DNA. Once added together, complementary 12 nt-ssDNA toeholds initiate the isothermal strand displacement reaction that promotes the formation of double-biotinylated DNA duplexes while releasing the RNA sequences to form functional DS RNAs (**Figure 7C**). The complete assembly of QDs and subsequent release of DS RNAs were achieved after ~10 minutes. In all three strategies of QD assembly, the addition of DNase to assembled 3D structures completely reversed the formation of assembled structures through the digestion of any DNA crosslinkers, resulting in the increased mobility of QDs. These results additionally confirm the DNA-driven organization of QDs.

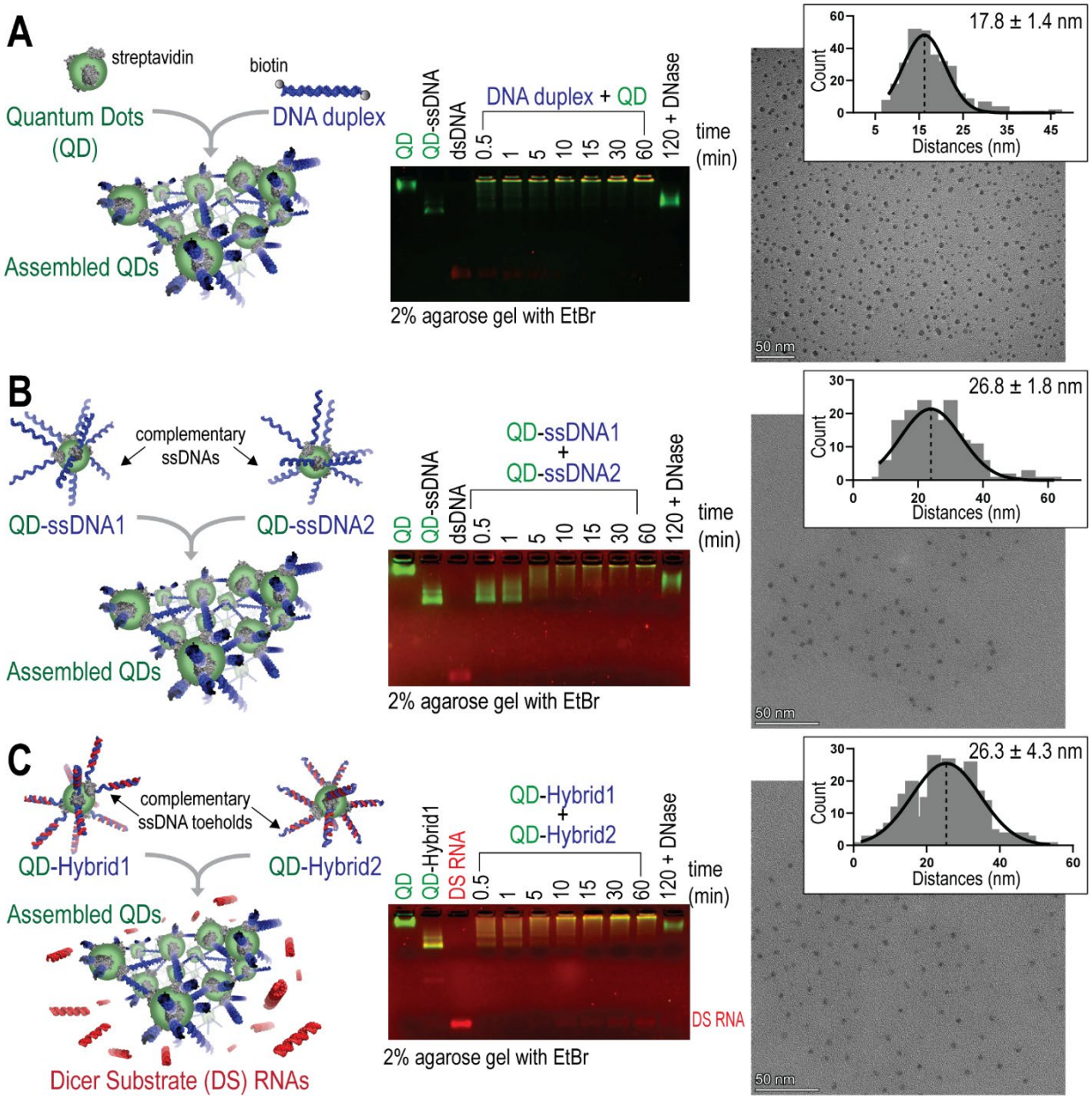

Figure 7. Three protocols of QD assembly with kinetics characterized by agarose gels. TEM images showing the distribution of QDs within their assemblies and measurements of the center-to-center distances presented in the histogram with their Gaussian fit for n=100 QDs. Scale bar = 50 nm. Mean center-to-center distances calculated from n=3 TEM images are shown ± SEM. (A) QDs mixed with double-biotinylated DNA duplexes. (B) QDs decorated with complementary ssDNA. (C) QDs decorated with RNA-DNA hybrids that re-associate via the complementary ssDNA toehold interaction and release Dicer Substrate (DS) RNAs.

All three methods of QD assembly were conducted, and the products were imaged by TEM. Analysis of the center-to-center distances between a given QD and its three nearest neighbors was assessed to compare QD distributions (**Figure A2**). For dsDNA duplex-driven QD assembly, the mean center-to-center distance was 17.8 ± 1.4 nm. For ssDNA-driven QD assembly, the mean center-to-center distance was 26.8 ± 1.8 nm. Finally, for hybrid-driven QD assemblies, the mean center-to-center distance was 26.3 ± 4.3 nm. The distributions of distances for 100 QDs are shown for each TEM image in **Figure 7A-C**. The assembled distances show much less distribution than free QDs in solution imaged at the same concentrations, for which the mean center-to-center distance was 76.6 ± 17.2 nm (**Figure A2**).

To fully take advantage of the programmable assemblies of inorganic QDs, assemblies were introduced into cells using a lipid-based carrier for their intracellular delivery. Their relative uptake and intracellular assembly in MDA-MB-231 human breast cancer cells were assessed by separately introducing QDs carrying complementary DNA/RNA hybrids. Cells were then visualized via fluorescence microscopy and analyzed by flow cytometry (**Figure 8A**). Micrographs labeled a-d correspond with the geometric mean fluorescence intensity (gMFI) shown to the right, wherein the stepwise introduction of materials for their intracellular assembly resulted in higher gMFI than for either QD component or assembly.

To confirm that the cognate QDs can form intracellular assemblies and thus co-localize inside cells, QD545 and QD605 carrying complementary hybrid DNA/RNA duplexes were introduced and the cells were analyzed by confocal microscopy (**Figure 8B**). The co-localization of the emission of each QD shown on the superposition image (1+2+3) demonstrates the heterogenous assembly of formations composed of both QDs and confirms the assembly of QDs

in cells. Additional confocal microscopy images of the co-localization studies are shown in **Figure A3**.

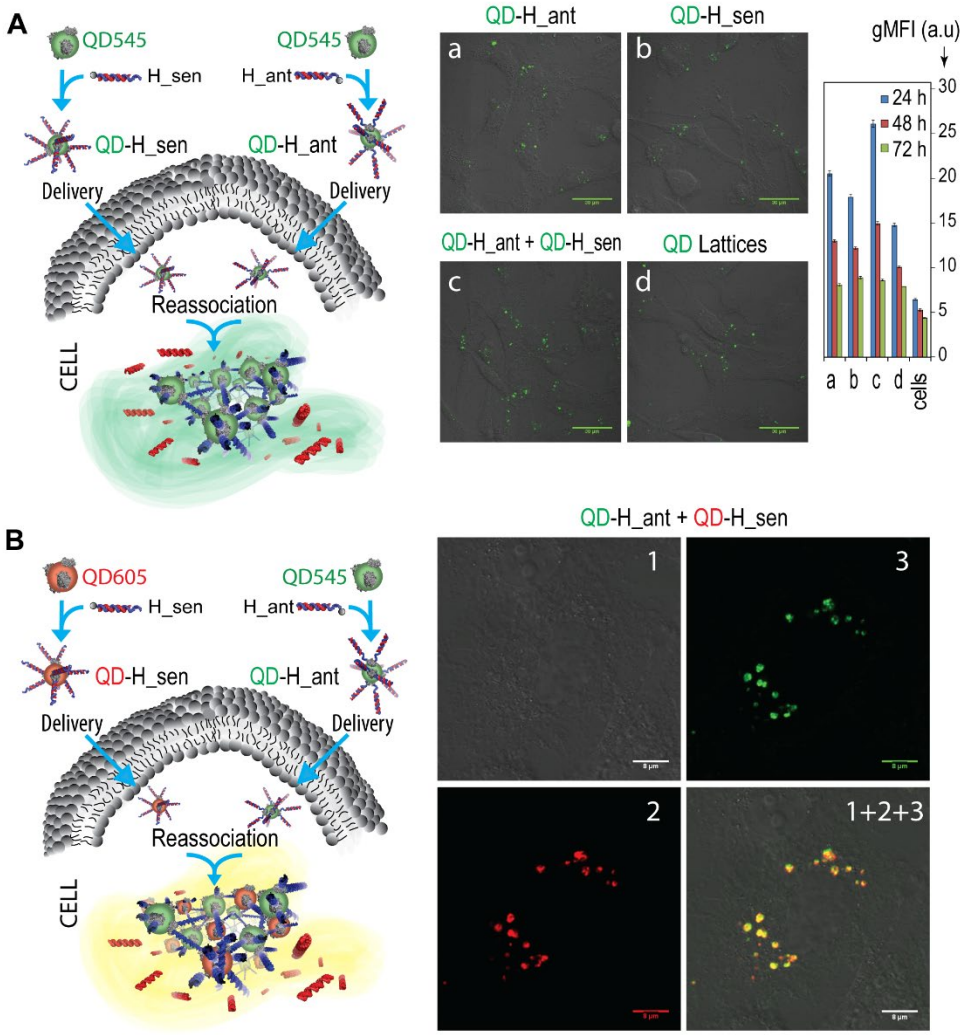

Figure 8. Relative uptake efficiencies and intracellular co-localization experiments. (A) The uptake of functionalized QD545 was analyzed by fluorescence microscopy and flow cytometry. Scale = 30 µm. Bars denote mean ± SEM of n=20,000 individual events. (B) Co-localization of QD545 (green) and QD605 (red) entering the composition of QD assemblies as analyzed by confocal microscopy. Image numbers correspond to (1) differential interference contrast (DIC), (2) QD605 emission, and (3) QD545 emission. Image (1+2+3) is the superposition of three different images, scale = 8 µm.

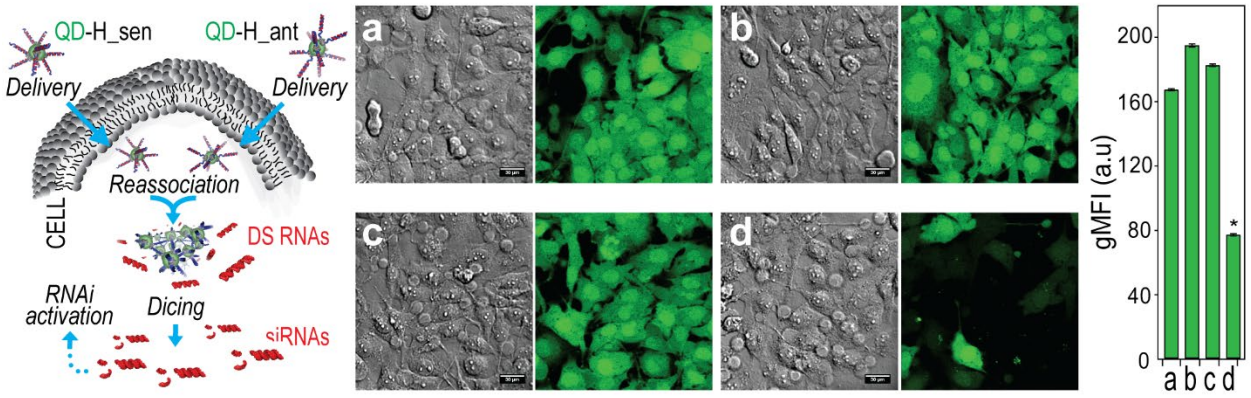

Figure 9. Activation of RNA interference in human breast cancer cells upon QD assembly formation. Intracellular QD assembly releases DS RNAs that trigger specific gene silencing upon dicing. Three days after the co-transfection of cells with QDs decorated with cognate hybrids, GFP silencing was confirmed by fluorescent microscopy and statistically analyzed with flow cytometry. Samples (a-d) have the same compositions for microscopy and flow cytometry experiments. (a) Untreated MDA-MB-231 eGFP cells show green fluorescence. Cells treated with either (b) QD-H_sen or (c) QD-H_ant show no fluorescence knockdown. Silencing is observed when (d) both QD-H_sen and QD-H_ant are transfected to reassociate in cells and drive the activation of RNAi. Final concentrations of nucleic acids are 10 nM and QDs are 1 nM. Bars denote mean ± SEM of n=20,000 individual events. Statistically significant results are indicated with asterisks (* = P-value < 0.05).

With uptake established, the potential for functional therapeutics imbued into the DNA/RNA assembly approach was further investigated. QDs carrying complementary hybrid duplexes were transfected stepwise into MDA-MB-231 cells engineered to express green fluorescent protein (GFP). The RNA sequences were designed to assemble into DS RNAs upon the reassociation of QDs inside the cell (**Figure 9**). With either QD or hybrid alone, the cells remained fluorescent with the expression of GFP. However, when both QDs were introduced to cells, the intracellular QD formation resulted in the silencing of GFP assessed after 72 hours. Flow cytometry confirmed a statistically significant reduction in gMFI as a result of the QD assembly. In timecourse studies, silencing with 10 and 20 nM QD assemblies was observed even after up to 14 days (**Figure A4**).

As the last step to confirm the downstream biological applications of these materials, their immunostimulation in cell lines was assessed. Hybrid duplexes and their reassociation were compared with assembled QDs, free QDs, QDs with hybrid duplexes, and the reassociation of

hybrid duplexes when one (QD-H_sen+H_ant) hybrid was bound to QDs. The relative production of cytokines hIL-1β, hIL-6, hIL-8, and hIFN-β in the human microglia-like cell line, hμglia, were assessed as normalized to cells treated only with a carrier, Lipofectamine 2000 (L2K) (**Figure 10**). The panel of these four cytokines was chosen due to their known roles as modulators of the inflammatory response: hIL-1β and hIL-6 as proinflammatory cytokines, hIL-8 as a chemokine, and hIFN-β as an interferon. Any recognition of exogenously introduced nucleic acids resulting in immunostimulation was expected to be observed from this representative panel, as their release has been previously documented from microglia in response to pathogen-associated molecular patterns (PAMPs) or pathogens[59-60]. Overall, no components of the QD assembly were identified as potent immune activators. Only QD-H_sen showed statistical significance in regard to relative hIL-1β production. The same panel of cytokines was also investigated for a human astrocyte-like cell line, U87-MG (**Figure A5**), in which no conditions demonstrated statistically significant immune stimulation. Importantly, free QDs showed no statistically significant cytotoxicity in neither the hμglia nor MDA-MB-231 cell lines (**Figure A6**).

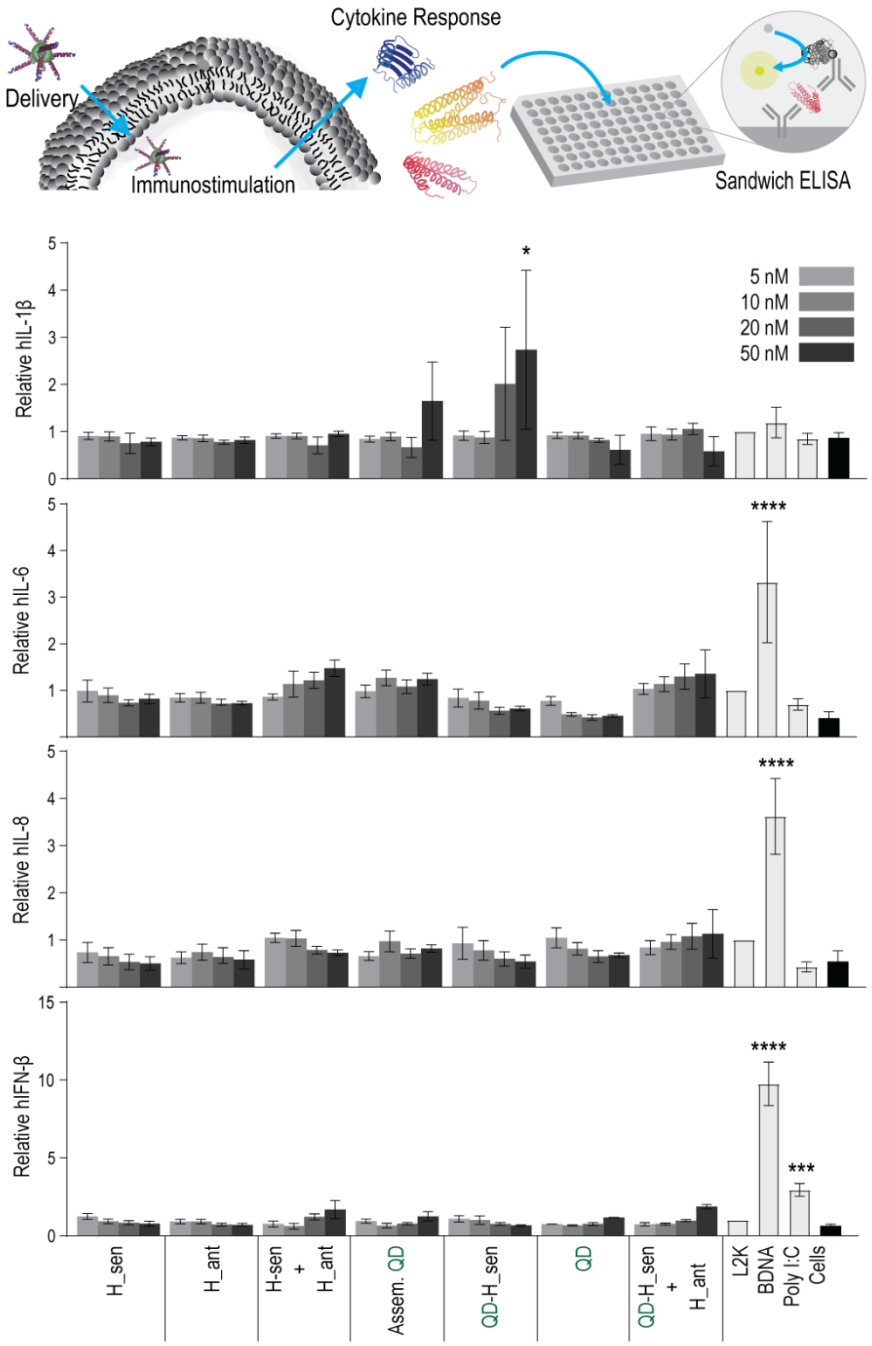

Figure 10. Immunostimulatory activity of QD assemblies. A human microglia-like cell line (hμglia) was transfected and cell supernatants were collected 24 hours later. Levels of hIL-1β, hIL-6, hIL-8, and hIFN-β were assessed by ELISA. Bars denote mean ± SEM of n=3 independent repeats. Statistically significant results are indicated with asterisks (**** = P-value < 0.0001, *** = P-value <0.001, * = P-value <0.05).

3.3 Conclusions

The colocalization of QDs 545 and 605 within human breast cancer cells demonstrates the assembly of QDs directly within the cellular environment, which is further validated by the significant fold knockdown of GFP in expressing cells via RNA interference upon QD formation. Importantly, despite the presence of large number of dsDNAs in their structures, QD assemblies and their components do not invoke a significant difference in the production of cytokines, which makes this theranostic approach feasible in addition to biosensing. While QDs alone exhibit narrow emission which is advantageous for tracking, assemblies of QDs offer more opportunities for sensing parameters.[43] For example, one avenue is that the centrifugation of assembled QDs results in the formation of a precipitate, while individual monomers show no precipitation (**Figure A7**).

Precise control over the assembly of complex networks of materials requires the coordination of all the individual components. Nucleic acids offer a straightforward route to scaffolding due to their programmable basepairing, but also allow for biologically relevant sequences to be implemented for therapeutic applications, as demonstrated here with the incorporation of RNA interference inducers. While three methods of assembly were demonstrated, their characterization shows similar morphologies despite variations in their kinetics. Variations in morphologies can also be achieved by changing the lengths of DNAs in the assembly composition, which could also allow for the integration of other functional nucleic acids. Further work to fine-tune the organization of QD assemblies may take advantage of nucleic acids' programmability in order to control size and shape of the network on a larger scale.

3.4 Experimental Section

3.4.1 Sequence design and preparation

DS RNAs designed against GFP and their complementary DNA sequences with 12 nt toeholds were purchased from Integrated DNA Technologies (IDT), as shown in previous work.[45]. Oligos were diluted in endotoxin-free HyClone™ HyPure Cell Culture Grade Water (Cytiva) before use.

3.4.2 Assembly of QDs

QD545s (Qdot™ 545 ITK™ Streptavidin Conjugate Kit, Catalog #Q10091MP) composed of a cadmium selenide core with a zinc sulfide and covalently attached streptavidin were purchased from Invitrogen™. QD545s were reported by the manufacturer to be 15-16 nm in diameter with an emission maximum of 545 ± 4 nm and were used for all studies. QD545s were assembled with either dsDNA, ssDNA, or DNA/RNA hybrid duplexes in endotoxin-free water with all QDs at 100 nM final concentration.

3.4.2.1 For (DNA duplex + QD) assembly

DNA duplexes were made by mixing complementary DNA oligos in an equimolar ratio. The mixture was heated at 95 °C for two minutes before assembly buffer (final concentration of 89 mM tris-borate (pH 8.2), 50 mM KCl, 2 mM $MgCl_2$) was added, followed by incubation at room temperature for 20 minutes[61]. Afterward, QDs were added with DNA duplex at a 1:10 QD:duplex molar ratio and incubated at 37 °C for 30 minutes.

3.4.2.2 For (QD + ssDNA1)+(QD + ssDNA2) assembly

QDs were assembled in two separate tubes with each DNA oligo in a 1:10 QD:DNA molar ratio in assembly buffer. Samples were incubated at 37 °C for 20 minutes. Afterward, the contents of the two tubes were mixed at a 1:1 volumetric ratio and incubated at 37 °C for 30 minutes.

3.4.2.3 For (QD + H_sen)+(QD + H_ant) assembly

Hybrid DNA/RNA duplexes were assembled in two separate tubes: H_sen ("DNA for Sense_12_Biotin" + "RNA Sense") and H_ant ("DNA for Antisense_12_Biotin" + "RNA Antisense.") The Hybrid Duplexes were prepared by adding their constituent oligos in an equimolar ratio, heating at 95 °C for two minutes, and adding assembly buffer, followed by incubation at room temperature for 20 minutes. QDs were added to each separate Hybrid Duplex tube in a 1:10 QD:duplex molar ratio and incubated at 37 °C for 30 minutes. Afterward, Hybrid Duplexes were mixed in a 1:1 volumetric ratio and incubated at 37 °C for 60 minutes. For cellular colocalization in Figure 4B, one hybrid duplex was added with QD545 while its conjugate was added with QD605 for the 30-minute incubation at 37 °C. For this, Qdot™ 605 Streptavidin Conjugate (Catalog # Q10101MP) composed of a cadmium selenide core, zinc sulfide shell, and polymer coating to allow for streptavidin conjugation was purchased from Invitrogen™. QD605s were reported to be 15-20 nm in diameter with an emission maximum of 608 ± 4 nm.

3.4.3 EMSA

To confirm assembly, QD assemblies were analyzed on a 2% agarose gel stained with 0.5 µg/mL ethidium bromide. Gels were run in 89 mM tris-borate, 2 mM EDTA (pH 8.2) for 20 minutes at 220 V, then visualized on a Bio-Rad™ ChemiDoc MP Imaging System using the Multichannel protocol for QD525 (used to view QD545) and QD605 (used to view ethidium bromide).

3.4.3.1 EMSAs of the kinetics of assembly

QDs were assembled in 40 µL volumes as described and incubated at 37 °C for 120 minutes as previously shown.[43] At the 0.5, 1, 5, 10, 15, 30, and 60-minute timepoints, 4 µL of assembling QDs were added to 4 µL of agarose loading buffer (30% glycerol, 0.25% bromophenol blue, 0.25%

xylene cyanol) in a tube, which was immediately placed on dry ice. At the 60-minute timepoint, 1 µL of RQ1 RNase-Free DNase (Promega) was added and allowed to incubate for an additional 30 minutes. Samples were visualized via EMSA as above by loading 4.0 µL of each sample per well by descending timepoint, along with controls.

3.4.4 Precipitation of QD assemblies

50 µL samples of assembled QDs (with final QD concentration of 100 nM) or controls were centrifuged at 4 °C for 5 minutes at 10, 5, 2.5, or 1 G on a ThermoScientific Sorvall Legend Micro 21R Centrifuge. All precipitates were immediately visualized on a Bio-Rad™ ChemiDoc MP Imaging System.

3.4.5 TEM

The QD assemblies were diluted by a factor of 100 in deionized water to a final concentration of ~1 nM for preparing TEM samples. Immediately after dilution, a drop of QD assembly in solution was allowed to dry on a TEM grid with an ultrathin amorphous carbon support film. Bright-field TEM images were acquired using a FEI Talos F200XG2 microscope with an accelerating voltage of 200 kV. Three representative images (**Figure A2**) chosen from each of the three methods of QD formation were assessed in ImageJ using the ND ImageJ plugin to calculate center-to-center distances.[62-63] After excluding edges, the radius (r_1) of each identified QD point was calculated as half the average of the width plus height. The distances from the edge of each QD to its three nearest neighbors (d) were averaged along with the average radii (r_2) of the three nearest neighbors using the ND ImageJ plugin. To calculate each center-to-center distance, r_1, r_2, and d were added together and averaged for the first 100 events in each of the three TEM images. The three average center-to-center distances were then averaged and the standard error of the mean (SEM) was calculated based on n=3 images. For visualizing the distribution of center-to-center

distances, the first 100 events in each of the images shown in **Figure 7** were plotted in a histogram and fit with a Gaussian distribution using GraphPad Prism version 9.0.0 for Windows, GraphPad Software, San Diego, California USA, www.graphpad.com. As a control, free QDs were analyzed at the same concentration.

3.4.6 Cell culture and transfection

The human breast cancer cell line MDA-MB-231(with or without GFP) was maintained in DMEM, 10% heat-inactivated fetal bovine serum (FBS), and 1% PenStrep in incubators at 37 °C, 5% CO_2. Cells were plated in 35 mm dishes to perform confocal visualization (Ibidi, Germany). Lipofectamine™ 2000 (L2K) was used for all experiments according to the manufacturer's guidelines. Briefly, plated cells were transfected for 4 hours in Opti-MEM using 10 nM of the nucleic acid transfected. Upon 4 hours, the medium was replaced with DMEM and the cells were further incubated for 3 days (silencing experiments) or 14 hours (uptake experiments). The cells were then washed 3 times in PBS and fixed with 4% paraformaldehyde prior to imaging.

3.4.7 Uptake and co-localization

Experiments were performed using a UV 510 confocal microscope (Carl Zeiss, Oberkochen) and a Plan-Apochromat 63x/1.4 Oil lens. To image QD545, a 488-laser beam was used for excitation and a BP filter 505-550 for detection. To image QD605, a 561 nm laser beam was used for excitation and a BP filter 575-615 for detection. All images were taken with a pinhole adjusted to 1 airy unit. Flow cytometry was performed on a BD Accuri C6 flow cytometer; CellQuest or the CFlow Sampler software was used to retrieve the geometric mean fluorescence intensity (gMFI). Data are expressed as the mean ± SEM for n=20,000 events per treatment.

3.4.8 Silencing assays

For silencing experiments, cells were visualized using a UV 510 confocal microscope (Carl Zeiss, Oberkochen) and a Plan-Neofluar 40×/1.3 Oil lens. To image GFP fluorescence, a 488-laser beam was used for excitation and detection was acquired using a BP filter 505-550. Flow cytometry was performed on a BD Accuri C6 flow cytometer; CellQuest or the CFlow Sampler software was used to retrieve the geometric mean fluorescence intensity (gMFI). To determine statistical significance, treatments were compared to cells-only using a one-way ANOVA followed by a Dunnett's multiple comparisons test performed in GraphPad Prism version 9.0.0 for Windows, GraphPad Software, San Diego, Californa USA, www.graphpad.com. Data are expressed as the mean ± SEM for n=20,000 events per treatment. A *P*-value of < 0.05 was considered statisitically significant.

3.4.9 Immune stimulation by ELISA

Dr. Jonathan Karn (Case Western Reserve University) generously provided the human microglia cell line, hμglia. Cells were maintained in Dulbecco's modified Eagle medium (DMEM) supplemented with 5% fetal bovine serum (FBS) and 100U/ml penicillin-100 μg/ml streptomycin at 37°C 5% CO_2. The immortalized human astrocytic cell line, U87-MG, was obtained from the American Type Culture Collection (ATCC; HTB-14) and maintained in Eagle's minimum essential media (EMEM) supplemented with 10% FBS and 100 U/ml penicillin-100 μg/ml streptomycin at 37°C 5% CO_2. Cells were transfected with final concentrations of 5, 10, 20, or 50 nM of each sample using lipofectamine 2000 (L2K, Invitrogen) according to the manufacturer's guidelines. Ligands were incubated for 30 minutes at room temperature with lipofectamine 2000 prior to transfection of cells with the indicated samples. Cells were incubated at 37 °C, 5% CO_2 for 4 hours with the transfection reaction. Afterward, media was aspirated and replaced with 1 mL

of fresh media. Cells supernatants were collected at 24 hours post transfection. IL-6, IFN-β, IL-1β, and IL-8 were quantified using specific capture ELISAs. IL-6 was detected using a rat anti-human IL-6 capture antibody (BD Pharmingen, cat # 554543; Clone Mq2-13A5) and a biotinylated rat anti-human IL-6 detection antibody (BD Pharmingen, cat# 554546; Clone MQ2-39C3). IFN-β was detected using a polyclonal rabbit anti-human IFN-β capture antibody (Abcam, cat# ab186669) and a biotinylated polyclonal rabbit anti-human IFN-β detection antibody (Abcam, cat# ab84258). IL-8 (R&D systems, cat# DY208) and IL-1β (R&D systems, cat # DY201) were detected using DuoSet ELISA kits. For all specific capture ELISAs, bound detection antibody was detected using streptavidin-HRP (BD Biosciences) followed by incubation with tetramethylbenzidine substrate. The cytokine concentration in cell supernatants was extrapolated from a standard curve generated using a dilution of recombinant cytokines. For each graph, the relative amount of cytokine production was normalized to the L2K-only treatment. To determine statistical significance, treatments were compared to L2K-only using a one-way ANOVA followed by Dunnett's multiple comparisons test performed in GraphPad Prism version 9.0.0 for Windows, GraphPad Software, San Diego, California USA, www.graphpad.com. Data are expressed as the mean ± SEM for a minimum of three independent experimental replicates. A *P*-value of < 0.05 was considered statistically significant.

3.4.10 Cell viability assay

To assess the cytotoxicity of QDs, MDA-MB-231 cells and hμglia cells were seeded in 96-well plates in their respective medias. Cells were transfected with final concentrations of 5, 10, 20, or 50 nM of each sample using L2K (Invitrogen) according to the manufacturer's guidelines. QD545s were incubated for 30 minutes at room temperature with L2K prior to transfection of cells with the indicated samples. Cells were incubated at 37 °C, 5% CO_2 for 4 hours with the transfection

reaction. Afterward, media was aspirated and replaced with fresh media. Cells were assessed 24 hours post-transfection using a CellTiter 96® AQ_{ueous} One Solution Cell Proliferation Assay (MTS, Promega) according to the manufacturer's guidelines. For each graph, the relative percent cell viability was normalized to the cells-only treatment. To determine statistical significance, treatments were compared to cells-only using a one-way ANOVA followed by a Dunnett's multiple comparisons test performed in GraphPad Prism version 9.0.0 for Windows, GraphPad Software, San Diego, Californa USA, www.graphpad.com. Data are expressed as the mean ± SEM for a minimum of n=3 independent experimental replicates. A *P*-value of < 0.05 was considered statisitically significant.

3.5 References

1. Jooken, S.; de Coene, Y.; Deschaume, O.; Krylychkina, O.; Verbiest, T.; Clays, K.; Callewaert, G.; Bartic, C., Quantum Dot-Functionalized Extracellular Matrices for In Situ Monitoring of Cardiomyocyte Activity. *ACS Applied Nano Materials* **2020,** *3* (6), 6118-6126.
2. Freeman, R.; Girsh, J.; Willner, I., Nucleic Acid/Quantum Dots (QDs) Hybrid Systems for Optical and Photoelectrochemical Sensing. *ACS Appl Mater & Interfaces* **2013,** *5* (8), 2815-2834.
3. Yuan, Y.; Zhang, J.; An, L.; Cao, Q.; Deng, Y.; Liang, G., Oligomeric nanoparticles functionalized with NIR-emitting CdTe/CdS QDs and folate for tumor-targeted imaging. *Biomaterials* **2014,** *35* (27), 7881-7886.
4. Jahed, V.; Vasheghani-Farahani, E.; Bagheri, F.; Zarrabi, A.; Jensen, H. H.; Larsen, K. L., Quantum dots-βcyclodextrin-histidine labeled human adipose stem cells-laden chitosan hydrogel for bone tissue engineering. *Nanomedicine: Nanotechnology, Biology and Medicine* **2020,** *27*, 102217.
5. Rosi, N. L.; Thaxton, C. S.; Mirkin, C. A., Control of nanoparticle assembly by using DNA-modified diatom templates. *Angew Chem Int Edit* **2004,** *43* (41), 5500-5503.
6. Berry, V.; Rangaswamy, S.; Saraf, R. F., Highly selective, electrically conductive monolayer of nanoparticles on live bacteria. *Nano Letters* **2004,** *4* (5), 939-942.
7. Dujardin, E.; Peet, C.; Stubbs, G.; Culver, J. N.; Mann, S., Organization of metallic nanoparticles using tobacco mosaic virus templates. *Nano Letters* **2003,** *3* (3), 413-417.
8. Kahn, J. S.; Minevich, B.; Gang, O., Three-dimensional DNA-programmable nanoparticle superlattices. *Current Opinion in Biotechnology* **2020,** *63*, 142-150.
9. Nykypanchuk, D.; Maye, M. M.; van der Lelie, D.; Gang, O., DNA-guided crystallization of colloidal nanoparticles. *Nature* **2008,** *451* (7178), 549-552.
10. Park, S. Y.; Lytton-Jean, A. K. R.; Lee, B.; Weigand, S.; Schatz, G. C.; Mirkin, C. A., DNA-programmable nanoparticle crystallization. *Nature* **2008,** *451* (7178), 553-556.

11. He, M.; Gales, J. P.; Ducrot, É.; Gong, Z.; Yi, G.-R.; Sacanna, S.; Pine, D. J., Colloidal diamond. *Nature* **2020,** *585* (7826), 524-529.
12. Laramy, C. R.; O'Brien, M. N.; Mirkin, C. A., Crystal engineering with DNA. *Nat Rev Mater* **2019,** *4* (3), 201-224.
13. Afonin, K. A.; Viard, M.; Koyfman, A. Y.; Martins, A. N.; Kasprzak, W. K.; Panigaj, M.; Desai, R.; Santhanam, A.; Grabow, W. W.; Jaeger, L.; Heldman, E.; Reiser, J.; Chiu, W.; Freed, E. O.; Shapiro, B. A., Multifunctional RNA Nanoparticles. *Nano Letters* **2014,** *14* (10), 5662-5671.
14. Khaled, A.; Guo, S.; Li, F.; Guo, P., Controllable self-assembly of nanoparticles for specific delivery of multiple therapeutic molecules to cancer cells using RNA nanotechnology. *Nano Letters* **2005,** *5* (9), 1797-1808.
15. Goldsworthy, V.; LaForce, G.; Abels, S.; Khisamutdinov, E. F. J. N., Fluorogenic RNA aptamers: A nano-platform for fabrication of simple and combinatorial logic gates. *Nanomaterials (Basel, Switzerland)* **2018,** *8* (12), 984.
16. Panigaj, M.; Johnson, M. B.; Ke, W.; McMillan, J.; Goncharova, E. A.; Chandler, M.; Afonin, K. A., Aptamers as Modular Components of Therapeutic Nucleic Acid Nanotechnology. *ACS Nano* **2019**, 12301-12321.
17. Johnson, M. B.; Chandler, M.; Afonin, K. A., Nucleic acid nanoparticles (NANPs) as molecular tools to direct desirable and avoid undesirable immunological effects. *Adv Drug Delivery Reviews* **2021,** *173*, 427-438.
18. Ke, W.; Afonin, K. A., Exosomes as natural delivery carriers for programmable therapeutic nucleic acid nanoparticles (NANPs). *Adv Drug Delivery Reviews* **2021**, 113835.
19. Nordmeier, S.; Ke, W.; Afonin, K. A.; Portnoy, V., Exosome mediated delivery of functional nucleic acid nanoparticles (NANPs). *Nanomedicine: Nanotechnology, Biology and Medicine* **2020,** *30*, 102285.
20. Bindewald, E.; Afonin, K. A.; Viard, M.; Zakrevsky, P.; Kim, T.; Shapiro, B. A., Multistrand Structure Prediction of Nucleic Acid Assemblies and Design of RNA Switches. *Nano Letters* **2016,** *16* (3), 1726-1735.
21. Zakrevsky, P.; Parlea, L.; Viard, M.; Bindewald, E.; Afonin, K. A.; Shapiro, B. A., Preparation of a conditional RNA switch. In *RNA Nanostructures*, Springer: 2017; pp 303-324.
22. Achenbach, J. C.; Nutiu, R.; Li, Y., Structure-switching allosteric deoxyribozymes. *Interpretation, Design and Selection of Biomolecular Interactions* **2005,** *534* (1), 41-51.
23. Bath, J.; Green, S. J.; Turberfield, A. J., A free-running DNA motor powered by a nicking enzyme. *Angew. Chem. Int. Ed. Engl.* **2005,** *44* (28), 4358-4361.
24. Liu, X.; Lu, C.-H.; Willner, I., Switchable reconfiguration of nucleic acid nanostructures by stimuli-responsive DNA machines. *Accounts of Chemical Research* **2014,** *47* (6), 1673-1680.
25. Yurke, B.; Turberfield, A. J.; Mills, A. P.; Simmel, F. C.; Neumann, J. L., A DNA-fuelled molecular machine made of DNA. *Nature* **2000,** *406* (6796), 605-608.
26. Modi, S.; M G, S.; Goswami, D.; Gupta, G. D.; Mayor, S.; Krishnan, Y., A DNA nanomachine that maps spatial and temporal pH changes inside living cells. *Nature Nanotechnology* **2009,** *4* (5), 325-330.
27. Zhou, M.; Liang, X.; Mochizuki, T.; Asanuma, H., A light-driven DNA nanomachine for the efficient photoswitching of RNA digestion. *Angew. Chem. Int. Ed. Engl.* **2010,** *49* (12), 2167-2170.

28. Halman, J. R.; Satterwhite, E.; Roark, B.; Chandler, M.; Viard, M.; Ivanina, A.; Bindewald, E.; Kasprzak, W. K.; Panigaj, M.; Bui, M. N.; Lu, J. S.; Miller, J.; Khisamutdinov, E. F.; Shapiro, B. A.; Dobrovolskaia, M. A.; Afonin, K. A., Functionally-interdependent shape-switching nanoparticles with controllable properties. *Nucleic Acids Research* **2017,** *45* (4), 2210-2220.
29. Ke, W.; Hong, E.; Saito, R. F.; Rangel, M. C.; Wang, J.; Viard, M.; Richardson, M.; Khisamutdinov, E. F.; Panigaj, M.; Dokholyan, N. V.; Chammas, R.; Dobrovolskaia, M. A.; Afonin, K. A., RNA-DNA fibers and polygons with controlled immunorecognition activate RNAi, FRET and transcriptional regulation of NF-κB in human cells. *Nucleic Acids Research* **2019,** *47* (3), 1350-1361.
30. Kahn, J. S.; Hu, Y.; Willner, I., Stimuli-Responsive DNA-Based Hydrogels: From Basic Principles to Applications. *Accounts of Chemical Research* **2017,** *50* (4), 680-690.
31. De Fazio, A. F.; El-Sagheer, A. H.; Kahn, J. S.; Nandhakumar, I.; Burton, M. R.; Brown, T.; Muskens, O. L.; Gang, O.; Kanaras, A. G., Light-Induced Reversible DNA Ligation of Gold Nanoparticle Superlattices. *ACS Nano* **2019,** *13* (5), 5771-5777.
32. Cutler, J. I.; Auyeung, E.; Mirkin, C. A., Spherical Nucleic Acids. *Journal of the American Chemical Society* **2012,** *134* (3), 1376-1391.
33. Sun, D.; Gang, O., DNA-Functionalized Quantum Dots: Fabrication, Structural, and Physicochemical Properties. *Langmuir* **2013,** *29* (23), 7038-7046.
34. Matea, C. T.; Mocan, T.; Tabaran, F.; Pop, T.; Mosteanu, O.; Puia, C.; Iancu, C.; Mocan, L., Quantum dots in imaging, drug delivery and sensor applications. *Int J Nanomedicine* **2017,** *12*, 5421-5431.
35. Tikhomirov, G.; Hoogland, S.; Lee, P. E.; Fischer, A.; Sargent, E. H.; Kelley, S. O., DNA-based programming of quantum dot valency, self-assembly and luminescence. *Nature Nanotechnology* **2011,** *6* (8), 485-490.
36. Sun, D.; Gang, O., Binary Heterogeneous Superlattices Assembled from Quantum Dots and Gold Nanoparticles with DNA. *Journal of the American Chemical Society* **2011,** *133* (14), 5252-5254.
37. Martynenko, I. V.; Litvin, A. P.; Purcell-Milton, F.; Baranov, A. V.; Fedorov, A. V.; Gun'ko, Y. K., Application of semiconductor quantum dots in bioimaging and biosensing. *Journal of Materials Chemistry B* **2017,** *5* (33), 6701-6727.
38. Gill, R.; Zayats, M.; Willner, I., Semiconductor quantum dots for bioanalysis. *Angew Chem Int Ed Engl* **2008,** *47* (40), 7602-7625.
39. Michalet, X.; Pinaud, F. F.; Bentolila, L. A.; Tsay, J. M.; Doose, S.; Li, J. J.; Sundaresan, G.; Wu, A. M.; Gambhir, S. S.; Weiss, S., Quantum dots for live cells, in vivo imaging, and diagnostics. *Science (New York, N.Y.)* **2005,** *307* (5709), 538-544.
40. Opazo, F.; Eiden, L.; Hansen, L.; Rohrbach, F.; Wengel, J.; Kjems, J.; Mayer, G., Modular Assembly of Cell-targeting Devices Based on an Uncommon G-quadruplex Aptamer. *Mol Ther Nucleic Acids* **2015,** *4*, 251.
41. Wen, L.; Qiu, L.; Wu, Y.; Hu, X.; Zhang, X., Aptamer-Modified Semiconductor Quantum Dots for Biosensing Applications. *Sensors (Basel)* **2017,** *17* (8), 1736.
42. Efros, A. L.; Nesbitt, D. J., Origin and control of blinking in quantum dots. *Nat Nanotechnol* **2016,** *11* (8), 661-671.
43. Roark, B. K.; Tan, L. A.; Ivanina, A.; Chandler, M.; Castaneda, J.; Kim, H. S.; Jawahar, S.; Viard, M.; Talic, S.; Wustholz, K. L.; Yingling, Y. G.; Jones, M.; Afonin, K. A.,

Fluorescence blinking as an output signal for biosensing. *ACS Sensors* **2016,** *1* (11), 1295-1300.
44. Zhang, D. Y.; Seelig, G., Dynamic DNA nanotechnology using strand-displacement reactions. *Nature Chemistry* **2011,** *3* (2), 103-113.
45. Afonin, K. A.; Viard, M.; Martins, A. N.; Lockett, S. J.; Maciag, A. E.; Freed, E. O.; Heldman, E.; Jaeger, L.; Blumenthal, R.; Shapiro, B. A., Activation of different split functionalities upon re-association of RNA-DNA hybrids. *Nature Nanotechnology* **2013,** *8* (4), 296-304.
46. Qian, L.; Winfree, E., Scaling up digital circuit computation with DNA strand displacement cascades. *Science* **2011,** *332* (6034), 1196-1201.
47. Afonin, K. A.; Desai, R.; Viard, M.; Kireeva, M. L.; Bindewald, E.; Case, C. L.; Maciag, A. E.; Kasprzak, W. K.; Kim, T.; Sappe, A.; Stepler, M.; KewalRamani, V. N.; Kashlev, M.; Blumenthal, R.; Shapiro, B. A., Co-transcriptional production of RNA–DNA hybrids for simultaneous release of multiple split functionalities. *Nucleic Acids Research* **2014,** *42* (3), 2085-2097.
48. Afonin, K. A.; Viard, M.; Tedbury, P.; Bindewald, E.; Parlea, L.; Howington, M.; Valdman, M.; Johns-Boehme, A.; Brainerd, C.; Freed, E. O., The use of minimal RNA toeholds to trigger the activation of multiple functionalities. *Nano Letters* **2016,** *16* (3), 1746-1753.
49. Espanol, P.; Warren, P., Statistical mechanics of dissipative particle dynamics. *Europhysics Letters* **1995,** *30* (4), 191.
50. Warren, P. B., Dissipative particle dynamics. *Current Opinion in Colloid & Interface Science* **1998,** *6* (3), 620-624.
51. Deaton, T. A.; Aydin, F.; Li, N. K.; Chu, X.; Dutt, M.; Yingling, Y. G. In *Dissipative Particle Dynamics Approaches to Modeling the Self-Assembly and Morphology of Neutral and Ionic Block Copolymers in Solution*, Foundations of Molecular Modeling and Simulation, Singapore, 2021//; Maginn, E. J.; Errington, J., Eds. Springer: Singapore, 2021; pp 75-100.
52. Li, N. K.; Fuss, W. H.; Tang, L.; Gu, R.; Chilkoti, A.; Zauscher, S.; Yingling, Y. G., Prediction of solvent-induced morphological changes of polyelectrolyte diblock copolymer micelles. *Soft Matter* **2015,** *11* (42), 8236-8245.
53. Walker, C. L.; Lukyanov, K. A.; Yampolsky, I. V.; Mishin, A. S.; Bommarius, A. S.; Duraj-Thatte, A. M.; Azizi, B.; Tolbert, L. M.; Solntsev, K. M., Fluorescence imaging using synthetic GFP chromophores. *Current Opinion in Chemical Biology* **2015,** *27*, 64-74.
54. Svaneborg, C., LAMMPS framework for dynamic bonding and an application modeling DNA. *Computer Physics Communications* **2012,** *183* (8), 1793-1802.
55. Plimpton, S., Fast parallel algorithms for short-range molecular dynamics. *Journal of Computational Physics* **1995,** *117* (1), 1-19.
56. Li, N. K.; Kuang, H.; Fuss, W. H.; Zauscher, S.; Kokkoli, E.; Yingling, Y. G., Salt Responsive Morphologies of ssDNA-Based Triblock Polyelectrolytes in Semi-Dilute Regime: Effect of Volume Fractions and Polyelectrolyte Length. *Macromolecular Rapid Communications* **2017,** *38* (20), 1700422.
57. Ge, W.; Li, N. K.; McCormick, R. D.; Lichtenberg, E.; Yingling, Y. G.; Stiff-Roberts, A. D., Emulsion-Based RIR-MAPLE Deposition of Conjugated Polymers: Primary Solvent Effect and Its Implications on Organic Solar Cell Performance. *ACS Appl Mater & Interfaces* **2016,** *8* (30), 19494-19506.

58. Li, N. K.; Fuss, W. H.; Yingling, Y. G., An Implicit Solvent Ionic Strength (ISIS) Method to Model Polyelectrolyte Systems with Dissipative Particle Dynamics. *Macromolecular Theory and Simulations* **2015,** *24* (1), 7-12.
59. Burmeister, A. R.; Marriott, I., The Interleukin-10 Family of Cytokines and Their Role in the CNS. *Frontiers in Cellular Neuroscience* **2018,** *12* (458).
60. Chauhan, V. S.; Sterka, D. G.; Gray, D. L.; Bost, K. L.; Marriott, I., Neurogenic Exacerbation of Microglial and Astrocyte Responses to Neisseria meningitidis and Borrelia burgdorferi. *The Journal of Immunology* **2008,** *180* (12), 8241.
61. Afonin, K. A.; Grabow, W. W.; Walker, F. M.; Bindewald, E.; Dobrovolskaia, M. A.; Shapiro, B. A.; Jaeger, L., Design and self-assembly of siRNA-functionalized RNA nanoparticles for use in automated nanomedicine. *Nat Protocols* **2011,** *6* (12), 2022-2034.
62. Schneider, C. A.; Rasband, W. S.; Eliceiri, K. W., NIH Image to ImageJ: 25 years of image analysis. *Nat Methods* **2012,** *9* (7), 671-675.
63. Haeri, M.; Haeri, M., ImageJ plugin for analysis of porous scaffolds used in tissue engineering. *Journal of Open Research Software* **2015,** *3* (1), 1-4.

3.6 Appendices: Supporting Information for Controlled Organization of Inorganic Materials Using Biological Molecules for Activating Therapeutic Functionalities

3.6.1 Sequences

DNA strands were designed to form RNA/DNA hybrids with sense and antisense strands of Dicer Substrate RNAs (DS RNAs) selected against Green Fluorescent Protein. Once formed, those hybrids have single-stranded DNA toeholds (underlined) which are designed to interact with each other to initiate branch migration.

DNA for Sense_12_Biotin
5’-/5Biosg/GGAGACCGTGACCGGTGGTGCAGATGAACTTCAGGGTCA

DNA for Antisense_12_Biotin
5’-/5Biosg/TGACCCTGAAGTTCATCTGCACCACCGGTCACGGTCTCC

RNA Sense
5’-/5Phos/ACCCUGAAGUUCAUCUGCACCACCG

RNA Antisense
5’-CGGUGGUGCAGAUGAACUUCAGGGUCA

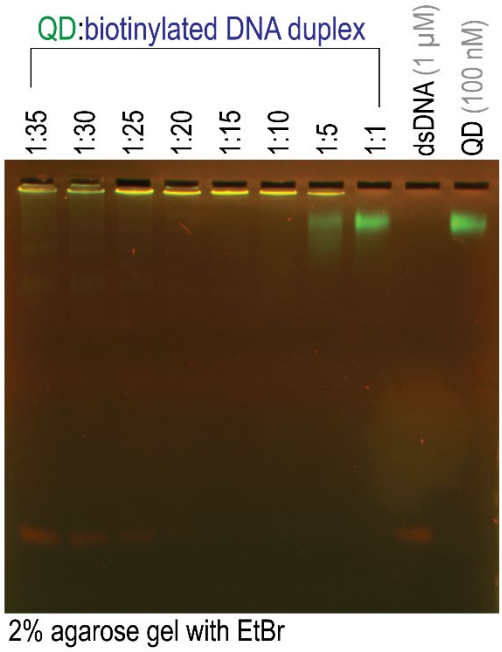

Figure A1. Binding assay of QD545 with increasing concentrations of biotinylated DNA duplexes used to confirm the number of biotin binding sites per QD required for assembly. QD is 100 nM in all conditions. The band corresponding to excess dsDNA becomes faintly visible beginning at the 1:15 ratio, so a 1:10 ratio was used for all QD:nucleic acid assemblies.

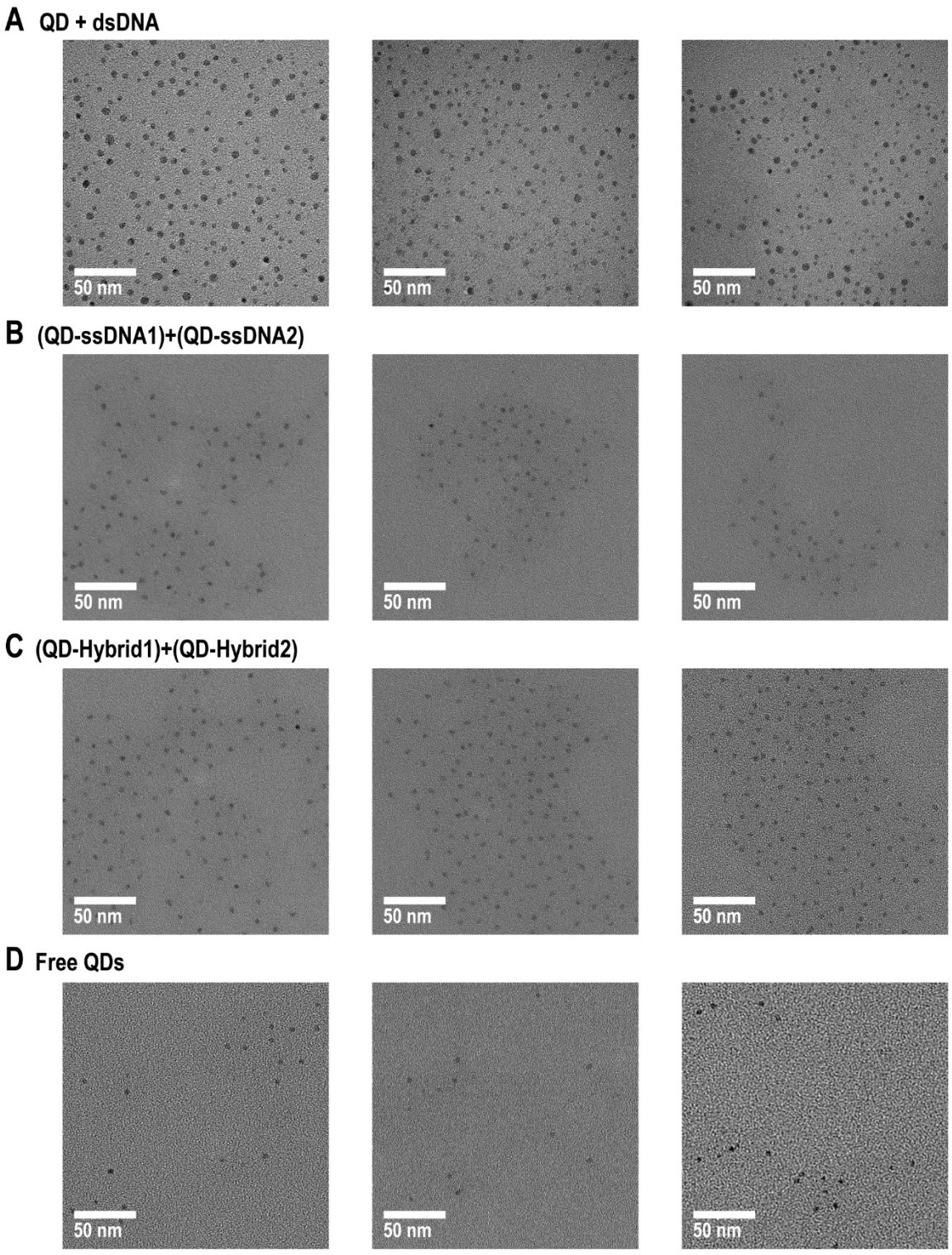

Figure A2. Three representative TEM images were used for calculations of center-to-center distances in ImageJ. Assemblies were formed via (A) QD+dsDNA, (B) (QD-ssDNA1)+(QD-ssDNA2), and (C) (QD-Hybrid1)+(QD-Hybrid2). (D) Free QDs were used as a control.

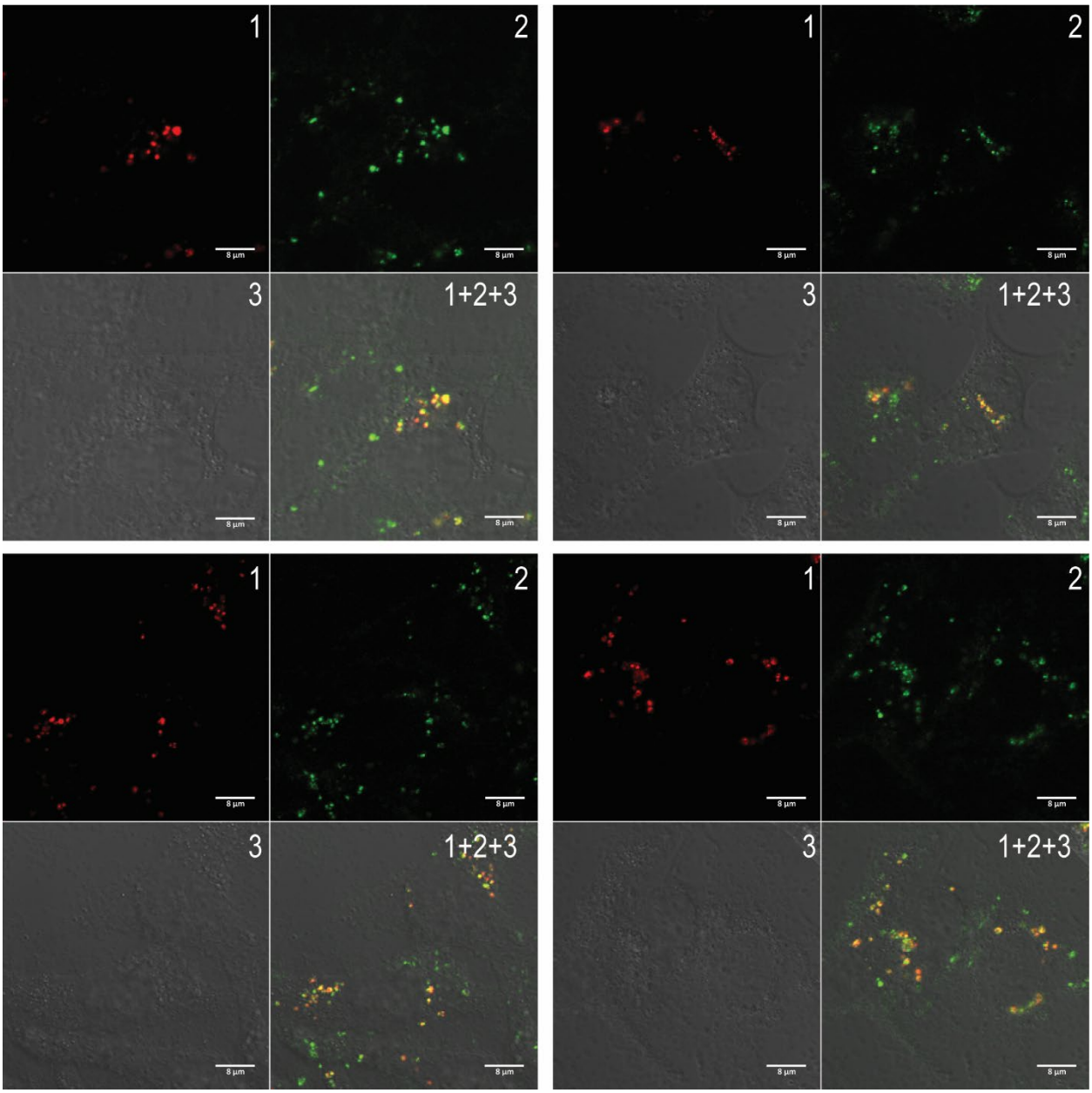

Figure A3. Co-localization of QD545 (green) and QD605 (red) entering the composition of intracellularly assembled QDs analyzed by confocal microscopy. Image numbers correspond to: (1) QD605 emission, (2) QD545 emission, and (3) differential interference contrast (DIC) images. Images (1+2+3) are the superposition of three different images. Scale = 8 μm.

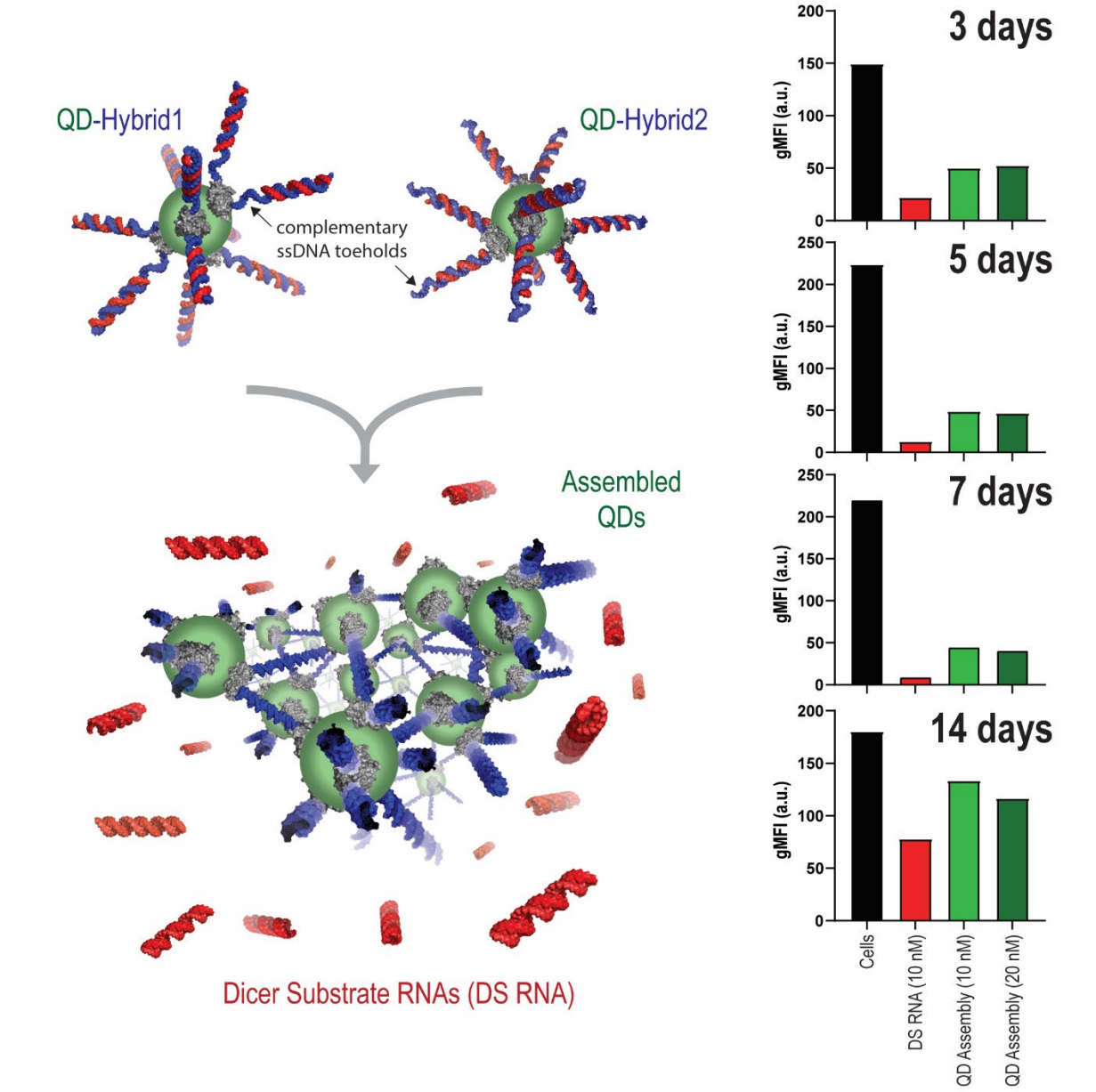

Figure A4. Activation of RNAi through QD assembly and release of DS RNAs using GFP knockdown assays for human breast cancer cells expressing GFP. Three, five, seven, and fourteen days after the co-transfection of cells with hybrid-functionalized QDs, GFP expression was analyzed with flow cytometry. As a control, transfections with the pre-formed DS RNA duplexes against GFP were used. gMFI corresponds to the geometric mean fluorescence intensity. Bars denote mean ± SEM of n=20,000 individual events.

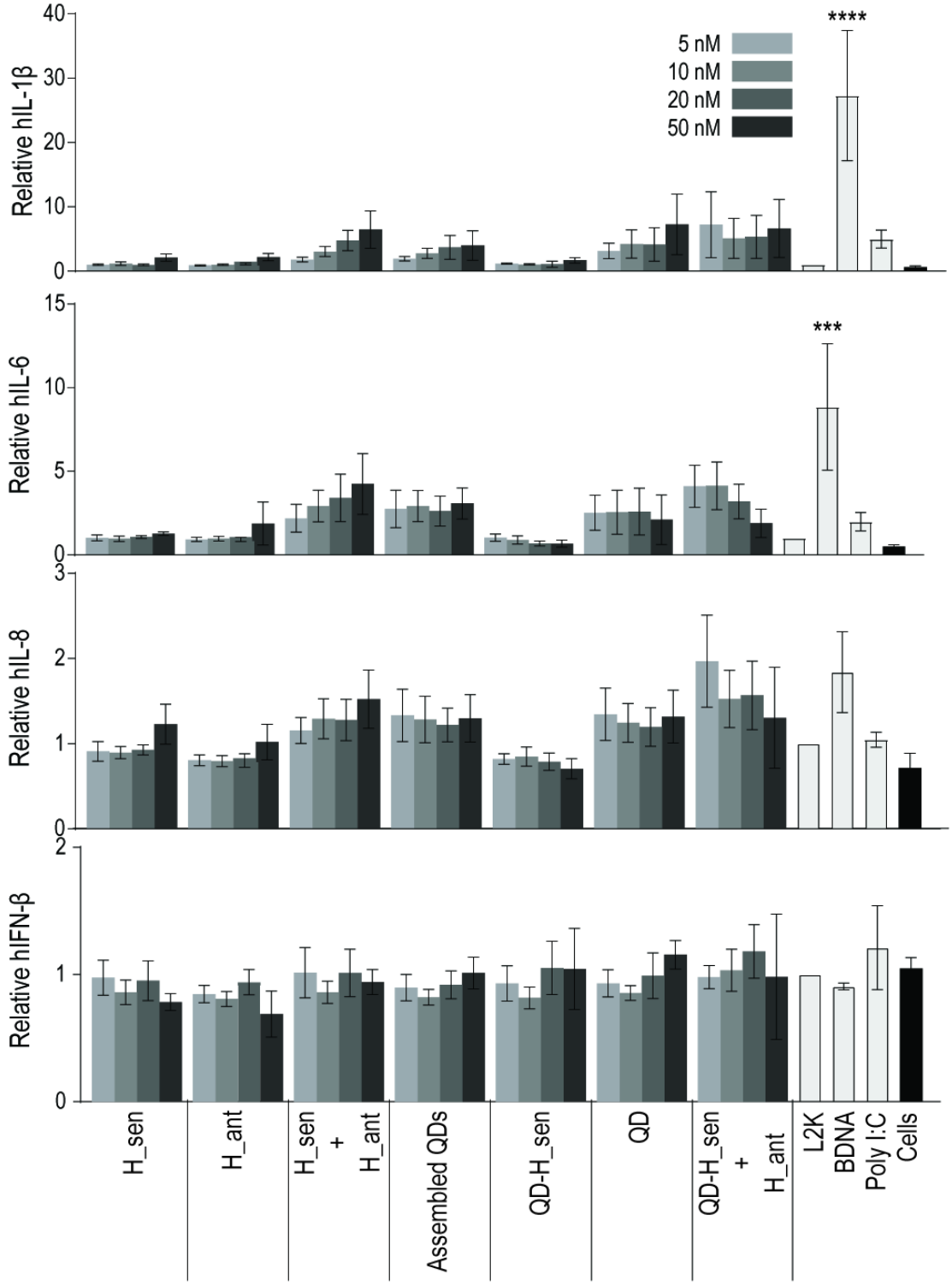

Figure A5. Immunostimulatory activity of QD assemblies in the human astrocyte-like cell line U87-MB. Cells were transfected and cell supernatants were collected 24 hours later. Levels of hIL-1β, hIL-6, hIL-8, and hIFN-β were assessed by specific-capture ELISA. Bars denote mean ± SEM of n=3 independent repeats. Statistically significant results are indicated with asterisks (**** = P-value < 0.0001, *** = P-value <0.001)

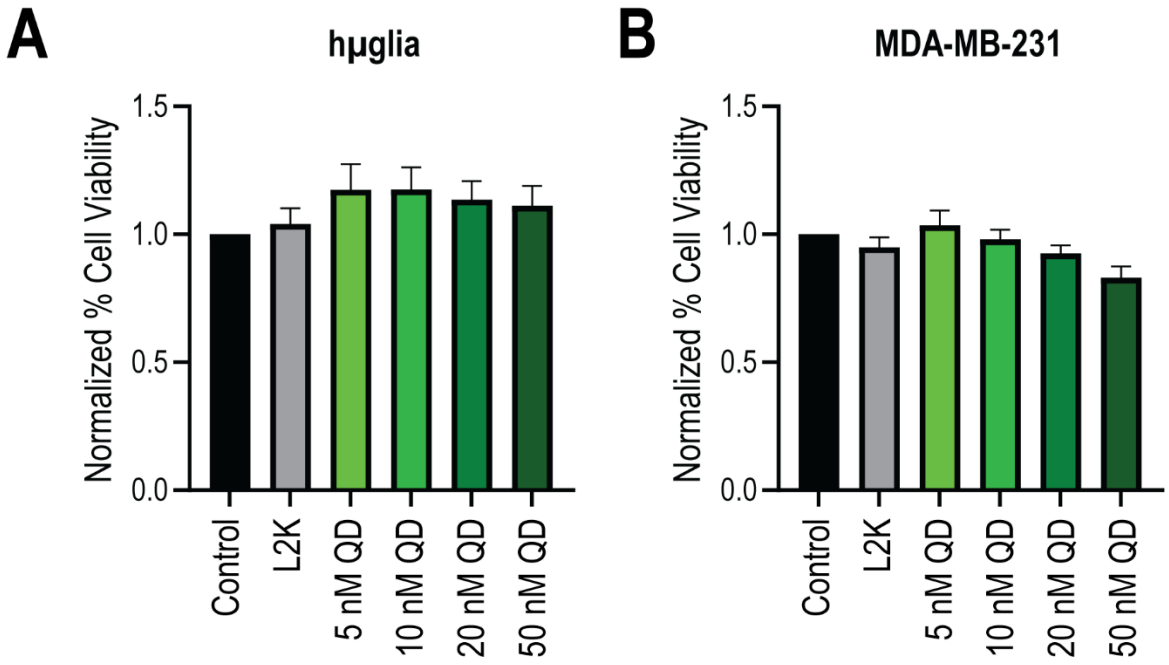

Figure A6. Cell viability assays of QDs in (A) hμglia and (B) MDA-MB-231 cell lines after 24 hours. Bars denote means ± SEM of n=4 independent repeats for control (cells-only), L2K, and 5-20 nM QD and n=3 independent repeats for 50 nM QD.

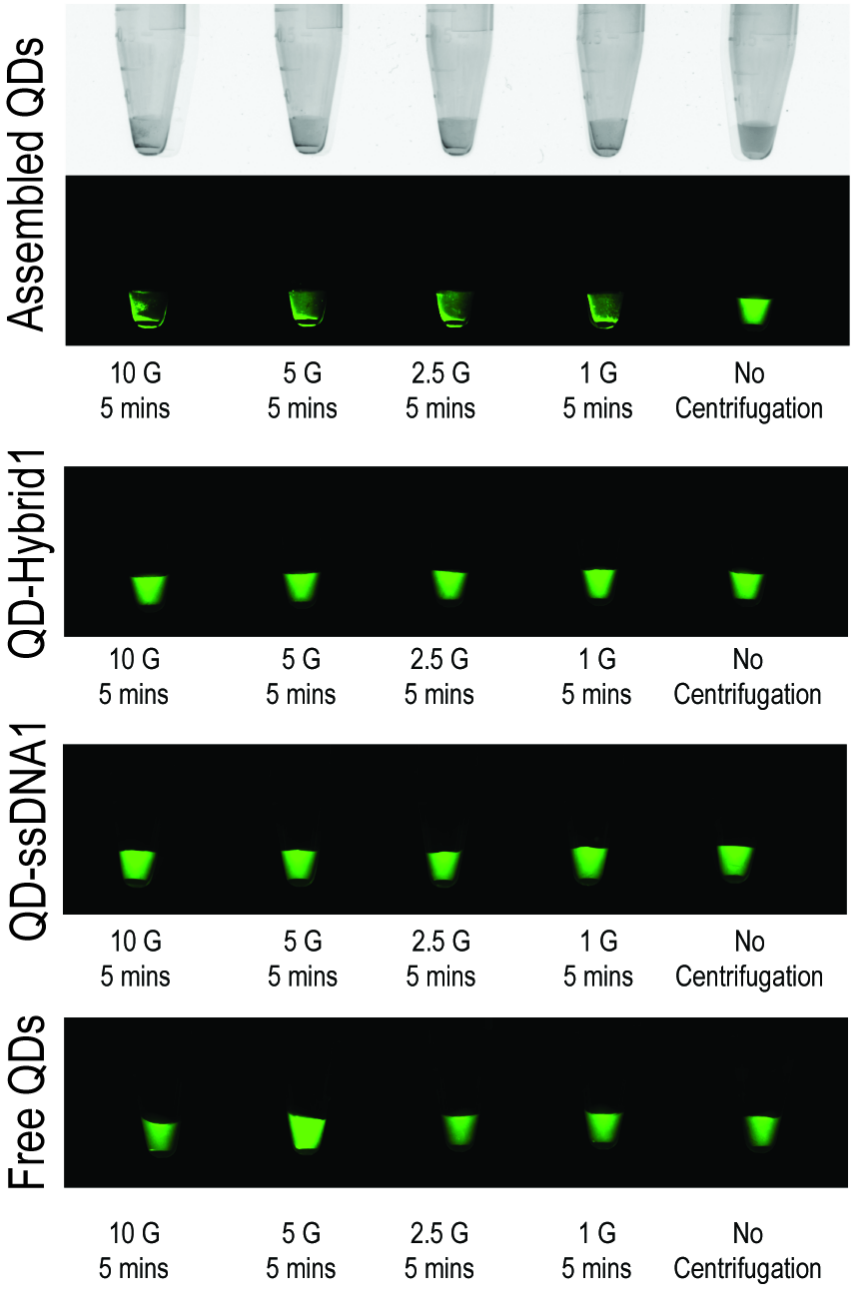

Figure A7. Precipitation of QD assemblies. Assembled QDs were centrifuged for 5 minutes at different speeds and show the formation of a solid pellet in the bottom of the tube. For all other QD samples which are not assembled, no precipitation is observed.

4 CHAPTER 4: SPATIAL ARRANGEMENT OF THERAPEUTIC MOIETIES DETERMINES THEIR IMMUNOSTIMULATION

4.1 Introduction

Within the cell, pattern recognition receptors (PRRs) specific for the detection of nucleic acids as pathogen or damage-associated molecular patterns (PAMPs or DAMPs) have evolved to pass the final judgement on which nucleic acids are "self" and which are not[1-4]. Endosomal Toll-Like Receptors (TLRs) bind to PAMPs to activate a signaling cascade which results in the downstream expression of various cytokines and interferons. In humans, there are four main TLRs which are generally activated by nucleic acids: broadly, TLR3 detects double-stranded RNAs, TLR7 and TLR8 detect single-stranded RNA, and TLR9 detects DNA and unmethylated CpG motifs[5]. Meanwhile, cytosolic DNA and RNA are readily sensed by the cGAS-STING and RIG-I-like receptor (RLR)-MAVS pathways[6].

As a result of their nucleic acid composition, nucleic acid nanoparticles (NANPs) which have been designed for biological applications interact with PRRs in the same language as innate nucleic acids[1, 7]. While unknown properties of the immunorecognition of assembled nucleic acids have historically been a major hurdle to their optimization and clinical transition, recently elucidated patterns of NANP recognition can now be incorporated directly to inform their design phase[8-11]. The ability to control which interactions with PRRs are occurring with NANPs also determines the overall downstream production of cytokines and cell signaling responses.

Previous work has investigated the structure-activity relationships between NANP designs and the way in which they interact with PRRs to stimulate an immune response. From these studies, some overall trends have been elucidated in NANPs' dimensionality (three-dimensional NANPs are more immunostimulatory than two-dimensional, which are more immunostimulatory than one-dimensional), composition (RNA-based NANPs are more

immunostimulatory than their DNA counterparts), and functionalization with therapeutic nucleic acids (TNAs) (with more TNAs yielding a higher immune response)[12]. Previous work on Dicer Substrate (DS) RNA-functionalized RNA fibers found that varying the orientation of the TNAs brought about a higher immune response[13]. However, this trend in orientation has not been explored for other NANP scaffolds. Particularly because the fiber is a one-dimensional structure known for lower immunostimulation, a greater flexibility in the stimulation brought about by TNA functionalization could be utilized to optimally co-deliver TNAs alongside a favorable immune profile.

To explore these trends, we have developed a panel of NANP rings composed entirely of RNA which are functionalized with DS RNAs against green fluorescent protein (GFP) as proof-of-concept. The assembly of rings has been previously established by our group[14-16] and is based on the intramolecular interactions of each of six RNA monomers to reveal the potential for intermolecular interactions between adjacent monomers to form ~120° kissing loop motifs[17]. Rings have been shown to be highly uniform in assembly, with the potential to incorporate TNAs modularly by extending the sequences in their hexameric composition. A variety of TNA-functionalized NANP rings have been utilized as carriers of aptamers, fluorophores, and DS RNAs into cells[14, 18-22].

4.2 Results

Owing to their hexameric nature, a maximum of up to six functionalities were incorporated into each NANP ring. This allows for various combinations of functionalization ranging from zero to six, with rings of two, three, and four DS RNAs available in three different orientations each. Here, all rings are referred to by the number of DS RNAs in their composition, *i.e.* Ring 5 has five DS RNAs, and those with multiple orientations are followed by A, B, or C, as

shown in **Figure 11.** The controlled programmable assembly of these precise combinations is possible due to the modular nature of the ring design, which has six distinct kissing loop interactions so that all monomers' intermolecular interactions are assured[17]. The assembly of this panel was confirmed by atomic force microscopy (AFM) and electrophoretic mobility shift assays (EMSA)(**Figure 11**).

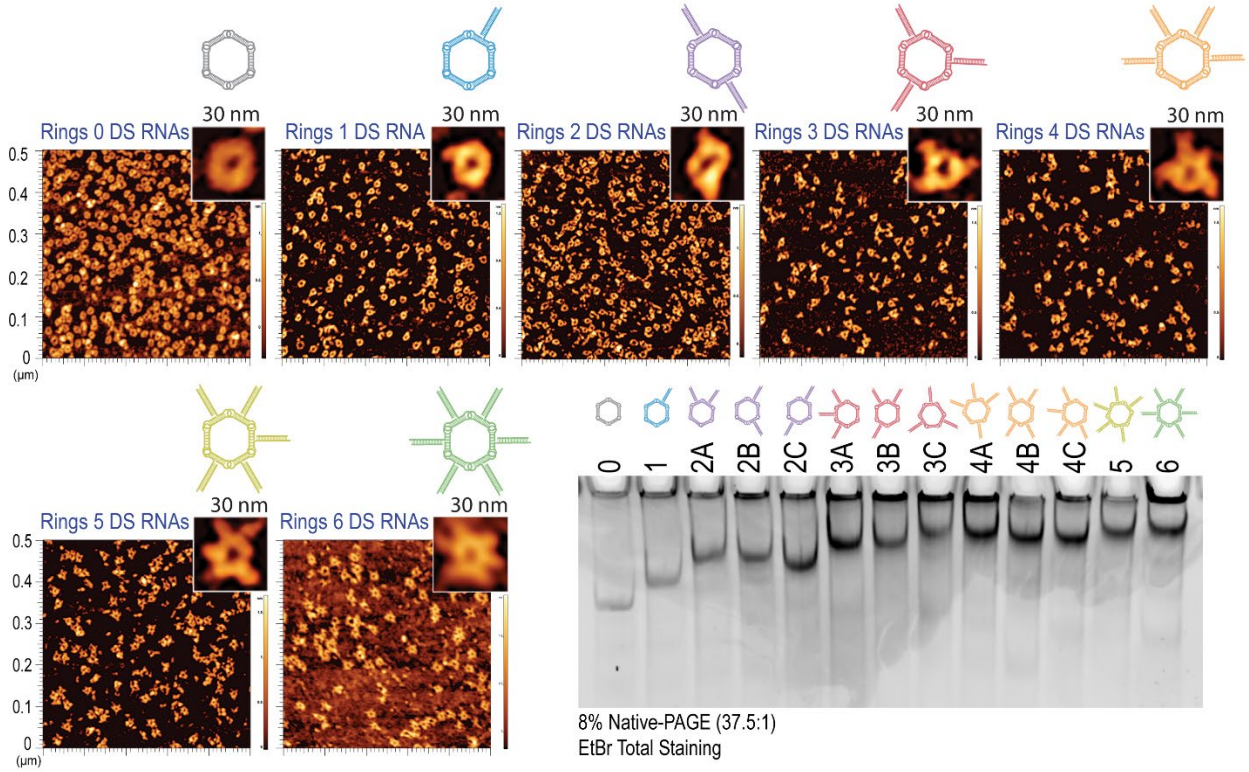

Figure 11. Orientations of functionalized GFP nanorings. All possible orientations were assembled and visualized on a Native-PAGE stained with EtBr (bottom right). Schemes show their design with the nomenclature described in-text. AFM images of one ring from each number of DS RNAs are shown (top).

To confirm the biological activity of all assembled rings, the panel was introduced into the human breast cancer cell line MDA-MB-231 expressing GFP. Lipofectamine 2000 (L2K) was used as a carrier for the intracellular delivery of rings into the cytosol, where the DS RNAs of each ring were designed to enter the RNA interference (RNAi) pathway. After dicing and subsequent incorporation into the RNA-induced silencing complex (RISC), the antisense strand

complementary to the GFP-coding mRNA was intended to drive its post-transcriptional knockdown. After 72 hours, cells were assessed via fluorescent microscopy to visualize the expression of GFP (**Figure 12**).

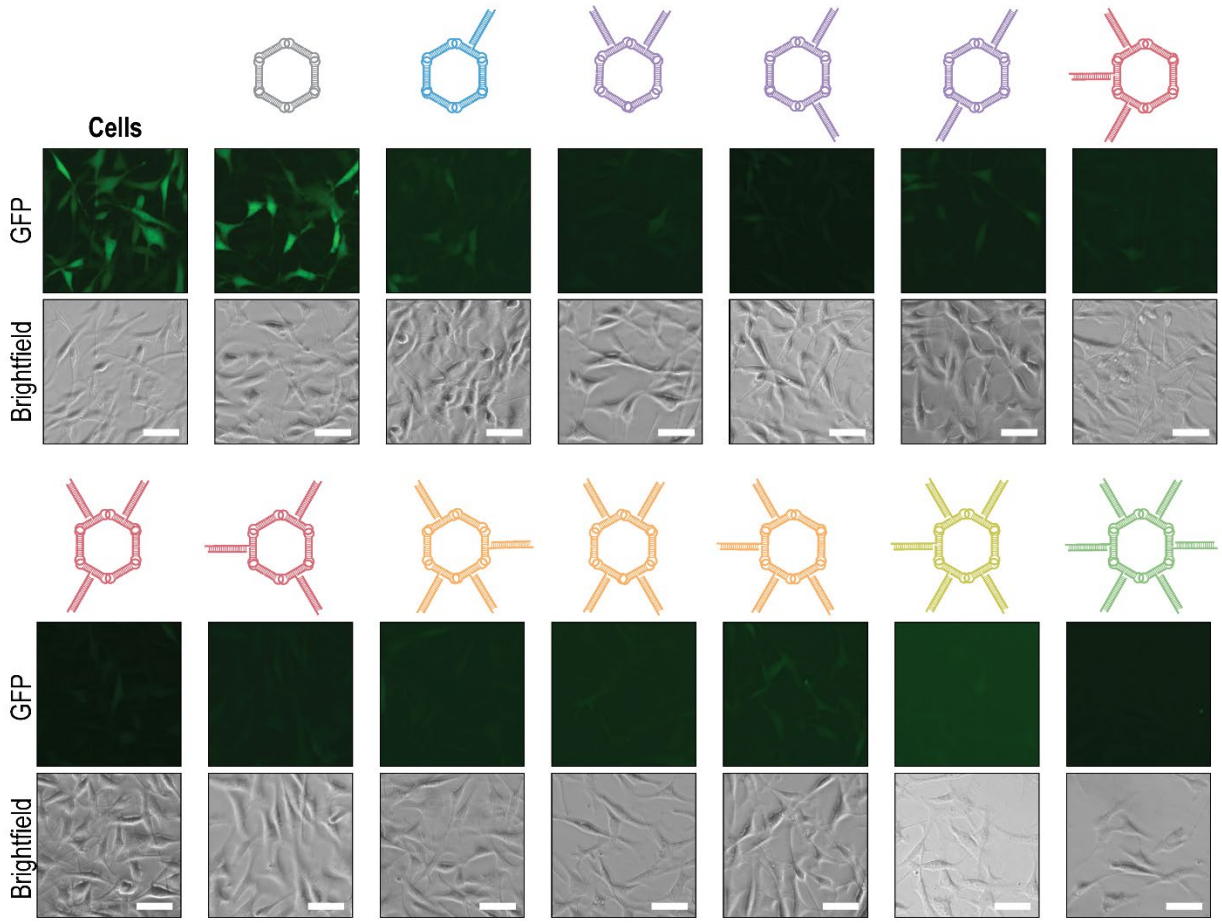

Figure 12. Fluorescent microscopy images of a human breast cancer cell line expressing GFP (MDA-MB-231 eGFP) 72 hours after transfection with functionalized rings. The same population of cells was imaged for GFP and brightfield after transfection with each ring shown. Scale bar = 50 μm.

To investigate the immunostimulatory properties of the ring panel using previously established protocols[7], peripheral blood mononuclear cells (PBMCs) were isolated from the freshly drawn blood of healthy human donors using resources from the Nanotechnology Characterization Laboratory in Frederick, Maryland. Three repeats were performed for each of *N*=4 donors to account for inter-donor variability. Rings of various TNA orientations conjugated

to L2K were added to PBMCs seeded at 200k cells per well[23]. ODN 2216, a known oligonucleotide immune activator, served as a positive control[24]. After 20 hours, the production of type I and III interferons (IFNs), IFN-α, β, ω, and λ, was assessed using a multiplex assay (**Figure 13**). The mean of each donor is represented by a different color point.

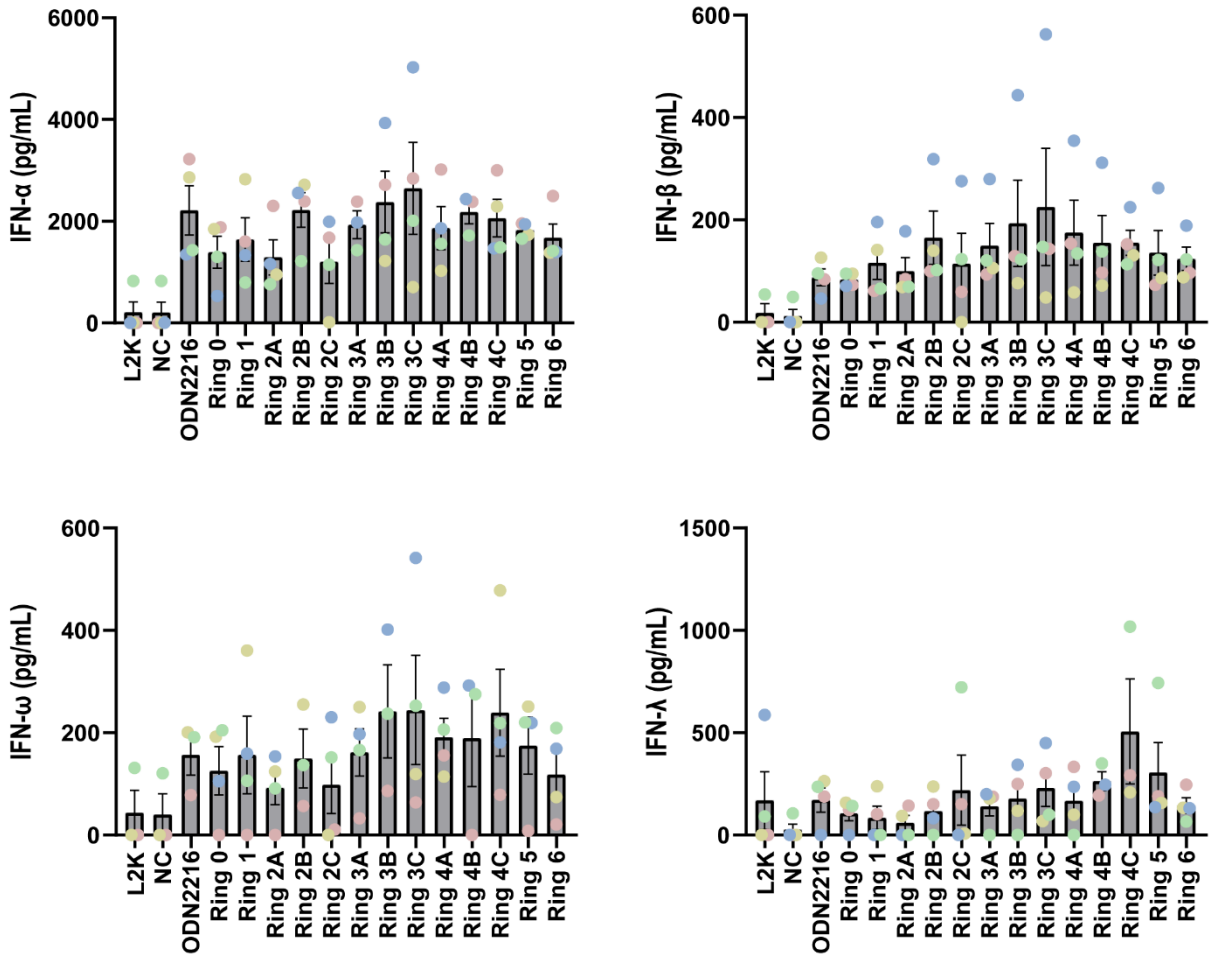

Figure 13. Results from a multiplex assay for type I and type III IFNs (IFN-α, -β, -ω, and -λ) 20 hours after the transfection of PBMCs with rings using L2K. All rings were 10 nM final concentration. Each point represents the mean of three measurements from one donor, for a total of *N*=4 donors per bar. Error bars denote mean ± SEM. Negative control (NC) is untreated cells, positive control is ODN2216, and vehicle control is L2K only.

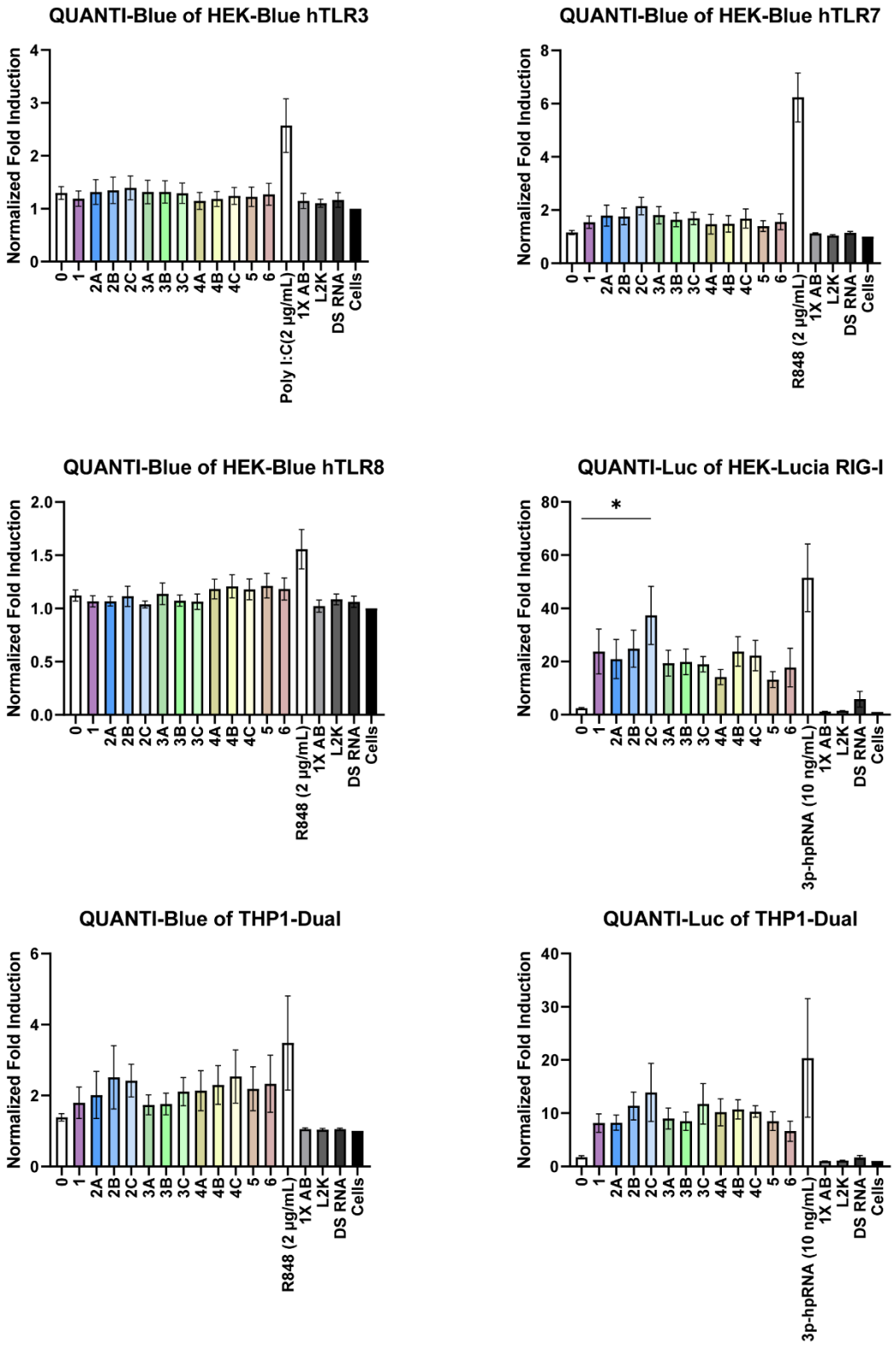

Figure 14. Normalized fold induction 24 hours after the transfection of rings into immune reporter cell lines. All values are normalized to the cells-only control and rings are 10 nM final

concentration. The positive control for each cell line is shown as the uncolored bar. 1X assembly buffer (AB), L2K, and DS RNA (10 nM) are additional controls. Each bar represents the mean of *N*=5 biological replicates. Errors bars denote mean ± SEM. A one-way ANOVA followed by a Tukey's multiple comparisons test was used to assess statistical significance between rings. A *P*-value of <0.05 as denoted by * was considered statistically significant.

Building upon this overall picture of immunostimulation, immune reporter cell lines from Invivogen were utilized to determine which PRRs are activated for each ring orientation **(Figure 14**). HEK-Blue™ hTLR3, hTLR7, and hTLR8 cell lines are engineered to overexpress their respective TLR upstream of an NF-κB-inducible secreted embryonic alkaline phosphatase (SEAP) reporter gene. Rings were transfected at the same concentrations as in PBMC studies (10 nM) using L2K as a carrier and were analyzed after 24 hours. Likewise, HEK-Lucia™ RIG-I cells engineered to overexpress RIG-I upstream of an IRF pathway-induced Lucia reporter were transfected and assessed with QUANTI-Luc™ assays to determine the overall contribution of RIG-I. THP1-Dual™ cells which express both reporters were used as an overall determination of whether the NF-κB or IRF pathways were involved.

4.3 Discussion

Rings were assembled with high batch-to-batch consistency for use in downstream experiments for biological activity and were confirmed via EMSA. While a distinct band confirmed the assembly of all orientations, the migration of each ring through the well is influenced by its shape (**Figure 11**). The distinct shapes of each combination are discernible via AFM, owing to the modularity of the assembly strategy.

All rings showed some silencing activity in MDA-MB-231 eGFP cells, resulting in decreased fluorescence by GFP (**Figure 12**). The untreated cells and those transfected with Ring 0 showed no visible knockdown as expected, since no DS RNAs were introduced. With the increasing addition of DS RNAs, there was visibly decreased GFP expression in cells, but high overall viability of cell populations. Throughout all silencing experiments, the concentration of

overall ring was kept constant at 5 nM in order to observe the fold reduction in fluorescence; Ring 6 should yield a 30 nM concentration of DS RNAs, while Ring 5 should yield a 25 nM DS RNA concentration. While Ring 6 appeared to show the most silencing activity by eye, future work will evaluate fluorescence more quantitatively using flow cytometry. From this approach, the fold-change in fluorescence, if any, should be more observable, as should any variations between ring orientations of the same number of DS RNAs.

With increasing DS RNAs added to the ring scaffolds, it was initially expected that the number of functionalities would be the determining variable of immunostimulatory capabilities. However, in PBMC assays (**Figure 13**), this was not the case. While Ring 0 showed low overall immunostimulation in agreement with previous work[25], Ring 6 was not the highest mean for any of the IFN results. Instead, Ring 3C showed the highest stimulation of type I IFNs (-α, -β, and -ω). For IFN-λ, a type III IFN, Ring 3C showed higher stimulation than either Ring 0 or 6, but the highest immunostimulation came from Ring 4C. Inter-donor variability was present within the panel from four donors, which are presented as individual means per point. For some donors, the baseline level of IFNs was higher, as observed in the L2K and negative control (NC) groups.

To address the differences in immunostimulation observed in PBMCs and inform the type of interactions with PRRs, immune reporter cell lines were transfected with 10 nM of each ring orientation along with L2K (**Figure 14**). The QUANTI-Blue assay of the THP1-Dual cell line was used to determine overall NF-κB pathway activation, for which differences in the normalized fold induction were present between rings with the same number of DS RNAs. To assess the activity of TLRs upstream of the NF-κB pathway, cell lines specifically expressing hTLR3 or hTLR8 showed no apparent trends between ring orientations. However, hTLR7

showed distinctions between orientations, with Ring 2C resulting in almost two-fold the amount of stimulation by Ring 0.

The trend was more apparently observed using QUANTI-Luc assays to determine the contribution of recognition by the IRF pathway and confirmed by RIG-I reporter cells that this pathway and cytosolic receptors play a role in their distinct recognition patterns. Here, the difference between Ring 2C and Ring 0 was statistically significant. Interestingly, Ring 2C also exhibited the greatest spacing between DS RNAs, approximately 180° apart.

Tailoring NANP design based on the intended immunorecognition is a burgeoning area of their further adaptation[9, 26]. For three-dimensional NANP cubes, the overall scaffold can be tuned from highly immunostimulatory to immunoquiescent by introducing an increasing number of DNA strands into the composition[27]. While the functionalization of NANPs with TNAs has been shown to increase immunostimulation overall with NANP fibers, the intermediate designs between a non- and fully-functionalized NANP are shown here for the first time. Specific design principles influencing ring recognition should be further explored, as the spacing between DS RNAs may play a role in recruiting an optimal number of receptors for recognition, as has been previously shown with double-stranded RNAs recognized by TLR3[28]. The pathway to immunorecognition has also been shown to be determined by the carrier[19-20, 29-30], and thus future studies towards in vivo work should utilize an alternative delivery vehicle to compare with in vitro work.

4.4 Materials and Methods

4.4.1 Nucleic Acid Preparation

Forward and reverse DNA primers and template strands (Integrated DNA Technologies (IDT), Inc.) were PCR-amplified using MyTaq™ Mix, 2x (Bioline), for the preparation of

double-stranded DNA templates containing the promoters for T7 RNA polymerase. The amplified products were purified using DNA Clean & Concentrator® (Zymo Research) and transcribed by in vitro run-off transcription with T7 RNA polymerase in the presence of 80 mM HEPES-KOH (pH 7.5), 2.5 mM spermidine, 50 mM DTT, 25 mM $MgCl_2$, and 5 mM each rNTP over 3.5 hours at 37 °C. Transcription was stopped by addition of RQ1 RNase-Free DNase (Promega, 3u/50 μL), followed by incubation for 30 minutes at 37 °C. The RNA strands produced were then purified through denaturing polyacrylamide gel electrophoresis (PAGE, 8%) in the presence of 8 M urea run in 89 mM tris-borate, 2 mM EDTA (TBE, pH 8.2) at 85 mA for approximately 1.5 hours. RNA bands were visualized by UV shadowing, cut out, and eluted overnight in 300 mM NaCl, TBE at 4 °C. The eluate was thoroughly mixed with 2.5 volumes of 100% EtOH and placed at -20 °C for 3 hours to precipitate. Afterwards, samples were centrifuged at 10.0 G for 30 minutes and the resulting pellet was washed twice with 90% EtOH between 10-minute centrifugations at 10.0 G. The supernatant was removed and the pelleted samples were dried in a CentriVap micro IR vacuum concentrator (Labconco) at 55 °C with IR. Pellets were dissolved in HyClone™ Water, Molecular Biology Grade (Cytiva) and the concentration of each strand was determined by measuring the absorbance at 260 nm on a NanoDrop 2000 (ThermoFisher).

For the assembly of all ring variations, twelve strands were separately prepared and stored at -20 °C until use. All sequences were previously established and are available in the Supporting Information. Modified oligos—including those with 5’-phosphorylation—were purchased directly from IDT, Inc.

4.4.2 NANP Assembly

All ring variations were prepared by the combination of strands A-F, where each side could be functionalized (*e.g.* GFP nrA) or non-functionalized (*e.g.* nrA). The combination of strands A-F were added in an equimolar ratio in endotoxin-free HyClone™ Water along with GFP Sense RNA in an equimolar ratio with the number of functionalized A-F strands. Samples were heated to 95 °C for two minutes, snap-cooled on ice for 2 minutes to promote the formation of intramolecular hydrogen bonds, and assembly buffer (AB) was added to a final concentration of 89 mM tris-borate (TB, pH 8.2), 2 mM $MgCl_2$, 50 mM KCl. Samples were then incubated at 30 °C for 30 minutes and were stored on ice or at 4 °C until use.

4.4.3 EMSA

Rings were visualized on a native-PAGE (8%, 37.5:1 acrylamide:bis-acrylamide) prepared on a Mini-PROTEAN® Tetra Cell system (Bio-Rad). Gels were pre-run for 5 minutes at 150 V in 89 mM TB, 2 mM $MgCl_2$ and 2 µL of 1 µM ring were loaded per each well with 2 µL of native loading buffer (AB, 30% glycerol, bromophenol blue, xylene cyanol). Loaded gels were run for 30 minutes at 300 V, washed with double-deionized water (ddiH_2O), and stained with ethidium bromide (EtBr, 0.5 µg/mL). Gels were then imaged on a ChemiDoc™ MP (Bio-Rad).

4.4.4 AFM

AFM of rings was performed as previously described on a freshly cleaved 1-(3-aminopropyl) silatrane-modified mica surface. All images were collected from a MultiMode AFM Nanoscope IV system (Bruker Instruments) in tapping mode.

4.4.5 Cell Silencing

MDA-MB-231 eGFP cells were maintained at 37 °C and 5% CO_2 in DMEM (Gibco) containing 10% heat-inactivated FBS (Atlanta Biologicals), 100 U/mL penicillin, and 100 µg/mL streptomycin. Cells were seeded in 12-well plates at 40,000 cells per well 24 hours before transfection. For a final concentration of 5 nM rings per well, the rings were incubated with Lipofectamine 2000 (Invitrogen, 2 µL per well) at room temperature for 30 minutes and were then brought up to 500 µL in Opti-MEM (Gibco). Media was aspirated from each well and replaced with the treatment in Opti-MEM for 4 hours of incubation at 37 °C and 5% CO_2. Afterwards, the treatment was aspirated and replaced with fresh media. Cells were kept in incubation and assessed after 72 hours.

4.4.6 Fluorescent Microscopy

Cells were viewed on an EVOS® FL cell imaging system (Thermo Fisher) equipped with a GFP light cube (488 abs, 507 em). Brightfield images were taken at 50% brightness, while GFP images of the same field were taken at 60% brightness.

4.4.7 Immunostimulation in PBMCs

A peripheral blood cytokine induction assay was performed following NCL Method ITA-10[31] as previously established for the evaluation of NANPs[7]. Whole blood was collected from healthy donor volunteers and mixed 1:1 v/v with phosphate-buffered saline (PBS, HyClone™, Cytiva), then layered 4:3 v/v with Ficoll-Paque (GE Healthcare) and centrifuged for 30 minutes at 900 g without brake. The resulting mononuclear cell layer was washed in three times the volume of Hank's balanced salt solution (HBSS, Gibco) and centrifuged for 10 minutes at 400 g, then the supernatant was discarded and an additional wash was completed. Cells were resuspended in complete Roswell Park Memorial Institute (RPMI)-1640 media with 10% heat-

inactivated FBS, 2 mM L-glutamine, 100 U/mL penicillin, and 100 µg/mL streptomycin (all from Hyclone, GE Life Sciences) and seeded at 200,000 cells in 160 µL per well in 96-well U-bottomed plates. For a final concentration of 10 nM rings per well, the rings were incubated with Lipofectamine 2000 (Invitrogen, 0.4 µL per well) at room temperature for 30 minutes and were then added to the wells in triplicate per donor. As a positive control, ODN2216 was added at 25 µg/mL. All samples were diluted in Opti-MEM™ (Gibco) to bring each well volume to 200 µL, including for the cells-only and Lipofectamine 2000 control treatments. Plates were incubated at 37 °C and 5% CO_2 for 20 hours. Afterwards, plates were spun down at 400 g for 5 minutes and supernatants were transferred to a new 96-well plate for analysis. A 4-plex interferon kit (Quansys Biosciences) was used to assess the amounts of IFN-α, IFN-β, IFN-ω, and IFN-λ (pg/mL) from supernatants following the supplier's protocol. Multiplex assays were read using a Quansys ImagePro reader equipped with Q-View software.

4.4.8 Immune Reporter Cells

THP1-Dual™, HEK-Blue™ hTLR3, HEK-Blue™ hTLR7, HEK-Blue™ hTLR8, HEK-Blue™ hTLR9, and HEK-Lucia™ RIG-I cells (InvivoGen) were maintained according to the supplier's instructions in an incubator at 37 °C and 5% CO_2. For all experiments, cells were seeded at 40,000 cells per well in a flat-bottomed 96-well plate (Corning™ Costar™) 24 hours before transfection (for HEK cells) or immediately before transfection (for THP1 cells). For a final concentration of 10 nM rings per well, the rings were incubated with Lipofectamine 2000 (Invitrogen, 0.375 µL per well) at room temperature for 30 minutes and were then added to the wells in technical triplicate repeats. A panel of positive controls (all from InvivoGen) for each receptor were used as follows: 2 µg/mL 2'3'-cGAMP and 2 µg/mL R848 for THP1-Dual™ (IRF and NF-κB pathways, respectively); 10 ng/mL 3p-hpRNA with 0.375 µL L2K per well

(following 30 minutes of incubation) for HEK-Lucia™ RIG-I; 2 µg/mL R848 for HEK-Blue™ hTLR7 and HEK-Blue™ hTLR8; 2 µg/mL Poly I:C for HEK-Blue™ hTLR3. L2K (0.375 µL per well), AB (equal to the volume of ring added per well), and GFP RNA duplex (10 nM, 0.375 µL L2K per well) were used as additional controls. 24 hours after the transfection, THP1-Dual™ and HEK-Blue™ cells were assessed using QUANTI-Blue™ assays (InvivoGen) according to the manufacturer's guidelines and the plates were read on a Tecan Spark plate reader at an absorbance of 638 nm. All well values were the averages of sixteen-point reads. THP1-Dual™ and HEK-Lucia™ cells were assessed using QUANTI-Luc™ assays (InvivoGen) according to the manufacturer's guidelines. Plates were read immediately on a Tecan Spark plate reader for luminescence with a 100 ms reading time. Within each plate, all samples were assessed in technical triplicates, averaged, and normalized to the cells-only treatment for assessment of normalized fold induction. N=5 biological replicates were completed and averaged to evaluate the mean and standard error of the mean (SEM). To assess statistical significance between rings, a one-way ANOVA followed by a Tukey's multiple comparisons test was performed using GraphPad Prism version 9.0.0. A P-value of < 0.05 was considered to be statistically significant.

4.4.9 Presentation and Statistical Analysis

Figures were prepared in Adobe Illustrator 2020, v24.0.2 (64-bit). Graphs were prepared and statistical analysis was performed using GraphPad Prism version 9.0.0. for Windows, GraphPad Software, San Diego, California USA, www.graphpad.com.

4.5 References

1. Johnson, M. B.; Chandler, M.; Afonin, K. A., Nucleic acid nanoparticles (NANPs) as molecular tools to direct desirable and avoid undesirable immunological effects. *Adv Drug Delivery Reviews* **2021,** *173*, 427-438.
2. Johnson, M. B.; Halman, J. R.; Burmeister, A. R.; Currin, S.; Khisamutdinov, E. F.; Afonin, K. A.; Marriott, I., Retinoic acid inducible gene-I mediated detection of bacterial nucleic acids in human microglial cells. *Journal of Neuroinflammation* **2020,** *17* (1), 139.

3. Ori, D.; Murase, M.; Kawai, T., Cytosolic nucleic acid sensors and innate immune regulation. *International reviews of immunology* **2017,** *36* (2), 74-88.
4. Roers, A.; Hiller, B.; Hornung, V., Recognition of Endogenous Nucleic Acids by the Innate Immune System. *Immunity* **2016,** *44* (4), 739-54.
5. Kawasaki, T.; Kawai, T., Toll-Like Receptor Signaling Pathways. **2014,** *5* (461).
6. Ablasser, A.; Hur, S. J. N. i., Regulation of cGAS-and RLR-mediated immunity to nucleic acids. **2020,** *21* (1), 17-29.
7. Dobrovolskaia, M. A.; Afonin, K. A., Use of human peripheral blood mononuclear cells to define immunological properties of nucleic acid nanoparticles. *Nature protocols* **2020,** *15* (11), 3678-3698.
8. Chandler, M.; Panigaj, M.; Rolband, L. A.; Afonin, K. A., Challenges to optimizing RNA nanostructures for large scale production and controlled therapeutic properties. *Nanomedicine (Lond)* **2020**.
9. Chandler, M.; Johnson, M. B.; Panigaj, M.; Afonin, K. A., Innate immune responses triggered by nucleic acids inspire the design of immunomodulatory nucleic acid nanoparticles (NANPs). *Curr Opin Biotech* **2020,** *63*, 8-15.
10. Dobrovolskaia, M. A., Nucleic Acid Nanoparticles at a Crossroads of Vaccines and Immunotherapies. *Molecules* **2019,** *24* (24).
11. Afonin, K. A.; Dobrovolskaia, M. A.; Church, G.; Bathe, M., Opportunities, Barriers, and a Strategy for Overcoming Translational Challenges to Therapeutic Nucleic Acid Nanotechnology. *ACS nano* **2020**.
12. Chandler, M.; Afonin, K. A., Smart-Responsive Nucleic Acid Nanoparticles (NANPs) with the Potential to Modulate Immune Behavior. *Nanomaterials* **2019,** *9* (4), 611.
13. Rackley, L.; Stewart, J. M.; Salotti, J.; Krokhotin, A.; Shah, A.; Halman, J. R.; Juneja, R.; Smollett, J.; Lee, L.; Roark, K.; Viard, M.; Tarannum, M.; Vivero-Escoto, J.; Johnson, P. F.; Dobrovolskaia, M. A.; Dokholyan, N. V.; Franco, E.; Afonin, K. A., RNA Fibers as Optimized Nanoscaffolds for siRNA Coordination and Reduced Immunological Recognition. *Advanced Functional Materials* **2018,** *28* (48), 1805959.
14. Yourston, L.; Rolband, L.; West, C.; Lushnikov, A.; Afonin, K. A.; Krasnoslobodtsev, A. V. J. N., Tuning properties of silver nanoclusters with RNA nanoring assemblies. **2020,** *12* (30), 16189-16200.
15. Afonin, K. A.; Grabow, W. W.; Walker, F. M.; Bindewald, E.; Dobrovolskaia, M. A.; Shapiro, B. A.; Jaeger, L., Design and self-assembly of siRNA-functionalized RNA nanoparticles for use in automated nanomedicine. *Nat Protocols* **2011,** *6* (12), 2022-2034.
16. Afonin, K. A.; Kireeva, M.; Grabow, W. W.; Kashlev, M.; Jaeger, L.; Shapiro, B. A., Co-transcriptional Assembly of Chemically Modified RNA Nanoparticles Functionalized with siRNAs. *Nano Letters* **2012,** *12* (10), 5192-5195.
17. Grabow, W. W.; Zakrevsky, P.; Afonin, K. A.; Chworos, A.; Shapiro, B. A.; Jaeger, L., Self-Assembling RNA Nanorings Based on RNAI/II Inverse Kissing Complexes. *Nano Letters* **2011,** *11* (2), 878-887.
18. Afonin, K. A.; Viard, M.; Koyfman, A. Y.; Martins, A. N.; Kasprzak, W. K.; Panigaj, M.; Desai, R.; Santhanam, A.; Grabow, W. W.; Jaeger, L.; Heldman, E.; Reiser, J.; Chiu, W.; Freed, E. O.; Shapiro, B. A., Multifunctional RNA Nanoparticles. *Nano Letters* **2014,** *14* (10), 5662-5671.
19. Halman, J. R.; Kim, K.-T.; Gwak, S.-J.; Pace, R.; Johnson, M. B.; Chandler, M. R.; Rackley, L.; Viard, M.; Marriott, I.; Lee, J. S.; Afonin, K. A., A cationic amphiphilic co-

polymer as a carrier of nucleic acid nanoparticles (Nanps) for controlled gene silencing, immunostimulation, and biodistribution. *Nanomedicine: Nanotechnology, Biology and Medicine* **2020,** *23*, 102094.

20. Juneja, R.; Vadarevu, H.; Halman, J.; Tarannum, M.; Rackley, L.; Dobbs, J.; Marquez, J.; Chandler, M.; Afonin, K.; Vivero-Escoto, J. L., Combination of Nucleic Acid and Mesoporous Silica Nanoparticles: Optimization and Therapeutic Performance In Vitro. *ACS applied materials & interfaces* **2020,** *12* (35), 38873-38886.
21. Parlea, L.; Bindewald, E.; Sharan, R.; Bartlett, N.; Moriarty, D.; Oliver, J.; Afonin, K. A.; Shapiro, B. A., Ring Catalog: A resource for designing self-assembling RNA nanostructures. *Methods* **2016,** *103*, 128-137.
22. Sajja, S.; Chandler, M.; Fedorov, D.; Kasprzak, W. K.; Lushnikov, A.; Viard, M.; Shah, A.; Dang, D.; Dahl, J.; Worku, B.; Dobrovolskaia, M. A.; Krasnoslobodtsev, A.; Shapiro, B. A.; Afonin, K. A., Dynamic Behavior of RNA Nanoparticles Analyzed by AFM on a Mica/Air Interface. *Langmuir* **2018,** *34* (49), 15099-15108.
23. Hong, E.; Halman, J. R.; Shah, A.; Cedrone, E.; Truong, N.; Afonin, K. A.; Dobrovolskaia, M. A., Toll-Like Receptor-Mediated Recognition of Nucleic Acid Nanoparticles (NANPs) in Human Primary Blood Cells. *Molecules (Basel, Switzerland)* **2019,** *24* (6), 1094.
24. Zamanian-Daryoush, M.; Marques, J. T.; Gantier, M. P.; Behlke, M. A.; John, M.; Rayman, P.; Finke, J.; Williams, B. R., Determinants of cytokine induction by small interfering RNA in human peripheral blood mononuclear cells. *Journal of interferon & cytokine research : the official journal of the International Society for Interferon and Cytokine Research* **2008,** *28* (4), 221-33.
25. Hong, E.; Halman, J. R.; Shah, A. B.; Khisamutdinov, E. F.; Dobrovolskaia, M. A.; Afonin, K. A., Structure and Composition Define Immunorecognition of Nucleic Acid Nanoparticles. *Nano Lett* **2018,** *18* (7), 4309-4321.
26. Johnson, M. B.; Chandler, M.; Afonin, K. A., Nucleic acid nanoparticles (NANPs) as molecular tools to direct desirable and avoid undesirable immunological effects. *Advanced drug delivery reviews* **2021,** *173*, 427-438.
27. Halman, J. R.; Satterwhite, E.; Roark, B.; Chandler, M.; Viard, M.; Ivanina, A.; Bindewald, E.; Kasprzak, W. K.; Panigaj, M.; Bui, M. N.; Lu, J. S.; Miller, J.; Khisamutdinov, E. F.; Shapiro, B. A.; Dobrovolskaia, M. A.; Afonin, K. A., Functionally-interdependent shape-switching nanoparticles with controllable properties. *Nucleic Acids Research* **2017,** *45* (4), 2210-2220.
28. Lee, E. Y.; Takahashi, T.; Curk, T.; Dobnikar, J.; Gallo, R. L.; Wong, G. C. L., Crystallinity of Double-Stranded RNA-Antimicrobial Peptide Complexes Modulates Toll-Like Receptor 3-Mediated Inflammation. *ACS nano* **2017,** *11* (12), 12145-12155.
29. Avila, Y. I.; Chandler, M.; Cedrone, E.; Newton, H. S.; Richardson, M.; Xu, J.; Clogston, J. D.; Liptrott, N. J.; Afonin, K. A.; Dobrovolskaia, M. A., Induction of Cytokines by Nucleic Acid Nanoparticles (NANPs) Depends on the Type of Delivery Carrier. *Molecules* **2021,** *26* (3), 652.
30. Ke, W.; Afonin, K. A., Exosomes as natural delivery carriers for programmable therapeutic nucleic acid nanoparticles (NANPs). *Adv Drug Delivery Reviews* **2021**, 113835.
31. Potter, T.; Cedrone, E.; Neun, B.; Dobrovolskaia, M., NCL Method ITA-10. 2020.

4.6 Appendices: Supporting Information for Spatial Arrangement of Therapeutic Moieties Determines Their Immunostimulation

4.6.1 Sequences

Nanoring strands are denoted by "nr." Nanoring strands functionalized with an antisense sequence for GFP are denoted by "GFP" with the antisense sequence shown as lowercase.

nrA
5'-GGGAACCGUCCACUGGUUCCCGCUACGAGAGCCUGCCUCGUAGC

nrB
5'-GGGAACCGCAGGCUGGUUCCCGCUACGAGAGAACGCCUCGUAGC

nrC
5'-GGGAACCGCGUUCUGGUUCCCGCUACGAGACGUCUCCUCGUAGC

nrD
5'-GGGAACCGAGACGUGGUUCCCGCUACGAGUCGUGGUCUCGUAGC

nrE
5'-GGGAACCACCACGAGGUUCCCGCUACGAGAACCAUCCUCGUAGC

nrF
5'-GGGAACCGAUGGUUGGUUCCCGCUACGAGAGUGGACCUCGUAGC

GFP nrA
5'-GGGAACCGUCCACUGGUUCCCGCUACGAGAGCCUGCCUCGUAGCuucgguggugcag
augaacuucaggguca

GFP nrB
5'-GGGAACCGCAGGCUGGUUCCCGCUACGAGAGAACGCCUCGUAGCuucgguggugcag
augaacuucaggguca

GFP nrC
5'-GGGAACCGCGUUCUGGUUCCCGCUACGAGACGUCUCCUCGUAGCuucgguggugcag
augaacuucaggguca

GFP nrD
5'-GGGAACCGAGACGUGGUUCCCGCUACGAGUCGUGGUCUCGUAGCuucgguggugcag
augaacuucaggguca

GFP nrE
5'-GGGAACCACCACGAGGUUCCCGCUACGAGAACCAUCCUCGUAGCuucgguggugcag
augaacuucaggguca

GFP nrF
5’-GGGAACCGAUGGUUGGUUCCCGCUACGAGAGUGGACCUCGUAGCuucgguggugcag
augaacuucaggguca

GFP Sense
5’-/5Phos/ACCCUGAAGUUCAUCUGCACCACCG

5 CHAPTER 5: CONCLUSIONS

The modularity of dynamic nucleic acid nanoparticles (NANPs) makes them highly amenable to a number of applications as therapeutics, biosensors, and programmable materials. Owing to their diverse natural functions in the cellular environment as messenger RNAs (mRNA), long non-coding RNAs, short interfering RNAs, ribozymes, riboswitches, aptamers, and more, the development of therapeutic nucleic acids (TNAs) can allow for control as mimics of these naturally occurring processes. This is readily demonstrated by the growing repertoire of TNAs which have been clinically approved, the increasing number of TNA candidates in development and moving through the preclinical pipeline, and the swift adaptation of preexisting TNA technologies for the development of mRNA vaccines against SARS-CoV-2. As presented in this dissertation, three articles detail the design of nucleic acid-based systems for interactions with targeted nucleic acids, receptors of the innate immune system, and cellular pathways such as RNA interference. Interactions between pattern recognition receptors (PRRs) with known pathogen-associated molecular patterns (PAMPs) and damage-associated molecular patterns (DAMPs) are the foundation for nucleic acids' recognition by the immune system to initiate the downstream production of cytokines and interferons. These pre-evolved pathways have also been shown to dictate the immunostimulation by NANPs in primary human peripheral blood mononuclear cells (PBMCs). Changes to the composition (DNA or RNA), dimensionality (from globular to planar to fibrous), and degree of functionalization (with TNAs) of a NANP dictate the resulting immunostimulatory response. Depending on the design strategy, a NANP can be tailored to interact with a particular receptor in the cytosol or endosome.

In the first article, the split fluorescent RNA aptamer Broccoli is demonstrated for the conditional activation of RNA function. Separately, each half of the aptamer (Broc or Coli) is

non-functional, but upon their assembly, the complete aptamer's function is restored to bind the dye DFHBI-1T. This conditional response is an example of an AND logic gate which introduces a regulatory component. Fluorescence activation is also shown to be controlled by factors such as the addition of enzymes, Mg^{2+} or EDTA, and temperature.

In the second study, DNA and DNA/RNA hybrid duplexes are combined for the programmed assembly of quantum dots (QDs). Three different assembly strategies result in different kinetics but are shown to assemble via electrophoretic mobility shift assays (EMSA) and transmission electron microscopy (TEM). The assembled QDs are demonstrated to be non-immunostimulatory and their uptake is demonstrated in a human breast cancer cell line, MDA-MB-231. As the third approach to QD assembly, the use of DNA/RNA hybrid duplexes allows for complementary DNA toeholds to drive a strand displacement reaction, resulting in DNA duplexes which link QDs and the release of Dicer Substrate (DS) RNAs. When these materials were assembled in MDA-MB-231 cells expressing green fluorescent protein (GFP), DS RNAs against GFP were shown to result in significant gene knockdown.

Finally in the third study, NANP ring designs are introduced. The rings are hexameric assemblies of RNA which require each strand to form intramolecular hydrogen bonds in order to promote the subsequent intermolecular binding of 120° kissing loop motifs. In this study, the ring was functionalized with a DS RNA against GFP in every possible design orientation in order to study the effect of TNA orientation on immunostimulation. Silencing of GFP is demonstrated in the MDA-MB-231 cell line and the assemblies are verified via EMSA and atomic force microscopy. The rings are then introduced into PBMCs isolated from four different donors which show that the orientation of TNAs does have an affect on its overall recognition. Furthermore, immune reporter cell lines expressing specific individual receptors were transfected

with the ring orientations to determine which receptors were the most essential to their recognition.

Taken together, these articles represent the progression of NANPs towards more dynamic design influence, where the therapeutic effects of TNAs can be activated conditionally or favorably depending on the assembly. Tailoring NANPs' designs to take advantage of the functional versatility of their nucleic acid components is an ongoing effort for the development of individualized therapeutics and personalized medicine.